Novel Inhibitors of Fibroblast Activation Protein

Synthesis and labelling with Fluorine-18

Nawid Esmailkhel

Dissertation for the degree Master of Pharmacy
Section of Pharmaceutical Chemistry
45 credits

Department of Pharmacy
Faculty of Mathematics and Natural Science

UNIVERSITY OF OSLO

October 2021

Novel Inhibitors of Fibroblast Activation Protein

Nawid Esmailkhel

Dissertation for the degree of Master of Pharmacy

Department of Pharmaceutical Chemistry

School of Pharmacy

Faculty of Mathematics and Natural Science

UNIVERSITY OF OSLO

October 2021

Supervisors

Jo Klaveness

Dag Erlend Olberg

Vegard Torp Lien

2021

Novel Inhibitors of Fibroblast Activation Protein

Nawid Esmailkhel

http://www.duo.uio.no/

Printed: Reprosentralen, University of Oslo

Acknowledgements

This thesis is dedicated to my late uncle Hashmat, who had a profound impact on my life and always inspired and encouraged me to do my best no matter the circumstances. I would not be able to complete my studies without his continuous support. Also, a huge thank you to my dear uncle Jalani and aunt Zarina who passed away while I was trying to make them proud.

I would like to express my enormous gratitude to Professor Jo Klaveness, Associate Professor Dag Erlend Olberg and Dr. Vegard Torp Lien for their expertise and guidance throughout the latest year. It was extremely inspiring to work with some of the brightest minds in the Norwegian pharmaceutical community. The circumstances were extraordinary, but they made sure to include me and make me feel at ease in their company. Therefore, I would like to thank my supervisors for their support, both inside and outside the laboratory.

I would also like to shed some light on senior engineer Gunnar Hagelin, who I met almost daily throughout my time in the laboratory. He is undoubtedly one of the kindest people I have had the opportunity to meet, and he helped me tremendously with all his knowledge and life experience while I was there. He would always be there to support me and help me academically no matter how busy he was, and for that I am forever grateful.

Lastly, I would like to send a thank you to all my friends and family who stood beside me through the most difficult year of my life. You were there for me when I needed you the most and supported me throughout this journey. It is hard to find the right words to express how grateful I truly am for all of you.

Blindern, October 2021

Nawid Esmailkhel

Abstract

In recent years, the advances in cancer therapy and diagnostics have led researchers to explore the role tumour microenvironment plays in the development of various cancers. This has led to the discovery of fibroblast activation protein alpha (FAP), a membrane-bound glycoprotein, as a novel target for cancer therapy and diagnostics. It is reported that a higher expression of FAP in the tumour microenvironment correlates with poor prognosis for some cancer patients. FAP is also found to be upregulated in various cancers but is only present in minimal amounts in normal adult tissue. This allows for selective targeting with a new class of small molecule compounds, commonly called FAPIs.

FAPIs can in many cases be utilized for radioisotopic labelling and thus for diagnostic use through positron emission tomography (PET). Fluorine-18 is a radioisotope with many desirable attributes and is relatively unexplored with regards to FAPIs. Several radiotracers with other radioisotopes have been synthesized for such use, but it remains to get the first one approved by the authorities and available for regular use in clinics. However, there has been extensive research to study the structure-activity relationship and increase the imaging properties of radiolabelled FAPIs, and this has led to the discovery of promising compounds with nanomolar potency and high selectivity.

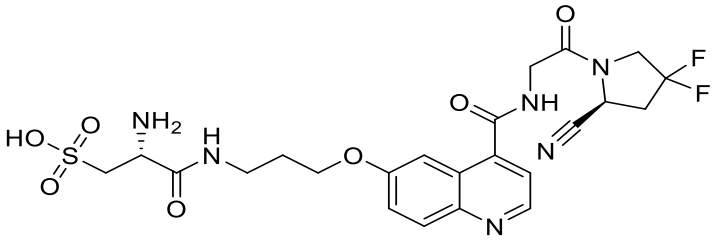

1

In this thesis, a novel precursor **1** was synthesized based on the existing knowledge of FAPIs and labelled with fluorine-18. Despite this, further studies must still be conducted to elucidate the pharmacological effects of this compound. There is also a need to synthesize analogues of the novel precursor and study the properties of these.

Abbreviations

[^{18}F]FDG	[^{18}F]Fluorodeoxyglucose
Boc	*tert*-Butyloxycarbonyl
BJP	British Journal of Pharmacology
CAFs	Cancer-associated fibroblasts
CNS	Central nervous system
CT	Computerized tomography
DCM	Dichloromethane
DIPEA	Diisopropylethylamine
DMF	Dimethylformamide
DMSO	Dimethyl sulfoxide
DNA	Deoxyribonucleic acid
DPP	Dipeptidyl peptidase
ECM	Extracellular matrix
EMT	Epithelial-mesenchymal transition
ESI	Electrospray ionization
Et_3N	Triethylamine
EtOAc	Ethyl acetate
FAP	Fibroblast activation protein alpha
FAPI	Fibroblast activation protein inhibitor
HATU	Hexafluorophosphate azabenzotriazole tetramethyl uronium
HBTU	Hexafluorophosphate benzotriazole tetramethyl uranium
HOAt	1-Hydroxy-7-azabenzotriazole
HOBt	Hydroxybenzotriazole
HRMS	High-resolution mass spectrometry

keV	Kiloelectron volt
LC-MS	Liquid chromatography-mass spectrometry
LG	Leaving group
mAbs	Monoclonal antibodies
MeCN	Acetonitrile
MS	Mass spectrometry
MsCl	Methanesulfonyl chloride
NAS	Nucleophilic aromatic substitution
NMR	Nuclear magnetic resonance
NPY	Neuropeptide Y
PET	Positron emission tomography
PREP	Prolyl oligopeptidase
Prep-HPLC	Preparative high performance liquid chromatography
PTSA	*p*-Toluenesulfonic acid
SAR	Structure-activity relationship
SERM	Selective estrogen receptor modulator
SPECT	Single photon emission computed tomography
TFA	Trifluoroacetic acid
TFAA	Trifluoroacetic anhydride
THF	Tetrahydrofuran
TIPS	Triisopropyl silane
TME	Tumour microenvironment

Table of contents

1 Introduction

1.1 Cancer and Fibroblast Activation Protein

1.1.1 Cancer

In broad terms, cancer can be defined as a group of diseases characterized by unregulated cell growth. One must distinguish between benign and malignant tumours, primarily because the latter is able to invade surrounding tissue, and travel with the blood or lymph system to other organs and thus metastasize. This feature is not observed in benign tumours, which are localized and not metastatic [1]. However, benign tumours can indeed become malignant, and therefore cancerous through tumour progression [2,3]. There is a broad consensus that cancer is a genetic disease, with alterations in oncogenes, tumour-suppressor genes and stability genes being responsible for carcinogenesis [4].

In their highly influential review article published in 2000, the cancer biologists Hanahan and Weinberg listed six hallmarks of cancer they believed were fundamental in the characterization of cancer and tumour progression. These six hallmarks included evasion of apoptosis, self-sufficiency in growth signals, insensitivity to anti-growth signals, tissue invasion and metastasis, limitless replicative potential, and sustained angiogenesis [5]. In a 2011 update, the list was extended to include four additional hallmarks: reprogramming of energy metabolism, genome instability and mutation, evading immune destruction, and tumour-promoting inflammation [6].

Cancer is one of the most important health problems in the world today. In 2020 alone, over 19 million new cases of various cancers were documented, and nearly 10 million deaths in the world were attributed to cancer in the same year (Fig. 1) [7]. In Norway, there were 34979 new cancer cases in 2019 [8]. As of 2021, the overall cancer incidence and cancer-associated deaths are increasing [9]. These numbers only highlight the ever-increasing demand for high-quality treatment and the early diagnosis of cancers.

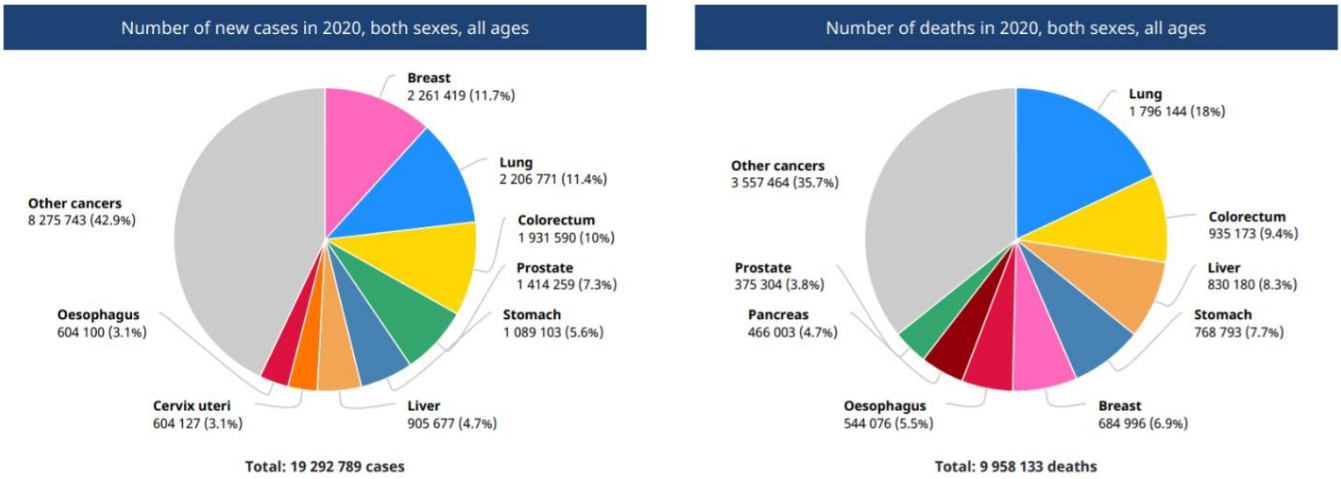

Figure 1. An overview of deaths and new cancer cases in 2020. The illustration also differentiates between the various types of cancers. The image is from the International Agency for Research on Cancer [7].

1.1.2 A shift towards personalized therapy

The diseases commonly referred to as cancer have captivated humans since ancient times. Ever since the first instances of cancerous growths in humans were discovered in approximately 3500-year-old Egyptian and Peruvian mummies, cancer has been an ever-present part of both human life and modern medicine [10]. The Hippocratic corpus from the Classical period of ancient Greece dealt with pathogenesis and treatment of various cancers. Some examples include the use of an intravaginal clyster containing the inner part of a cucumber mixed with honeycomb in water to prevent cancer, or simple advice to drink the juice of a squirting cucumber to combat cancer after a digestive disorder [11].

The knowledge of cancer management increased with time, and Goodman *et al*. eventually became among the first to demonstrate the efficacy of an anticancer therapy in humans during a study published in 1946. In this study, 67 patients were treated with the first chemotherapeutic agents, more precisely halogenated alkyl amine chlorides derived from mustard gas for Hodgkin disease, lymphosarcoma (previously used to describe a malignant tumour of lymphatic tissue), leukaemia and other related diseases [10,12]. The exact reason why some patients responded positively to the treatment was not known at the time, but it was later revealed that these compounds, today known as alkylating agents, formed covalent bonds with DNA that resulted in apoptosis of cancer cells. This led to a paradigm shift in cancer treatment, because the increased understanding coupled with the development of alkylating agents in the following decades built on the initial discoveries made by Goodman and his peers [13]. However, one of

the main drawbacks of these agents was that they also targeted healthy cells in addition to the cancer cells. This led to adverse events and fueled the interest of those who wanted new drugs that could target cancer cells with more selectivity. This led to the development of new drugs such as Tamofixen during the late 1970s, a selective estrogen receptor modulator (SERM) that blocked estrogen action necessary for hormone-dependent cancers, by binding to the estrogen receptor [14].

Further scientific advances and the Human Genome Project accelerated the shift towards tailored, personalized therapy. It was discovered that several mutations were associated with the different types of cancer, and varied a great deal between the individual patients [14]. This new understanding meant that researchers had to change their approach once again, the historical one-size-fits-all treatments could no longer be the norm. As a result, cancer therapy today, evolves very much around a selection of very specific molecules that play a key role in carcinogenesis.

1.1.3 The tumour microenvironment

The ever-growing understanding of cancers has led researchers to shift their attention towards malignant cells and the stroma. The stroma consists of non-malignant cells such as vascular cells, inflammatory cells, and fibroblasts, and makes up most of the tumour microenvironment (TME). Although is it well established that the tumour microenvironment is critical for tumour survival and factors such as growth signals and nutritional support, it has only recently been a growing acceptance among researchers that the tumour and its microenvironment collaborate to form an intricate network critical for the progression into aggressive cancers [15,16]. It is reported that the stroma can make up more than 90 % of the total tumour mass in some cancers, including breast cancer, pancreatic cancer, and colorectal cancer [17].

As previously mentioned, the stroma and the components associated with it are critical for the overall tumour survival, but also other related processes, ranging from proliferation and angiogenesis, to migration and invasion. The tumour microenvironment is subjected to structural changes, but may also recruit stromal cells such as fibroblasts, produce a modified extracellular matrix (ECM), or even induce secretion of various growth factors. Adjacent growth factors and cytokines play a big role in mediating the abovementioned processes, which

in turn leads to poor prognosis for patients with some cancers. These growth factors are secreted by cancer cells and activated fibroblasts but can also be derived from the extracellular matrix (ECM) through protease activity [16].

Cancer-associated fibroblasts (CAFs), also known as myofibroblasts, are complex cells of heterogenous origin, that are present in the stroma and viewed as a subpopulation of fibroblasts [18,19]. They do not appear in normal healthy tissue but are present in big numbers during natural wound repair, in tumours and in diseases involving remodeling of the extracellular matrix, e.g., lung fibrosis, chronic inflammation and myocardial infarction [20]. When these stromal cells are activated, they stimulate angiogenesis, induce the epithelial-mesenchymal transition (EMT) and modify the extracellular matrix, which all in turn promote tumor growth and metastasis [21]. Another key feature of cancer-associated fibroblasts is its expression of fibroblast activation protein α, more commonly known as FAP [16].

1.1.4 Fibroblast activation protein alpha

Fibroblast activation protein α is a proline-selective, type II membrane-bound glycoprotein with both dipeptidyl peptidase and endopeptidase activity, that belongs to the dipeptidyl peptidase (DPP) family. For this enzymatic activity to be possible, a catalytic triad and homodimerization of the enzyme is required [15]. To date, known natural substrates of FAP include α_1-antitrypsin, type I collagen and various neuropeptides [22]. FAP consists of 760 amino acids in total, with 734 amino acids in the extracellular domain, 20 amino acids in the transmembrane domain and 6 amino acids in the cytoplasmic tail [23].

FAP is expressed mainly by cancer-associated fibroblasts and pericytes [24]. Just like cancer-associated fibroblasts, FAP also plays an important role in the biology of cancers. FAP promotes ECM-remodeling through serine protease activity on type I collagen, and tumor growth through promoting angiogenesis [24,25]. More specifically, the observed density of microvessels was found to correlate with the amount of FAP present in human breast carcinoma cells [26]. Neuropeptide Y (NPY), which serves as a natural substrate for FAP, is also cleaved into a substance that has proangiogenic characteristics through its endopeptidase activity [27]. Consequently, all the above-mentioned factors help drive metastasis. Another key similarity with CAFs is its limited presence in healthy adult tissue, and upregulation in various conditions

and diseases, including rheumatoid arthritis, wound healing, fibrosis, and cancers. For example, FAP is upregulated in most carcinomas, which are cancers originating from epithelial cells. FAP is also present in tumour cells from lung cancer, breast cancer and pancreatic cancer, where it plays an important part during tumour development and progression [23, 28]. The negative attributes of FAP in some cancers were also discussed by Liu *et al*. in their 2014 meta-analysis, which concluded that an overexpression of FAP resulted in poor overall survival [29].

It must however be noted that the role of FAP as a tumour promoter has been disputed. Although there is much evidence that FAP is involved in processes such as cancer cell proliferation, migration, invasion, and degradation of the ECM, it has also been reported that FAP has a role in inhibition of carcinogenesis [15,30]. Another study even revealed that FAP expression in the stroma could be associated with longer overall survival in patients with breast cancer [31]. Despite these findings, there is still substantial evidence that FAP has a vital role in various cancers, and this makes it a promising and selective target for cancer therapy.

1.1.5 FAP targeting

As of February 2021, only one FAP-inhibitor has been tested in clinical trials (Fig.2). This agent, Val-boroPro (Talabostat), was administered to a group of patients with metastatic colorectal cancer, and although it demonstrated minimal clinical activity, it managed to inhibit approximately 20 % of the enzymatic activity of FAP *in vivo*. It was also well-tolerated in patients [32]. This boronic-acid based inhibitor developed by Point Therapeutics represents only one of many small molecules developed to inhibit the peptidase activity of FAP.

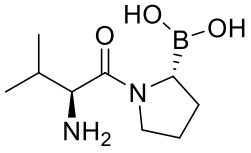

Figure 2. The molecular structure of Val-boroPro (Talabostat)

Another approach to target FAP is through the recent development of some monoclonal antibodies (mAbs), however this has yielded mixed results, and further studies are required to assess the role of these drugs [24]. One example here is the FAP-targeting monoclonal antibody sibrotuzumab, which was labelled with iodine-131 and administered to patients with FAP-positive cancers. The phase I study demonstrated a selective tumour uptake but did not address

the efficacy of the drug [33]. In a later trial, Hofheinz *et al*. were not able to detect any partial or complete tumour response [34]. A third approach is prodrug-based, and exploits the peptidase activity of FAP, by coupling a cytotoxic agent with a peptide containing a domain readily cleaved by FAP. When the prodrug interacts with the glycoprotein, it is cleaved, and the potent toxin can exert its activity on both surrounding cells and the FAP-expressing cell after crossing the cell membrane [15]. Immune-based therapies are also on the rise, but these are beyond the scope of this thesis.

One defining limitation with regards to the monoclonal antibodies, including ^{131}I-labelled sibrotuzumab, was their relatively slow clearance [20]. This limitation made it difficult to use these compounds for imaging, because the background signals made it challenging to both interpret and relate these signals to specific lesions or even tumours. The development of small, radiolabelled molecules helped pave the way for quinoline-based FAP-inhibitors (FAPIs) for use as theranostics – meaning for both diagnostic and therapeutic use. Coupling these molecules with chelators resulted in selective uptake and accumulation, and therefore also high-contrast images that could be used to produce excellent PET images for diagnostic use [15].

1.1.6 Structure-activity relationship of FAPIs

There is a serious need for compounds that can have a selective uptake in the tumour and exercise a satisfactory tracer retention at the site of action. This requires a fine-tuning of the molecular structures of the various FAPIs and is undoubtedly key to unlock the potential of these compounds for tumour diagnostics. The importance of tweaking the molecular structure was confirmed by Lindner *et al*., who demonstrated that replacing hydrogen atoms in the cyanopyrrolidine moiety with fluorine atoms resulted in an increased tumour uptake which was 100 % higher for FAPI-04 compared with FAPI-02 (Fig. 3) after 24 hours [35]. This underlines the sensitivity of these molecules for structural changes. The new compound showed promising results in two patients. They also emphasized that future drug discovery must focus on the synthesis of compounds that will incorporate radioisotopes other than ^{68}Ga and ^{90}Y for radiolabelling [35].

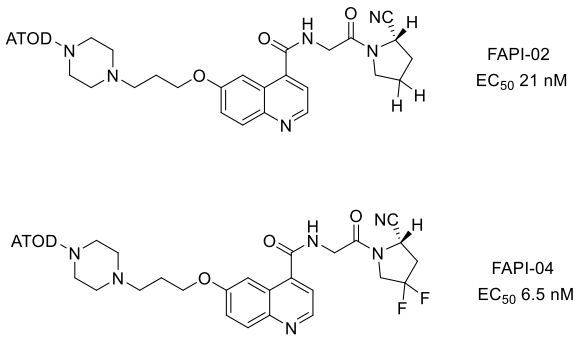

Figure 3. The molecular structures of FAPI-02 and FAPI-04

One distinct challenge when it comes to the development of FAPIs is the enzyme prolyl oligopeptidase (PREP). There is an overlap between FAP and PREP, which includes the characteristic endopeptidase activity that FAP possesses. This certainly makes the development of FAP-selective inhibitors more problematic, since both are known to be overexpressed by cells present in the tumour microenvironment of many cancers [36].

The development of UAMC110 (Fig. 4) by Decker *et al*. proved to be a major breakthrough, and it was argued that this could pave the way for other selective FAPIs for tumour imaging. This was followed by the development of several FAP-selective compounds by Haberkorn *et al*. in 2018, with all compounds building on the initial discoveries made by Decker and colleagues [37].

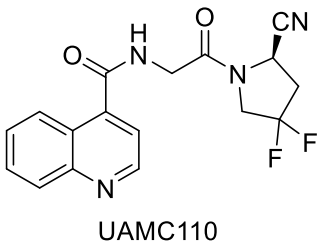

Figure 4. The molecular structure of UAMC110

Several studies have been conducted to assess the structure-activity relationship (SAR) of FAP inhibitors. Taking into consideration the recent advancements with regards to different FAPIs, it has been proposed that selected chemical structures play an especially important part in the biological activity of these compounds.

Jansen *et al*. studied how different chemical modifications on the 2-cyanopyrrolidine moiety and the aromatic quinoline ring system affected FAP potency. For the latter, substituents generally lowered the FAP potency, most likely due to steric hinderance and/or unfavorable

distribution of electron density. Substituents in the 5-position of the quinoline ring also resulted in lowered FAP potency. This phenomenon was observed when varying the position of the sp^2-hybridized nitrogen atom in the quinoline ring as well. At last, it was concluded that the molecule N-(4-quinolinoyl)-glycyl-(2-cyanopyrrolidine) was the most promising with regards to the development of selective FAPIs (Fig. 5). It was characterized by FAP affinity in the nanomolar-region, and favorable FAP/PREP selectivity [38].

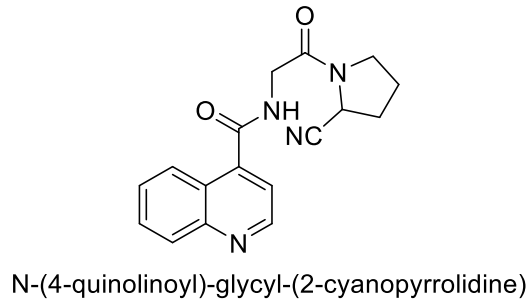

N-(4-quinolinoyl)-glycyl-(2-cyanopyrrolidine)

Figure 5. The molecular structure of N-(4-quinolinoyl)-glycyl-(2-cyanopyrrolidine)

In an article published by the same research group the following year, further investigations were made into the structure-activity relationship for this class of compounds. They studied the heterocyclic ring system, but also the glycine and cyanopyrrolidine moieties. The carbonitrile warhead-function was of particular interest, and it was explored how different electrophilic warhead types (e.g., chloromethyl ketone, boronic acid) affected the inhibitory potency. The following key findings were made by the group after developing 60 new inhibitors [36]:

- Replacing the glycine residue resulted in a significant reduction of FAP affinity. This was also observed when glycine was replaced by chemically similar amino acids, such as 1-amino-1-carboxycyclopropane and 2-aminopropanoic acid.
- Altering the amide bond adjacent to the quinoline ring resulted in a near complete loss of FAP potency. It is believed that this part of the molecule exhibits an interaction with FAP that is not present in PREP, because the same effect was not seen on PREP potency.
- Changing from a monofluorinated to a difluorinated pyrrolidine ring greatly increased the FAP potency. Both S and L-enantiomers of the monofluorinated product were studied but were not as ideal as the difluorinated molecule.

- With regards to the carbonitrile warhead, neither a boronic acid-based warhead or chloromethyl ketone showed combination of both satisfactory potency and FAP/PREP selectivity. The latter did not bind irreversibly to the target enzyme either.
- Replacing the quinoline ring with other azaheterocycles was deemed unsuccessful. Even the use of pyridine, which partly resembles the quinoline ring, resulted in a 6-fold reduction of ligand efficacy. The introduction of more than one nitrogen atom to the ring system did not have a positive effect either.
- Generally, the introduction of substituents affected the activity negatively. However, after coming to terms with the fact that the quinoline structure was optimal, numerous attempts were made to have substituents in the 5- and 7-position. This resulted in a handful compounds with preferred nanomolar FAP potency and FAP/PREP selectivity profiles. The activity was very sensitive to the type of substituent, as it was observed that bulky substituents did not result in optimal FAP potency. It was even revealed that 5-methoxy, considered to be a small substituent, resulted in a potency that was reduced by more than 1000 times. This only underlined the importance of how the quinoline ring interacts with the active center of the FAP enzyme.

The article concluded that the most promising molecule was compound 61 (Fig 6). In vitro pharmacokinetics and toxicity studies showed that it was not subject to fast oxidative metabolization, and that no signs of cytotoxicity were observed. Peroral and intravenous treatment of rats with the methoxy-quinoline did not result in any deaths. Oral administration resulted in a FAP-inhibition of at least 85 %, and the half-life was more than 6 hours [36].

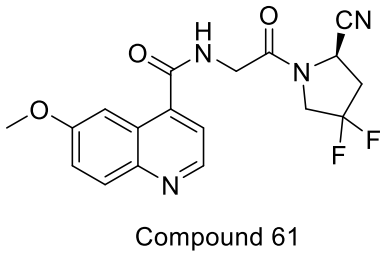

Compound 61

Figure 6. The molecular structure of compound 61

Compound 61 had favorable attributes compared with other FAP selective inhibitors, even when considering the extensive work with SAR studies carried out across many publications. Therefore, it was determined that this was the ideal molecule to use as a starting point for the development of a FAPI for radiolabelling with fluorine-18.

1.2 Positron emission tomography

1.2.1 An introduction to PET

Nuclear imaging can in simple terms be divided into two modalities, positron emission tomography and single photon emission computed tomography (SPECT). PET is a noninvasive imaging technique based on the use of positron-emitting radiopharmaceuticals, while SPECT is based on the direct detection of single gamma-rays emitted by radiopharmaceuticals [39]. Radiopharmaceuticals can be defined as chemical entities consisting of two parts – a defined molecular structure and a radioactive nuclide, with both often being connected by a linker. The molecular structure is typically responsible for the pharmacodynamics and pharmacokinetics of the radiopharmaceutical, and the radioactive nuclide plays the part with regards to the signaling and subsequent imaging of a tumour or tissue of interest [40].

The isotopes fluorine-18, gallium-68, carbon-11, oxygen-15, and nitrogen-13 are among the most widely used isotopes for PET (Table 1), whereas common isotopes for SPECT include technetium-99^{m}, indium-111, iodine-123 and gallium-67 [41]. The radiopharmaceuticals are usually injected in tracer amounts, meaning that they do not disrupt any physiological processes *in vivo* due to the low doses administered [42].

Table 1. The most used PET-isotopes and their respective half-lives [41]

Radionuclides	^{11}C	^{13}N	^{15}O	^{18}F	^{64}Cu	^{68}Ga	^{82}Rb	^{89}Zr
	20.39 minutes	9.97 minutes	2.04 minutes	109.77 minutes	13 hours	67.63 minutes	1.27 minutes	78.41 hours

As previously mentioned, PET is based on the use of positron-emitting radiotracers. The radionuclide emits positrons that collide with electrons *in vivo* after injection. This single collision triggers something called an annihilation event, in which energy is released in the form of two high-energy photons (511 keV) moving in the opposite direction of each other. The annihilation photon pair can be detected by a PET scanner, which in turn can produce high-quality images for use in eg. tumour diagnostics. Tomographic images are obtained by collecting the abovementioned data from various angles surrounding the patient. A gamma camera can also be used for this purpose but does not have the same sensitivity as a PET scanner [39,40].

A combination of PET and computerized tomography (CT), often abbreviated as PET/CT, is a preferred dual-modality scanner used for tumour diagnostics. PET compliments the ability of CT to give an overview of the anatomical structures being studied. For this to be possible, it is a prerequisite that the target molecule is overexpressed in the tumour compared with the surrounding and/or remaining tissue. Other requirements include at least some degree of selectivity, which is essential to achieve a low background signal, leading to high-contrast imaging. A high degree of selectivity is also important because this can facilitate the use of lower doses, which in turn can reduce adverse events because of radiation exposure to sensitive tissue and organs [22].

PET can be used to study many processes in humans, including metabolism, blood flow, transport of molecules, receptor density studies both inside and outside the CNS and more. Until recently, it has been used extensively to study the heart and brain, but oncology has been the driving force that has expanded PET and its routine clinical use [43]. This newfound success is mainly due to the discovery of [^{18}F]fluorodeoxyglucose, abbreviated [^{18}F]FDG, which has been the single most groundbreaking and flexible PET radiopharmaceutical to be developed [44]. It will be discussed more in detail later in this thesis.

1.2.2 General characteristics of PET tracers

There are many things to consider when developing a novel PET tracer. Sharma and Aboagye list and discuss some of these factors in their 2011 article *Development of radiotracers for oncology – the interface with pharmacology* published in the British Journal of Pharmacology (BJP). Firstly, there must be a high affinity for the target molecule, preferably in the subnanomolar or nanomolar region to the target of interest. This requirement is fulfilled for the latest FAP inhibitors that have been developed and screened. An ideal PET tracer should also result in limited radiation exposure, be selective, have either high clearance or low degree of plasma-protein binding, low toxicity, demonstrate *in vivo* stability, and not be readily metabolized. Obviously, the molecule in question must also be suitable for radiolabelling. For the further development of a radioligand into a ready-to-use radiopharmaceutical product, some requirements with regards to radiosynthesis must also be fulfilled. These requirements include sufficient yields and high radiochemical purity (usually $\geq$ 95 %) among other things [42].

1.2.3 Fluorine-18

Fluorine-18 is one of the most used radioisotopes in positron emission tomography. The first of the many merits of this isotope is the fitting half-life of 109.8 minutes, which makes it relatively practical to both produce and send from the site of production to a hospital [44,45]. It is also relatively easy to produce in larger quantities in medical cyclotrons and its chemistry is well-established through synthetic methods (either nucleophilic or electrophilic strategy), combined with low positron emission energy and high positron abundance [44,46]. Fluorine-18 was also shown to perform better than gallium-68, another popular PET radioisotope, because of its shorter positron range, half-life, and positron yield, with the two latter being higher than that for gallium-68 [47].

Most radioisotopes are produced in cyclotrons or other particle accelerators. When it comes to the vast majority of PET radioisotopes, including fluorine-18, their production is performed in a cyclotron, with the $^{18}O(p,n)^{18}F$ reaction being the dominating production method of fluorine-18. The exact way this happens for fluorine-18 is by initial loading of the target with ^{18}O-enriched water. The cyclotron then accelerates several high-energy, positive hydrogen ions (H^+) with the help of an electromagnetic field in a spiral before they bombard the target and produce the desired radionuclide – in this case fluorine-18. Initially, negative hydrogen ions are produced by an ion source, but later stripped of two electrons in the cyclotron to produce (H^+). The target, containing the irradiated water, is then transported through a tube-system to a hot-cell in the laboratory where the radiolabelling can happen [48]. It must be noted that fluorine-18 can be produced by other means than those described above, as Jacobson *et al*. describe in their article [49].

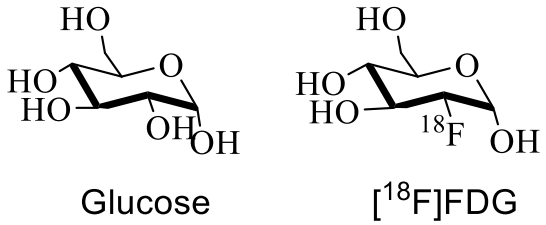

Figure 7. The molecular structures of glucose and [^{18}F]FDG, which is a glucose analogue.

Fluorodeoxyglucose, a glucose analogue radiolabelled with fluorine-18 (Fig. 7), remains by far one of the most utilized radiotracers in history [40]. It is used in a wide array of different disease states, including oncology, cardiology, neurology, infectious and inflammatory diseases [50-53]. Although it is very effective in the detection of malignant tumours where glucose

metabolism is upregulated, it has expected limitations due to its unspecific nature. FDG has for example been seen in non-cancerous tissue, in connection with infections and inflammations [40]. Even though FDG is considered the gold standard in the world of nuclear imaging of tumours, it still has its limitations, and this motivates researchers to develop new radiotracers that can offer even more value for clinicians and their patients.

1.3 Synthetic methods

1.3.1 HBTU/HATU coupling

HBTU and HATU are reagents classified as guanidinium salts and are among the most popular agents used in peptide coupling chemistry. HBTU was originally described in 1978 and was followed by the discovery of HATU in 1993 [54]. HBTU and HATU are characterized by their enhanced reactivity and ability to cause only low levels of racemization, thus making them excellent coupling agents for peptide synthesis [55,56]. They have also been hailed for their excellent reactivity with regards to avoiding side-reactions [56,57]. Under normal circumstances, HATU and HBTU mediate the conversion of a carboxylic acid to an active ester, that contains a HOAt or HOBt leaving group, depending on the type of reagent used. After this, a nucleophilic amine can react with the activate ester upon addition, and the resulting product will therefore be an amide [58]. It is important to note that both HATU and HBTU must not be used in excess, as this can hinder chain elongation. The general mechanism for a HATU coupling is shown below (Fig. 8).

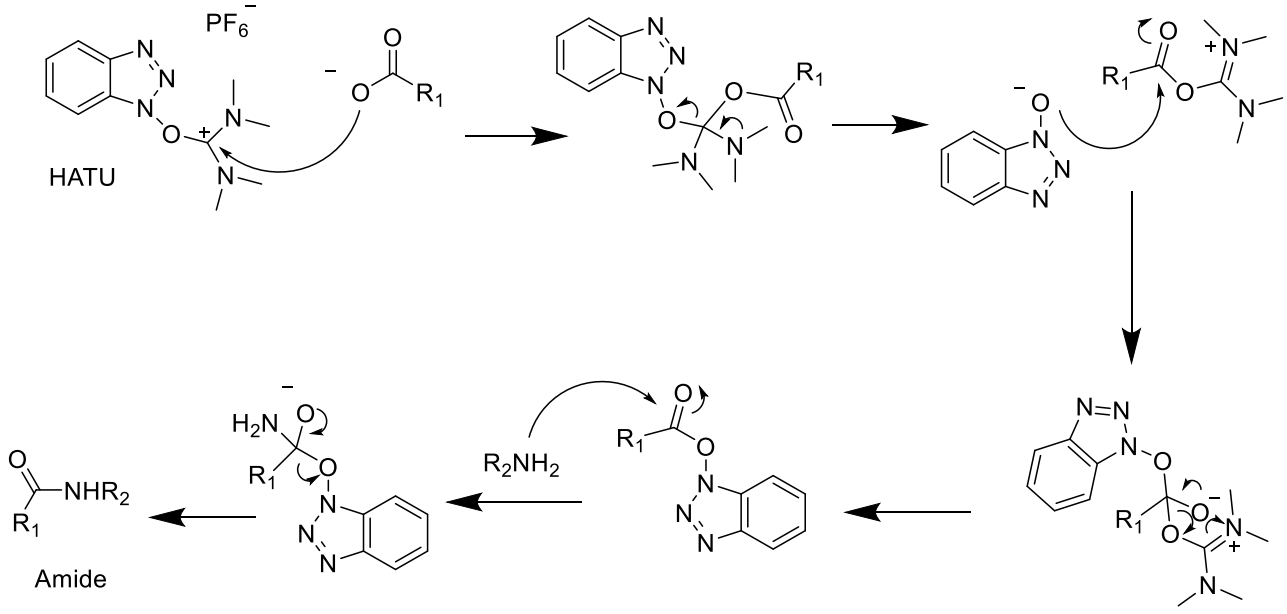

Figure 8. The general reaction mechanism for a HATU-mediated coupling when forming an amide. This mechanism applies for HBTU as well, but with small modifications [58].

2 Aim

2.1 Background

Fibroblast activation protein is shown to be upregulated in many common cancers, and this upregulation is not observed in normal adult tissue. Although some researchers question the role of FAP in specific cancers, there is still little to no doubt that high expression of FAP correlates with many of the processes vital for carcinogenesis. There are also new publications that hint at the use of FAPIs for other indications [59]. The observations described previously in this thesis combined with the potential for selective therapy and diagnosis have paved the way for the development of several FAP inhibitors.

Although some of these novel compounds have shown promising results in vitro and *in vivo*, there is still a lot of work remaining before a FAP inhibitor can be available for use in clinics. Researchers have carried out studies to explore the structure-activity relationship (SAR) for this class of compounds, and these recent advancements have served as a foundation for the latest developments in FAPI research. The new compounds are generally more potent and selective than before, and this has undoubtedly generated new interest within the pharmaceutical industry. Recently, the Swiss pharmaceutical company Novartis acquired the exclusive rights to develop and commercialize several FAPIs for cancer therapy [60].

The potential use of FAPIs for diagnostic applications has been the main motivation for this thesis. It can be argued that a pharmacophore is already determined, and that further research must focus on minor modifications of the chemical structure to optimize pharmacokinetics, as well as the use of other radioisotopes than the ones already studied. We had a particular focus on the radionuclide fluorine-18, which has several promising attributes and is relatively unexplored when it comes to radiolabelled FAPIs for diagnostic use with PET.

2.1.1 Overall aim of the thesis

The overall aim of this thesis was to synthesize a FAPI precursor and relevant analogues that could be radiolabeled with fluorine-18 for cancer diagnostics through PET.

2.1.2 Sub-aims of the thesis

- Develop a relevant precursor which is FAP-selective, based on the SAR studies that have been conducted through the recent years
- Explore the possibility to improve the synthesis towards a suitable precursor
- Synthesize a non-radioactive (“cold”) reference standard of the precursor
- Radiolabel the novel precursor with fluorine-18 and explore ways to improve this process

3 Results and discussion

3.1 An overview of the synthetic pathway

After extensive research, a precursor (**1)** for radiolabelling with fluorine-18 was synthesized (Fig. 9). The development of the precursor was based on available patent literature and published articles, but also trial and error with guidance from the supervisors named in this thesis.

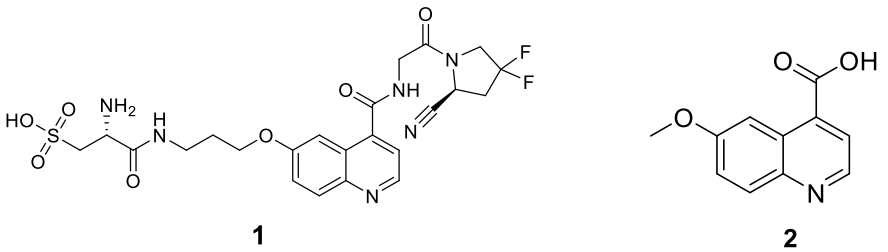

Figure 9. The precursor (**1)** to the left, and 6-methoxyquinoline-4-carboxylic acid (**2)** to the right

Four approaches were considered for the synthesis of the precursor (**1)**. Three out of the four methods included initial O-demethylation of the commercially available 6-methyoxyquinoline-4-carboxylic acid (**2**), based partly on the procedure specified in patent literature by Haberkorn *et al* [61]. The product 6-hydroxyquinoline-4-carboxylic acid (**3**) would then be going through one of the three procedures stated under:

1. Esterification of the carboxylic acid on (**3**), followed by alkylation of the phenol group with a Boc-protected propyl chain (**12**). The product of this reaction (**5**) would then undergo ester hydrolysis, followed by an amidation reaction with an amine building block (**13**) to produce compound (**7**). After deprotection of (**7**) to yield compound (**8**), a coupling reaction with Boc-L-cysteic acid (**17**) can be carried out. After yet another deprotection reaction, the final product would then be the desired precursor (**1**).
2. Amidation reaction between compound (**2**) and an amine building block (**13**), followed by alkylation with a Boc-protected propyl chain (**12**) on the phenol group of compound (**10**). The product (**7**) would then be deprotected, before a coupling reaction with Boc-L-cysteic acid (**17**) is done. After yet another deprotection, the desired precursor (**1**) is produced.

3. Initial dialkylation of compound (**3**) with a Boc-protected propyl chain (**12**), followed by ester hydrolysis of (**11**). The free carboxylic acid would then be able to partake in an amidation reaction with the amine building block (**13**). After this, the propyl chain can be deprotected and a new coupling with Boc-L-cysteic acid (**17**) can take place. After the last coupling reaction, deprotection would afford the precursor (**1**).

The fourth method involved a direct coupling of 6-methoxyquinoline-4-carboxylic acid (**2**) with the amine building block (**13**), before demethylation of the methyl ether on compound (**9**) could occur. This would be followed by alkylation on the hydroxy group, and a deprotection reaction to afford compound (**8**). Thereafter, coupling with Boc-L-cysteic acid (**17**) takes place before yet another deprotection affords the precursor (**1**), identical to the previous reaction schemes. A systematic overview of the four strategies is displayed below (Scheme 1).

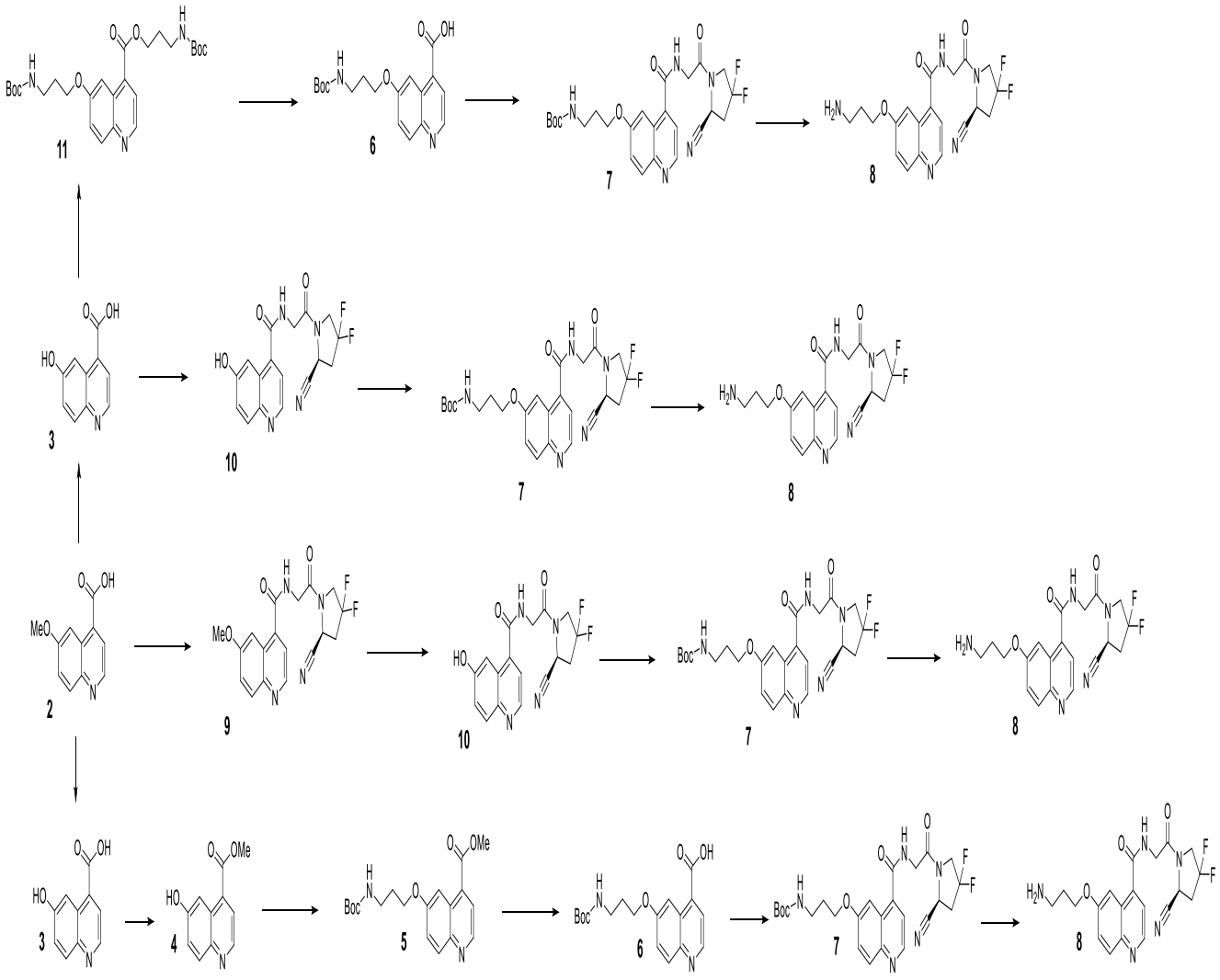

Scheme 1. A systematic overview of the four reaction pathways that were evaluated. The coupling reaction with Boc-L-cysteic acid and the following deprotection reaction is not included in the reaction scheme.

All four approaches were considered, but the third reaction pathway proved to be the least troublesome and was therefore preferred throughout this thesis. As stated, 6-methyoxyquinoline-4-carboxylic acid (**2**) was commercially available and only required a demethylation with hydrogen bromide at 130°C before further use (Scheme 2).

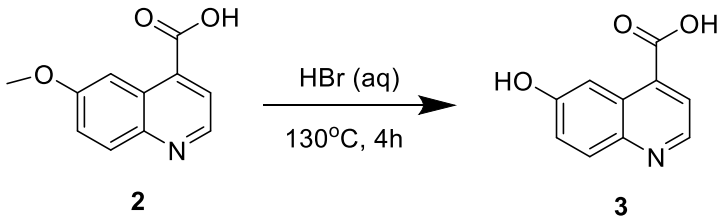

2 **3**

Scheme 2. Synthesis of compound **(3)**

Once demethylated, it was attempted to purify compound (**3**). Several different methods were evaluated, ranging from the use of a Sep-Pak cartridge to washing in a separatory funnel, or even purification on prep-HPLC. All methods were problematic because compound (**3**) had non-favourable solubility properties – it did not have any extra affinity towards either an organic or aqueous phase. This rendered purification with Sep-Pak or in a separatory funnel useless. In the end, prep-HPLC proved to be the most efficient way to purify compound (**3**). Nevertheless, the next reaction (Scheme 3) to yield the desired dialkylated product (**11**) was also deemed successful without any prior work-up, and purification of (**3**) was therefore disregarded in the end.

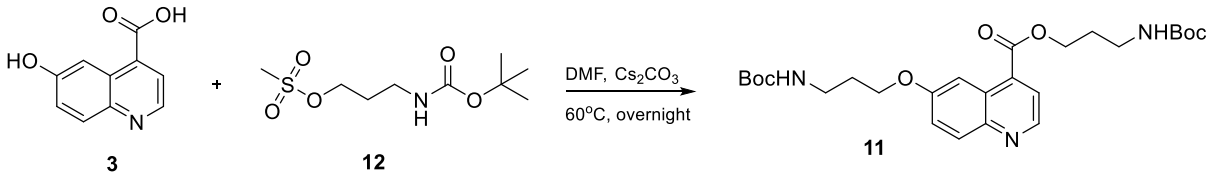

3 **12** **11**

Scheme 3. Synthesis of compound (**11**)

Compound (**11**) was obtained after reacting (**3**) with 3-((tert-butoxycarbonyl)amino)propyl methanesulfonate (**12**) in dimethylformamide (DMF) with caesium carbonate at 60°C. The reactant (**12**) used in this alkylation reaction was the product of a reaction between methanesulfonyl chloride (MsCl) and *tert*-butyl N-(3-hydroxypropyl) carbamate, dissolved in dry dichloromethane and triethylamine under argon atmosphere at 0°C [62]. Alkylation was

also attempted with 3-(bromopropyl)phtalimide and tert-butyl (3-bromopropyl)carbamate (Fig. 10), but these were harder to synthesize and were not considered to be as promising as compound (**12**) after having studied a handful number of reactions.

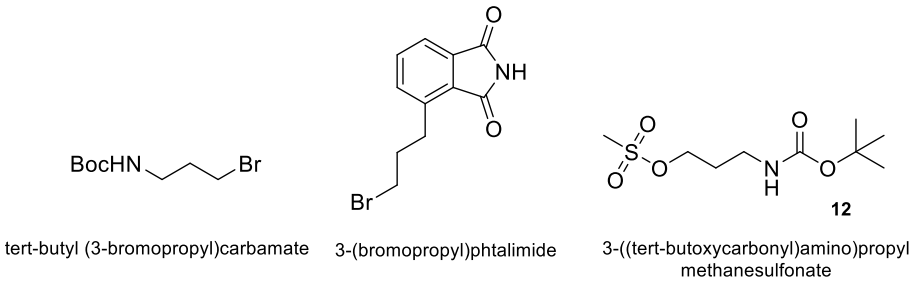

Figure 10. Three reactants that were studied in the alkylation reactions

Since a dialkylated product (**11**) was obtained, the ester was hydrolysed under basic conditions by the addition of sodium hydroxide (NaOH) and methanol (MeOH) (Scheme 4). This would afford compound (**6**), suitable for a direct coupling reaction with the amine building block (**13**). Prior to this, hydrolysis was attempted with 6.0 M NaOH in H_2O and MeCN multiple times, but without any success. The main theory was that the molecule broke down, possibly due to nucleophilic attack from MeCN under strong basic conditions.

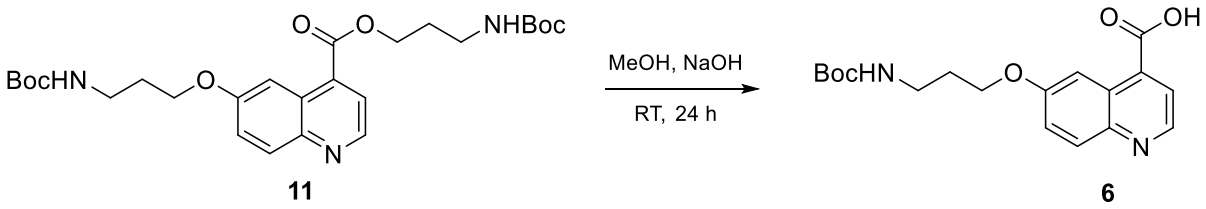

Scheme 4. Synthesis of compound (**6**)

The amine building block (**13**) that was to react with compound (**6**), had to be synthesized in 3 steps (Scheme 5) from the commercially available (S)-4,4-difluoropyrrolidine-2-carboxamide (**14**). These reactions had already been described by Jansen *et al.*, but were further simplified in this thesis [36]. The first reaction consisted of a HATU-mediated coupling of compound (**14**) with 2-(tert-butoxycarbonylamino) acetic acid, better known as Boc-Gly-OH, in dichloromethane (DCM) with Hünig's base (DIPEA). This yielded a Boc-protected product (**15**), which underwent dehydration from a primary amide to a nitrile (**16**) in the next step. This dehydration reaction required the Boc-protected reactant to be dissolved in dry tetrahydrofuran

(THF) at -15 ^{o}C, before the addition of pyridine and trifluoroacetic anhydride (TFAA). To synthesize the final amine, (S)-4,4-difluoro-1-glycylpyrrolidine-2-carbonitrile (**13**), only a deprotection of the Boc-group remained. This was done by dissolving the product from the last reaction in dry acetonitrile (MeCN) at 0^{o}C, adding p-Toluenesulfonic acid (PTSA) and then allowing it to react in room temperature.

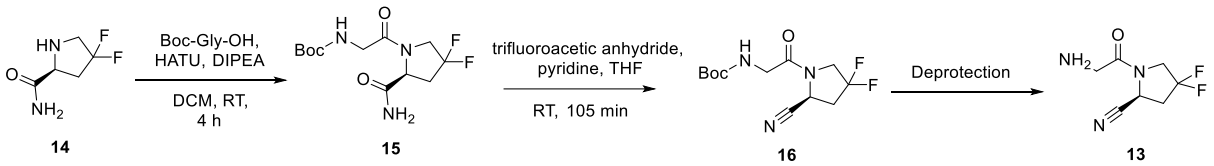

Scheme 5. Procedure for the synthesis of the amine building block (**13**)

The coupling reaction between compound (**13**) and the free carboxylic acid of compound (**6**) was done based on the general amidation protocol, provided by Lindner *et al*. in the supporting information of their 2018 research article from the Journal of Nuclear medicine [35]. In this instance, the coupling reaction was mediated by HATU with DIPEA in DMF (Scheme 6). For this step, several problems arose due to the sensitivity of the reactants involved, and no desired product was initially obtained. The conditions for this reaction were therefore evaluated in a successful test reaction involving compound (**2**) and 4-methylbenzylamine. The amine building block (**13**) was also tested in a successful test reaction with p-methoxybenzoic acid. This proved that the conditions, at least in theory, should be acceptable. Subsequently, both compounds (**6**) and (**13**) were purified on prep-HPLC, and this proved to be key in order to facilitate this reaction and obtain the desired compound (**7**).

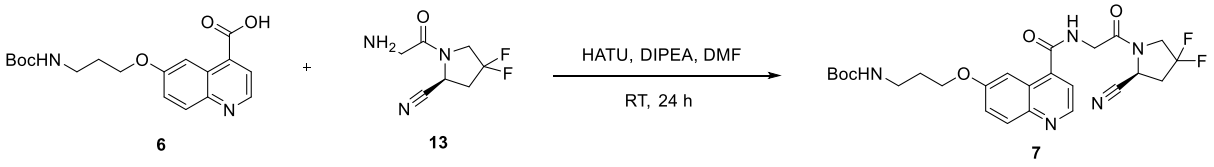

Scheme 6. Procedure for the synthesis of compound (**7**)

Previously, it was also attempted to couple the amine building block (**13**) with the quinoline (**2**) prior to demethylation (Scheme 1). This proved to be successful and was followed by the

demethylation of compound (**9**) under mild conditions with BBr_3. Subsequent attempts at alkylation with 3-(bromopropyl)phtalimide did not yield the desired compound.

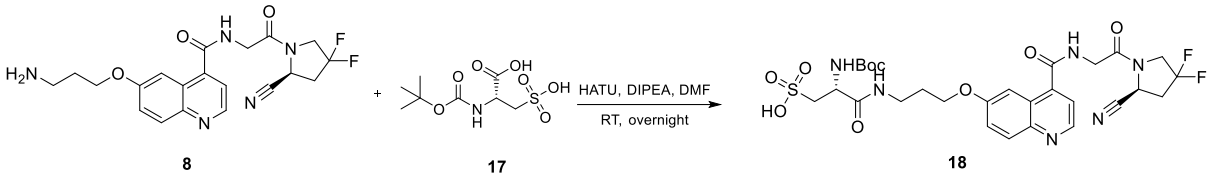

8 17 18

Scheme 7. Procedure for the synthesis of compound (**18**)

The amidation reaction to produce compound (**7**) was followed by a general Boc-deprotection in an acidic solution consisting of trifluoroacetic acid (TFA) and triisopropylsilane (TIPS) in water. The deprotected product (**8**) was then coupled with Boc-L-cysteic acid (**17**) in a HATU-mediated reaction to afford compound (**18**) (Scheme 7). Compound (**17**) was synthesized by reacting L-cysteic acid monohydrate with di-tert-butyl dicarbonate in anhydrous DMF with triethylamine, as reported by Bing *et al*. [63].

Boc-L-cysteic acid (**17**) was used as an important building block for the synthesis of the precursor molecule (**1**). The main contribution of compound (**17**) is the role it serves as a pharmacokinetic modifier, allowing for improved blood clearance and simultaneously reducing both hepatobiliary excretion and high protein binding. The latter two are often a result of high lipophilicity, which leads to poor tumour-to-background ratios that can affect imaging quality negatively. Compound (**17**) counters this by adjusting the cLogP value, which is often used as a measure of lipophilicity. Compound (**8**), without the cysteic acid moiety, has a cLogP value of 1.45, whereas the precursor molecule (**1**) is remarkably more hydrophilic with a cLogP value of -3.45. This is in many ways explained by the fact that cysteic acid is permanently charged at physiological pH (pH 7.4). The use of cysteic acid for this very purpose is well documented [64].

Compound (**18**) was then deprotected by following the same general procedure as already mentioned above. This resulted in the desired precursor (**1**), which was also reacted with 6-fluoropyridine-3-carboxylic acid in a HATU-mediated reaction with DIPEA in DMF, to afford the fluorinated reference standard (**19**) (Scheme 8).

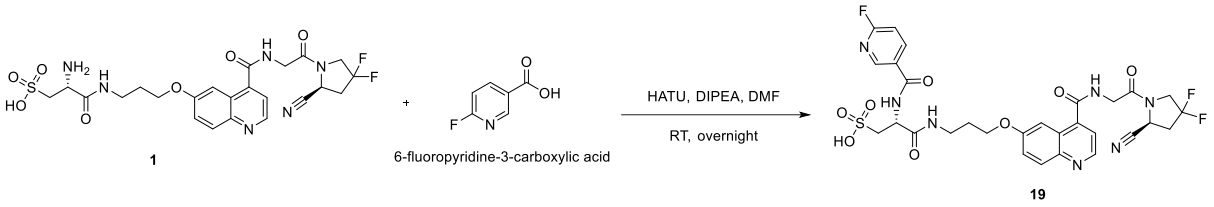

Scheme 8. Procedure for the synthesis of reference standard (**19**)

The FAPI-precursor (**1**) was radiolabeled in an amidation reaction with 6-[^{18}F]fluoronicotinic acid 2,3,5,6-tetrafluorophenyl ester ([^{18}F]F-Py-TFP), which acts as an active ester partly due to the electronegative attributes of the fluorine substituents in the tetrafluorophenyl moiety. The latter reactant was initially produced in a one-step radiosynthesis reaction, in which a trialkyl pyridin-2-ammonium nicotinic acid precursor underwent nucleophilic aromatic substitution (NAS), with the quaternary ammonium as a good leaving group (LG). The quaternary ammonium is a good LG in this instance because of the electron deficient nature of the positive nitrogen atom, as well as the ester group which draws electron density away from the already electron deficient pyridine ring. This synthesis followed the general reaction protocol initially reported by Olberg and Svadberg, but with the Chromabond PS-HCO_3 column heated to 65^{o}C, and the product being rinsed on a Waters tC18 Sep-Pak column to get rid of excess precursor before addition to a solution with the FAPI-precursor [65]. Different conditions were tested in order to produce the desired radiolabelled FAPI-molecule (**22**), and these are described more in detail in chapter 3.6 Radiosynthesis. A general overview of the process to obtain the desired radiolabelled compound (**22**) is presented below (Scheme 9).

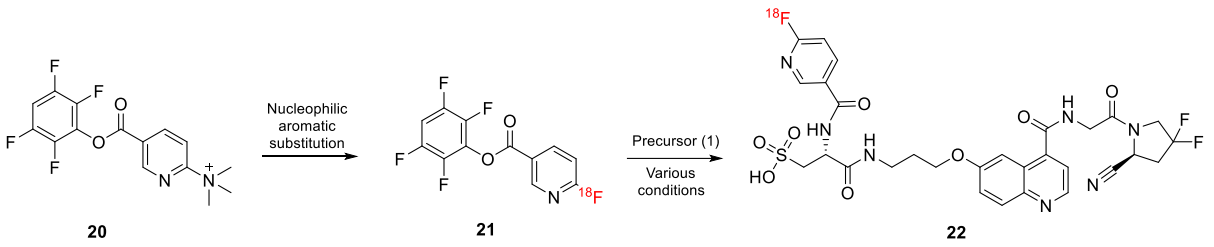

Scheme 9. A general overview of the radiolabelling process to produce compound (**22**)

3.2 Synthesis of the amine building block

3.2.1 Synthesis and characterization of tert-butyl (S)-(2-(2-carbamoyl-4,4-difluoropyrroloidin-1-yl)-2-oxoethyl)carbamate (15)

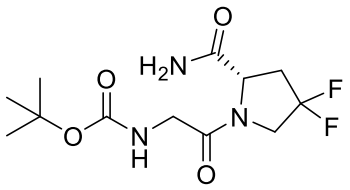

Figure 11. The molecular structure of compound (**15**)

The preparation of compound (**13**) was in part based on a reaction protocol reported by Jansen *et al*, but a few modifications were made to the original reaction scheme [36]. The first of the three steps to synthesize the desired amine building block (**13**), was carried out by obtaining the commercially available (S)-4,4-difluoropyrrolidine-2-carboxamide (**14**). Then, both Boc-Gly-OH and HATU were dissolved in DCM, before DIPEA was added. Both reactants formed an active ester intermediate after stirring for about 15 minutes, as illustrated in chapter 1.3.1. After this, a solution of compound (**14**) was prepared by dissolving the compound in DCM with DIPEA, which was then added dropwise to the reaction mixture and allowed to react for 4 hours in room temperature (RT). This is shown in Scheme 5. The addition of the nucleophilic amine allowed for the desired amide bond to be formed. After the reaction, the mixture was cooled, filtrated, recrystallized, and dried to give (**15**) as an off-white powder with a yield of 46.2 %.

Compound (**15**) was analysed with ^{1}H NMR spectroscopy and electrospray ionisation mass spectrometry (ESI-MS). The NMR spectrum (Figure A-3) correlates quite well with the peaks reported by Jansen, *et al* [36]. As one would expect, there is a characteristic, intense peak upfield at 1.38 ppm, which integrates for the protons (9H) from the Boc-group that was introduced in the reaction leading to compound (**15**). There are some impurities present, but the other signals also match up well with the literature data. The main peak in the MS spectrum has an *m/z* value of 330.123, which corresponds with the molecular mass of the sodium adduct (330.1241) of compound (**15**).

3.2.2 Synthesis and characterization of tert-butyl (S)-(2-(2-cyano-4,4-difluoropyrrolidin-1-yl)-2-oxoethyl)carbamate (16)

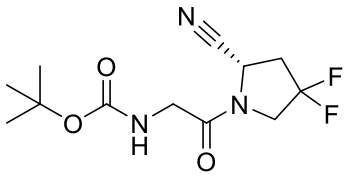

Figure 12. The molecular structure of compound (**16**)

The second step towards the desired amine (**13**) was a reaction that sought to convert the primary amide of compound (**15**) into a nitrile group through a dehydration reaction. This was once again based on the reaction reported by Jansen *et al* [36]. A cooling bath was prepared, before the (**15**) from the previous reaction was dissolved in dry tetrahydrofuran (THF) at -15^{o}C under argon atmosphere. This was followed by the consequent addition of 2.99 equivalents of pyridine, and then the dropwise addition of 2.19 equivalents of trifluoroacetic anhydride (TFAA). The cooling bath was removed, and the solution was stirred for 1.75 hours. After evaporating the solvents on a rotary evaporator, the mixture was dissolved in ethyl acetate (EtOAc) and washed with 1.0M HCl, $NaHCO_3$ and brine. This was followed by drying over magnesium sulfate ($MgSO_4$), filtration and evaporation of the solvents.

The use of TFAA and pyridine for dehydration reactions is indeed associated with many benefits. First, it is possible to use TFAA with milder conditions. and one can also avoid the formation of unwanted by-products. This eventually leads to better yields, at least in theory. The use of pyridine has dual benefits as well, not only by catalysing the reaction, but also through neutralization of the TFA formed during the course of the reaction [66].

Compound (**16**) was also analysed by ^{1}H NMR spectroscopy and electrospray ionisation mass spectrometry (ESI-MS). The ^{1}H NMR spectrum was almost identical to the reported shifts and peaks by Jansen, *et al* [36]. The MS spectrum (Fig. B-3) presented a main peak with the *m/z* value 312.113, which also translates well to the calculated sodium adduct (312.1135) of compound (**16**).

3.2.3 Synthesis and characterization of (S)-4,4-difluoro-1-glycylpyrrolidine-2-carbonitrile (13)

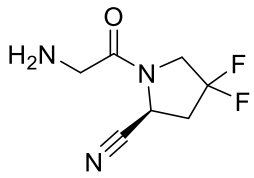

Figure 13. The molecular structure of compound (**13**)

The last step to obtain the desired amine building block (**13**) was a deprotection reaction to remove the Boc-protecting group. Compound (**16**) from the last reaction was dissolved in MeCN at 0^{o}C, before 1.49 equivalents of p-Toluenesulfonic acid monohydrate was added. The reaction mixture was slowly warmed to room temperature and allowed to stir for 20 hours. After evaporation of the solvent, the product was washed with ethyl acetate (EtOAc) and diethyl ether to yield a yellow oil. Compound (**13**) was later purified on prep-HPLC.

The molecular structure of the amine building block (**13**) was confirmed by ^{1}H NMR and ESI-MS analysis. In the ^{1}H NMR spectrum (Fig. A-5), most peaks appeared a bit more downstream compared to the peaks reported by Jansen, *et al*. [36]. However, they integrated for the same number of protons, and the recorded MS spectrum (Fig. A-5) displayed peaks with the *m/z* values of 190.079 and *m/z* 212.061. Both peaks correlate with the hydrogen adduct (190.0792) and sodium adduct (212.1555) of compound (**13**).

3.3 Synthesis of selected reactants

3.3.1 Synthesis and characterization of 3-((tert-butoxycarbonyl)amino)propyl methanesulfonate (12)

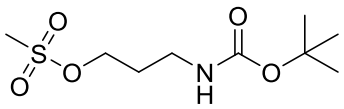

Figure 14. The molecular structure of compound (**12**)

The propyl chain (**12**) that would be used for alkylation was synthesized by following the reaction scheme provided in patent literature [62]. The compound was made by dissolving tert-butyl N-(3-hydroxypropyl) carbamate in dry DCM under argon atmosphere at 0^{o}C, followed by the addition of Et_3N (triethylamine) and MsCl. By converting the alcohol to a sulfonate through the action of MsCl, an excellent leaving group is prepared for further synthesis. After the complete addition of both, the reaction mixture was warmed to room temperature and stirred for two hours. The complete reaction was monitored and therefore confirmed with LC-MS. After this, the crude mixture was diluted with DCM and washed with water and brine, dried over $MgSO_4$ and filtrated, before the solvents were evaporated.

^{1}H NMR analysis, as well as ESI-MS, was performed on the product (**12**). The ^{1}H NMR spectrum (Fig. A-6) correlated well with the reported values by Gawandi and Fitzpatrick [67]. The main peak in the MS spectrum had the *m/z* value of 276.088, which corresponds to the sodium adduct (276.0881) of compound (**12**).

3.3.2 Synthesis and characterization of Boc-L-cysteic acid (17)

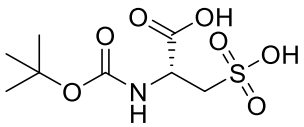

Figure 15. The molecular structure of compound (**17**)

Compound (**17**) was prepared by dissolving L-cysteic acid monohydrate in anhydrous DMF and adding triethylamine under argon atmosphere, followed by the dropwise addition of di-ter-butyl-dicarbonate dissolved in anhydrous DMF. This is in accordance with the reaction scheme reported by Bing *et al* [63]. The reaction mixture was stirred for 46 hours before the solvent was evaporated on the rotary evaporator to afford a light-yellow oil. Afterwards the residue was

dissolved in DCM, and a high volume of diethyl ether was added while stirring forcefully. A white precipitate was formed, and the remaining solvents were discarded. The residue was washed with diethyl ether before it was dried under vacuum overnight.

^{1}H NMR analysis confirmed the presence of a Boc-group in the molecule. Monitoring the reaction with LC-MS on negative ion mode had also confirmed a base peak that corresponded with the exact mass of the deprotonated molecule (268.056) minus one hydrogen atom.

3.4 Synthesis of the precursor

3.4.1 Synthesis and characterization of 6-hydroxyquinoline-4-carboxylic acid (3)

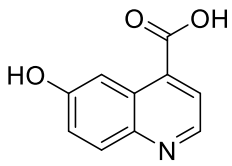

Figure 16. The molecular structure of compound (**3**)

The procedure for this reaction was based on patent literature [61]. The demethylated product (**3**) was synthesized by the addition of hydrogen bromide 48 % to 6-methyoxyquinoline-4-carboxylic acid (**2**). This reaction mixture was then refluxed for 4 hours at 130^{o}C, before the solvent was evaporated on a rotary evaporator. After this, the remaining product was dried overnight under vacuum. As previously explained, this compound (**3**) was synthesized numerous times, allowing it to react both overnight and for 4 hours under the same conditions. The main problem of this procedure was related to the solubility attributes of compound (**3**). This made it harder to purify the compound and thus get rid of both organic and inorganic impurities that had the opportunity to impact the following reactions.

The molecular structure was confirmed with ^{1}H NMR and ESI-MS. Looking at the NMR spectrum of compound (**2**) in Figure A-1, one can clearly see a peak integrating for the protons (3H) in the methyl group at 3.90 ppm. In Figure A-2, this peak is not present, meaning that the successful demethylation has occurred. This leaves 6 hydrogen atoms in the rest of the molecule, but only 5 hydrogen atoms are observed from the remaining signals due to the proton from the carboxylic acid not being visible. This was also the case for the starting material (**2**).

As mentioned, the MS spectrum was also recorded and showed a base peak for the *m/z* value of 212.032, which corresponds well with the sodium adduct (212.0323) of compound (**3**)

3.4.2 Synthesis and characterization of 3-((tert-butoxycarbonyl)amino)propyl 6-(3-((tert-butoxycarbonyl)amino)propoxy)quinoline-4-carboxylate (11)

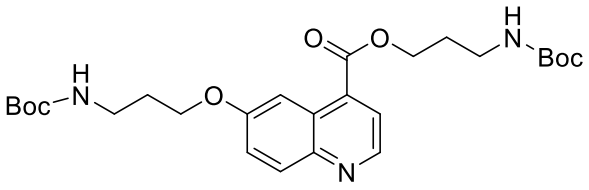

Figure 17. The molecular structure of compound (**11**)

Once demethylated, the product (**3**) from the previous reaction was dialkylated. This was done by dissolving the demethylated quinoline (**3**) in DMF, before adding cesium carbonate to deprotonate both the phenol and carboxylic acid. The mixture was then allowed to stir for 15 minutes, before the dropwise addition of compound (**12**) dissolved in DMF. The reaction mixture was then left to reflux at 60^{o}C overnight. The following day, the reaction mixture was allowed to reach room temperature, before DMF was evaporated on the rotary evaporator.

Recording of the ESI-MS spectrum revealed that the base peak had an *m/z* value of 526.252, which corresponds well with the calculated value for the sodium adduct (526.2529) of compound (**11**).

3.4.3 Synthesis and characterization of 6-(3-((tert-butoxycarbonyl)amino)propoxy) quinoline-4-carboxylic acid (6)

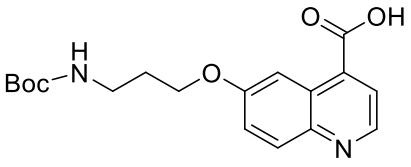

Figure 18. The molecular structure of compound (**6**)

Compound (**11**) was dissolved in methanol, before 1.0 M NaOH was added to facilitate the basic hydrolysis of the ester group. The reaction was monitored by LC-MS until all reactants were completely consumed, which took 24 hours. The crude mixture was then diluted with

water and neutralised with HCl before evaporation. The following day, compound (**6**) was purified on prep-HPLC. Evaporation of the solvent resulted in a snow-white powder.

The molecular structure of (**6**) was confirmed by LC-MS and ^{1}H NMR. The singlet at 1.36 ppm represents the protons found in the Boc group. The three peaks between 1.92-4.11 ppm integrates for a total of 6 protons, and these are most likely the ones expected from the propyl chain. Out of these, the peak at 1.92 is shielded the most and occurs upstream, because of its longer distance to the electronegative oxygen and nitrogen atoms. The coupling constants also confirm that these carbon atoms are connected. The triplet at 6.94 ppm most likely represents the proton connected with the amine. The 5 aromatic protons are found between 7.48-8.85 ppm, and the proton from carboxylic acid was not detected.

The recorded MS spectrum showed a base peak for the *m/z* value of 347.10, which corresponds with the calculated proton adduct (347,1607) of compound (**6**). The sodium adduct was also observed in the MS spectrum at *m/z* 369.12, and this also matches relatively well with the calculated value (369.1426).

3.4.4 Synthesis and characterization of tert-butyl (S)-(3-((4-((2-(2-cyano-4,4-difluoropyrrolidin-1-yl)-2-oxoethyl)carbamoyl)quinolin-6-yl)oxy)propyl)carbamate (7)

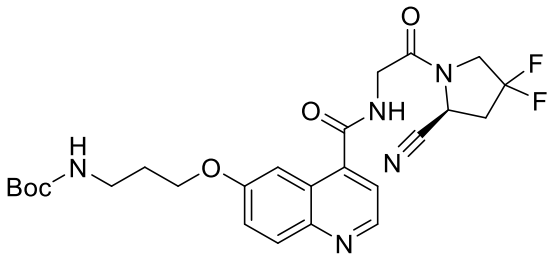

Figure 19. The molecular structure of compound (**7**)

The purified, monoalkylated quinoline (**6**) was then coupled with the amine building block (**13**) through a HATU-mediated reaction that lasted for 24 hours. The reaction was carried out by dissolving the monoalkylated quinoline (**6**) and HATU in DMF with DIPEA. This reaction mixture was stirred for 15 minutes, before the dropwise addition of the amine (**13**) dissolved in DMF. After the 24 hours that the reaction took, the solvents were evaporated, before compound (**7**) was purified on prep-HPLC.

The structure was confirmed once again with NMR and LC-MS. As one would expect, compound (**7**) takes longer to eluate compared with (**6**), mainly due to the loss of the free carboxylic acid which has hydrophilic properties. The base peaks observed in the recorded MS spectrum were also *m/z* 518.15 and *m/z* 540.23, which corresponds well with the calculated values for the hydrogen adduct (518.2215) and sodium adduct (540.2034) of (**7**).

Based on the molecular structure of (**7**), one would expect the signals in the ^{1}H NMR spectrum to integrate for a total of 29 protons, but in this case the total number is 28. A direct comparison between the ^{1}H NMR spectrums of (**6**) and (**7**) is not easy to carry out due to the different solvents used, but nonetheless it is obvious that the Boc-protecting group is still present. Based on the shifts and number of protons integrated for, it is also reasonable to assume that protons connected to the sp^3-hybridized carbons are present. Downfield, one would expect seven signals for the protons associated with the quinoline and the nitrogen atoms, respectively. However, one of the nitrogen-associated hydrogens atoms are not visible in the ^{1}H NMR spectrum.

3.4.5 Synthesis and characterization of (S)-6-(3-aminopropoxy)-N-(2-(2-cyano-4,4-difluoropyrrolidin-1-yl)-2-oxoethyl)quinoline-4-carboxamide (8)

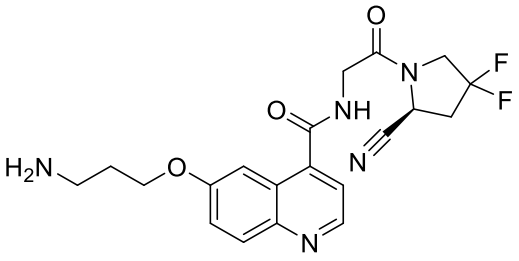

Figure 20. The molecular structure of compound (**8**)

The Boc-group that remained after the initial alkylation was then removed in a general Boc-deprotection reaction, with a solution consisting of trifluoroacetic acid (TFA) and triisopropylsilane (TIPS) in water. The reaction took approximately 30 minutes, and the desired product was confirmed on LC-MS. Evaporation and drying overnight yielded compound (**8**) as a brown, viscous solution.

The reaction was monitored with LC-MS. The limited retention proved that the product (**8**) was in fact more polar than compound (**7**), and the base peak of *m/z* 418.35 correlated relatively well with the calculated value for the hydrogen adduct (418.1690) of compound (**8**).

3.4.6 Synthesis and characterization of (R)-2-((tert-butoxycarbonyl)amino)-3-((3-((4-((2-((S)-2-cyano-4,4-difluoropyrrolidin-1-yl)-2-oxoethyl)carbamoyl)quinolin-6-yl)oxy)propyl)amino)-3-oxopropane-1-sulfonic acid (18)

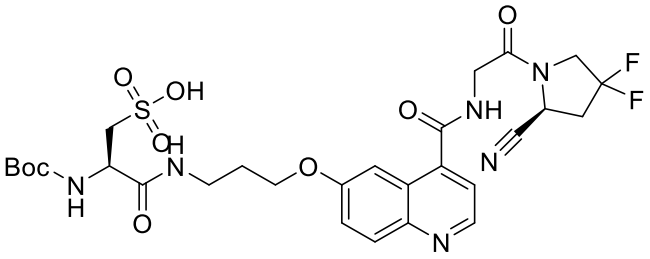

Figure 21. The molecular structure of compound (**18**)

Compound (**8**) would then react with the Boc-protected cysteic acid in a HATU-mediated reaction overnight. This happened by dissolving the cysteic acid and HATU in DMF with DIPEA. This reaction mixture was stirred for 15 minutes, before the dropwise addition of the amine dissolved in DMF. After the 24 hours that the reaction took, the solvents were evaporated, and the structure was confirmed once again with NMR and LC-MS.

The NMR data are not easy to interpret due to the size of the molecule and simultaneous presence of organic impurities. This is reflected in the ^{1}H and ^{13}C spectrums. However, the mass was confirmed by LC-MS, which showed the Boc protected molecule at *m/z* 669.14 and the deprotected variant at *m/z* 569.29. The first value corresponds with the calculated value for the proton adduct (669.2154) of compound (**18**).

3.4.7 Synthesis and characterization of (R)-2-amino-3-((3-((4-((2-((S)-2-cyano-4,4-difluoropyrrolidin-1-yl)-2-oxoethyl)carbamoyl)quinolin-6-yl)oxy)propyl)amino)-3-oxopropane-1-sulfonic acid (1)

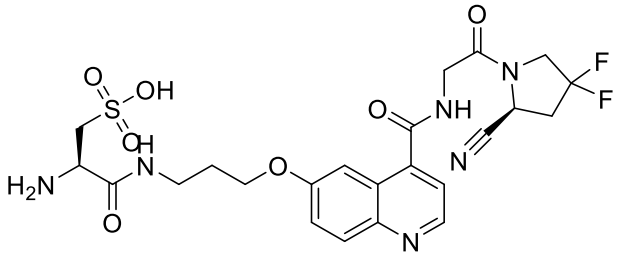

Figure 22. The molecular structure of compound (**1**)

The next reaction sought to remove the Boc-protecting group that remained after the reaction with Boc-L-cysteic acid (**17**). This was done by following a general Boc-deprotection reaction, in which the compound (**18**) was dissolved in a solution consisting of trifluoroacetic acid (TFA) and triisopropylsilane (TIPS) in water. The reaction took approximately 30 minutes, and the desired precursor compound (**1**) was confirmed with HRMS. The measured *m/z* value was 591.1444, and this was with regards to the molecular formula $C_{23}H_{26}F_2N_6NaO_7S$, which is the sodium adduct of compound (**1**). After the reaction, the precursor molecule (**1**) was purified on prep-HPLC.

3.5 Synthesis of the "cold" reference standard

3.5.1 Synthesis and characterization of (R)-3-((3-((4-((2-((S)-2-cyano-4,4-difluoropyrrolidin-1-yl)-2-oxoethyl)carbamoyl)quinolin-6-yl)oxy)propyl)amino)-2-(6-fluoronicotinamido)-3-oxopropane-1-sulfonic acid (19)

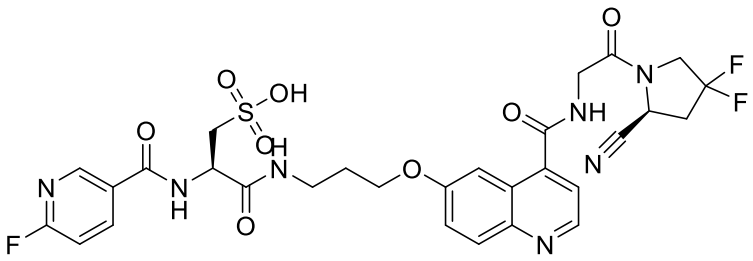

Figure 23. The molecular structure of compound (**19**)

The non-radioactive, "cold" reference standard was synthesized by dissolving 6-fluoropyrridine-3-carboxylic acid and HATU in DMF with DIPEA. The mixture was stirred for

15 minutes, before the dropwise addition of precursor in DMF to the reaction mixture. As not all the reactants were consumed, the reaction was stirred overnight. The following day, more of 6-fluoropyrridine-3-carboxylic acid and HATU in DMF with DIPEA was added. After 45 minutes, most of the precursor was consumed and the reference standard was synthesized. After rotary evaporation, prep-HPLC was performed, which yielded compound (**19**) (Fig. 23) as a light yellow/slightly green solid.

Based on the number of protons in the aromatic ring systems (8H) and hydrogen atoms connected to nitrogen (3H), one would expect a total of 11 signals in the aromatic region when studying the ^{1}H NMR spectrum for compound (**19**). This is confirmed in Figure A-13 and confirms the presence of the fluoronicotinamido moiety. It is difficult to assign the remaining signals upfield due to the large size of the molecule and the presence of organic impurities. However, the HRMS spectrum shows the measured m/z value 736.1385, which corresponds well with the calculated value of a double sodium-adduct minus a hydrogen atom (736.1387).

3.6 Radiosynthesis

3.6.1 Synthesis of 6-[^{18}F]fluoronicotinic acid 2,3,5,6-tetrafluorophenyl ester ([^{18}F]F-Py-TFP) (21)

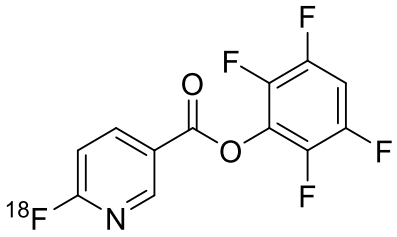

Figure 24. The molecular structure of compound (**21**)

Fluorine-18 in water was fixated on an anion exchange column (Chromabond PS-HCO_3) before the column was washed with anhydrous MeCN and dried for one minute under vacuum. The trialkyl pyridin-2-ammonium nicotinic acid precursor (12 mg) was then dissolved in MeCN/t-BuOH (0,5 mL) and pushed through the same anion exchange column, to produce ([^{18}F]F-Py-TFP). The solution was diluted with water and passed through a C18 cartridge which was washed with water. The desired product ([^{18}F]F-Py-TFP) (Fig. 24) was then eluted with MeCN.

3.6.2 Synthesis of (R)-3-((3-((4-((2-((S)-2-cyano-4,4-difluoropyrrolidin-1-yl)-2-oxoethyl)carbamoyl)quinolin-6-yl)oxy)propyl)amino)-2-(6-(^{18}F)nicotinamido)-3-oxopropane-1-sulfonic acid (22)

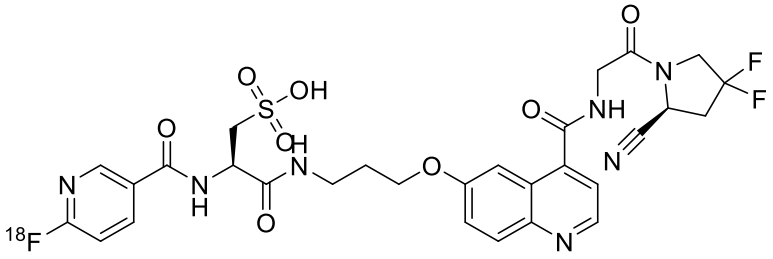

Figure 25. The molecular structure of compound (**22**)

Approximately 1 mg of the FAPI precursor was added to several vials, and dissolved in various solvents using a variety of bases before the addition of ([18F]F-Py-TFP), to produce the desired radiolabelled compound (**22**) (Fig. 25).

The first attempt to produce (**22**) included dissolving compound (**1**) in two vials containing 0.5 mL THF and 2-butanone, respectively. It was discovered that this was challenging due to solubility issues of the precursor compound (**1**). The addition of 1 µL DIPEA to THF, and the subsequent analysis with radio-HPLC led to the belief that ([^{18}F]F-Py-TFP) was being hydrolyzed before the amidation reaction between compounds (**21**) and (**1**) could take place. Because of this, it was decided to remove any excess water by drying the solvents over $MgSO_4$ prior to use. Another problem was that a substantial amount of ([^{18}F]F-Py-TFP) was not getting consumed in the reaction. After the extra addition of 2 µL DIPEA and heating with a blow-dryer for a while, this problem was limited, as shown in Figure E-12. Unfortunately, minimal amounts of the desired compound (**22**) were observed even though most of the starting material was consumed in the end.

Because the results from the previous experiment were worse than expected, it was decided to use another combination of solvent and bases. The precursor compound was dissolved in absolute ethanol, before the addition of triethylamine and hydrogen carbonate. The reaction mixture was heated after the addition of ([^{18}F]F-Py-TFP). The radiochromatogram (Fig. E-7) revealed that some product was obtained and that most reactants had been consumed, but hydrolysis was still significant.

Since the use of 2-butanone as a solvent for the precursor molecule was deemed non-favorable, a combination consisting of DMSO, 2-butanone, DIPEA with heating was tested instead. The radiochromatogram from Figure E-5 shows that this combination proved to be better in terms of producing the desired compound (**22**), but the yield was still considered to be low.

As observed on all radiochromatograms, the desired product was not produced in satisfying amounts under the various conditions. Generelly, the reaction resulted in three different main products. The largest signal and impurity typically appear between 2 and 3 minutes, and this is the hydrolyzed ^{18}F-Py-TFP being converted to the free acid, before amidation with the precursor could occur. It cannot be ruled out that the FAPI molecule may possess some degree of esterase activity, and that it is responsible for cleavage of the ester linkage, as experience have shown that amide formation with ^{18}F-Py-TFP is in general quite robust. The second main signal came right before the 4-minute mark, and this is the desired fluorine-18 labelled product (**22**). The third signal, occurring after approximately 7 minutes, is the unconsumed labelling reactant (**21**). The hydrophobic nature of compound (**21**) is also a natural explanation for the longer retention time.

A few other conditions were tested as well, including but not limited to DMSO and DIPEA, as well as different phosphate buffer systems. The reaction was attempted at pH 7.75 in both room temperature and with heating, and at pH 8.60. Two recurring problems with the buffer solutions was that the labelling reactant (**21**) was not getting consumed, and the presence of other unknown impurities. Despite this, the yield was still considered to be a lot higher than some of the other reactions. Another solution containing ethanol absolute, lutidine and DIPEA was also tested, but this resulted mainly in the hydrolyzed product. The conditions described are summed up below (Table 2).

Table 2. Selected conditions that were tested to produce compound (**22**)

Solvent	**Base**	**Time (min)** **Temperature (ºC)**	**Results**
THF	DIPEA	Unspecified time Heated with blow-dryer	Not satisfactory
Ethanol absolute	Triethylamine Hydrogen carbonate	Unspecified time Heated with blow-dryer	Not satisfactory
2-butanone and DMSO	DIPEA	Unspecified time	Improved results

		Heated with blow-dryer	
DMSO	DIPEA	Unspecified time Heated with blow-dryer	Not satisfactory
Phosphate buffer (pH 7.75)	N/A	Unspecified time Room temperature	Not satisfactory
Phosphate buffer (pH 7.75)	N/A	Unspecified time Heated with blow-dryer	Improved results
Phosphate buffer (pH 8.60)	N/A	Unspecified time Heated with blow-dryer	Not satisfactory
Ethanol absolute	DIPEA 2,6-lutidine	Unspecified time Room temperature	Not satisfactory

4 Conclusion and further studies

The initial focus of this thesis was to synthesize a FAPI precursor and relevant analogues that could be radiolabelled with fluorine-18 for cancer diagnostics with PET. After many attempts, a suitable FAPI precursor was developed, and radiolabelling with fluorine-18 also proved to be possible.

Several synthetic strategies were evaluated, with varying results. The main issue for this class of compounds was the attributes related to solubility, which often led to difficulties when isolating and purifying the various compounds. This resulted in many non-selective reactions where the desired product was either produced in small amounts or not even observed at all, exemplified by the amidation reaction involving the amine building block and quinoline.

Radiolabelling with fluorine-18 was also proved to be possible but did only produce small amounts of the desired product, most likely due to hydrolysis of the ester group before amidation was possible. It was proposed that the FAPI molecule might have esterase activity, something that may explain the observed phenomenon. This warrants further investigation, especially to study if varying the substituents or the length of the linker moiety affects the radiolabelling with fluorine-18.

Due to time constraints, pharmacological testing of the novel FAP precursor was not possible. In the future, it could be interesting to see if there is any real-world promise with this specific precursor. Pharmacological testing should be considered, and several new analogues may also be synthesized for this very purpose.

5 Experimental procedures

5.1 Methods for organic chemistry

The reactions were carried out as described in the experimental section. Most reactions were monitored with liquid chromatography-mass spectrometry (LC-MS), using Thermo Finnigan Surveyor LCQ DECA XP Plus with a Phenomenex Kinetex C18 column (2.6 µm, 50 x 2.1 mm) with UV detection. The mobile phase consisted of 0.1 % trifluoroacetic acid (TFA) in water, and acetonitrile. Some reactions were also monitored using thin layer chromatography, with plates based on silica gel coated with the fluorescent indicator F254.

A few compounds were also purified by HPLC, using a Walters Delta Prep 4000 with a Phenomenex Luna C18 column (5 µm, 250 x 21.20 mm) and UV detection on dual-wavelength mode (214, 254 nm). The mobile phase varied depending on the molecular properties of the relevant compound. The different conditions used with regards to the mobile phase are listed under (Table 3):

Table 3. The different mobile phases used for the purification of certain compounds

Compound	Gradient/isocratic	Mobile phase	Time
(S)-4,4-difluoro-1-glycylpyrrolidine-2-carbonitrile (**13**)	Gradient	A: 0,1 % TFA in H_2O B: MeCN (2-40 %)	60 minutes
6-(3-((tert-butoxycarbonyl) amino)propoxy)quinoline-4-carboxylic acid (**6**)	Gradient	A: 0,1 % TFA in H_2O B: MeCN (10-80 %)	60 minutes
tert-butyl (S)-(3-((4-((2-(2-cyano-4,4-difluoropyrrolidin-1-yl)-2-oxoethyl)carbamoyl) quinolin-6-yl)oxy)propyl) carbamate (**7**)	Gradient	A: 0,1 % TFA in H_2O B: MeCN (10-80 %)	60 minutes
(R)-2-amino-3-((3-((4-((2-((S)-2-cyano-4,4-difluoropyrrolidin-1-yl)-2-	Gradient	A: 0,1 % TFA in H_2O B: MeCN (5-60 %)	60 minutes

oxoethyl)carbamoyl)quinolin-6-yl)oxy)propyl)amino)-3-oxopropane-1-sulfonic acid (**1**)			
(R)-3-((3-((4-((2-((S)-2-cyano-4,4-difluoropyrrolidin-1-yl)-2-oxoethyl)carbamoyl) quinolin-6-yl)oxy)propyl) amino)-2-(6-fluoronicotin amido)-3-oxopropane-1-sulfonic acid (**19**)	Gradient	A: 0,1 % TFA in H_2O B: MeCN (5-60 %)	60 minutes

Analysis of the radiolabelled compounds was done using the Agilent 1200 series HPLC system. This was used together with an ACE C18 chromatography column (3 µm, 50 x 4.6 mm) and Raytest Gabi radioactivity detector.

NMR spectroscopy with Bruker AVIII HD 400 400 MHz was used regularly to study the molecular structures of the synthesized compounds. In some cases, the compounds were also delivered to the MS laboratory at the University of Oslo for high-resolution mass spectrometry (HRMS).

5.1.1 Procedure for the synthesis of tert-butyl (S)-(2-(2-carbamoyl-4,4-difluoropyrrolidin-1-yl)-2-oxoethyl)carbamate (15)

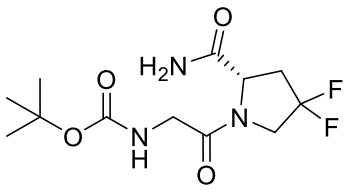

2-(tert-butoxycarbonylamino)acetic acid (2.252 g, 12.85 mmol) was dissolved in DCM (12.0 mL) in a round-bottom flask, before DIPEA (2.245 mL) was added. After 15 minutes, a solution containing compound (**14**) in DCM (16.0 mL) and DIPEA (3.74 mL) was added dropwise to the round-bottom flask. The reaction mixture was stirred for 4 hours, before it was cooled, filtrated, recrystallized, and dried over $MgSO_4$ to provide compound (**15**) as an off-white powder (1.544 g, 46.2 % yield). ^{1}H NMR (400 MHz, DMSO) δ 7.70 – 7.10 (m, 3H), 6.87 (dt, *J* = 10.7, 5.8 Hz, 1H), 4.45 (dd, *J* = 9.7, 4.2 Hz, 1H), 4.06 (p, *J* = 14.3, 13.5 Hz, 1H), 3.98 – 3.86 (m, 1H), 3.80 (ddd, *J* = 16.9, 6.0, 3.0 Hz, 1H), 3.74 – 3.64 (m, 1H), 2.94 – 2.63 (m, 1H), 2.35 (qd, *J* = 14.6, 4.3 Hz, 1H), 1.38 (d, *J* = 2.3 Hz, 9H). MS (ESI) *m/z* 330.123 $[M+Na]^+$

5.1.2 Procedure for the synthesis of tert-butyl (S)-(2-2-cyano-4,4-difluoropyrrolidin-1-yl)-2-oxoethyl)carbamate (16)

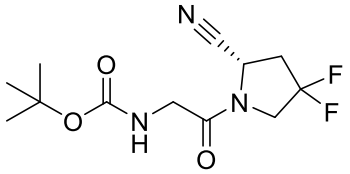

Compound (**15**) was dissolved in dry THF (55 mL) at -15 ^{o}C under argon atmosphere. Pyridine (1.25 mL, 15.52 mmol) and TFAA (1.6 mL, 11.51 mmol) was added dropwise to the solution. The reaction mixture was slowly warmed to room temperature and stirred for 105 minutes, before the solvent was evaporated. The contents were then dissolved in EtOAc (30 mL) and transferred to a separatory funnel, where it was washed with HCl (10 mL, 1.0 M), saturated $NaHCO_3$ (3 x 10 mL) and brine (3 x mL), before being dried over $MgSO_4$ and filtrated. The solvent was evaporated to yield compound (**16**) as an off-white oil (1.670 g, 114.9 %). ^{1}H NMR (400 MHz, $CDCl_3$) δ 5.34 (s, 1H), 4.97 (t, *J* = 6.6 Hz, 1H), 4.04 – 3.76 (m, 4H), 2.75 (ddd, *J* = 14.8, 9.0, 6.1 Hz, 2H), 1.50 (d, *J* = 38.3 Hz, 9H). MS (ESI) *m/z* 312.113 $[M+Na]^+$

5.1.3 Procedure for the synthesis of (S)-4,4-difluoro-1-glycylpyrrolidine-2-carbonitrile (13)

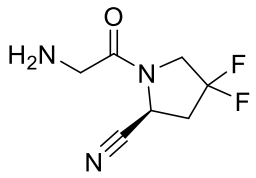

p-Toluenesulfonic acid monohydrate (1.636 g, 8.60 mmol) was added to a solution of compound (**16**) (1.661 g, 5.742 mmol) in dry MeCN (20 mL) at 0°C. The reaction mixture was allowed to reach room temperature, before it was stirred for 20 hours. The solvent was then evaporated, and the residue was washed with EtOAc and diethyl ether. Evaporation of the solvents and purification on prep-HPLC resulted in compound (**13**) as a yellow oil (0.673 g, 62.0 %). ^{1}H NMR (400 MHz, D_2O) δ 7.72 – 7.68 (m, 2H), 7.40 – 7.36 (m, 2H), 5.19 – 5.15 (m, 1H), 4.18 – 3.96 (m, 4H), 3.03 – 2.89 (m, 2H), 2.40 (s, 3H). MS (ESI) *m/z* 190.0792 $[M+H]^+$

5.1.4 Procedure for the synthesis of 3-((tert-butoxycarbonyl)amino)propyl methanesulfonate (12)

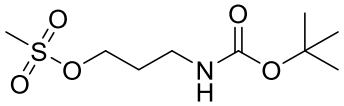

tert-butyl N-(3-hydroxypropyl)carbamate (1.984 g, 11.32 mmol) was dissolved in dry DCM (10 mL) at 0 °C under argon atmosphere, before triethylamine (3.2 mL, 22.96 mmol) and MsCl (1.35 mL, 17.44 mmol) were added. The reaction mixture was stirred for 2 hours after reaching room temperature. The crude mixture was diluted with DCM (15 mL) and washed with H_2O (3 x 10 mL) and brine (3 x 10 mL) in a separatory funnel. The solution was dried over $MgSO_4$ and filtrated before the solvents were evaporated to afford compound (**12**) as an orange solid (3.069 g, 107.0 %). ^{1}H NMR (400 MHz, $CDCl_3$) δ 4.29 (t, *J* = 6.0 Hz, 2H), 3.24 (d, *J* = 6.8 Hz, 2H), 3.02 (s, 3H), 1.93 (p, *J* = 6.2 Hz, 2H), 1.43 (s, 9H). MS (ESI) *m/z* 276.088 $[M+Na]^+$

5.1.5 Procedure for the synthesis of Boc-L-cysteic acid (17)

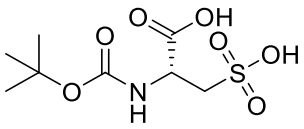

L-cysteic acid monohydrate (2.014 g, 10.76 mmol) was added to a round-bottom flask and dissolved in anhydrous DMF (35 mL) and triethylamine (3 mL, 21.53 mmol) under argon atmosphere. Di-tert-butyl dicarbonate (2.823 g, 12.93 mmol) was measured in a pear-shaped flask and dissolved in anhydrous DMF (17.5 mL). The solution containing di-tert-butyl dicarbonate was added dropwise to the round-bottom flask, and the reaction mixture was stirred for 46 hours before the solvent was evaporated. The residue was dissolved in DCM (10 mL) before diethyl ether (60 mL) was added under vigorous stirring. The organic solvents were discarded, leaving a white precipitation in the flask. The residue was washed with diethyl ether (10 mL) again before being discarded. Drying overnight resulted in compound (**17**) as solid, white crystals (4.114 g, 142.1 %). ^{1}H NMR (400 MHz, D_2O) δ 4.52 (dd, *J* = 7.8, 4.3 Hz, 1H), 1.44 (s, 9H).

5.1.6 Procedure for the synthesis of 6-hydroxyquinoline-4-carboxylic acid (3)

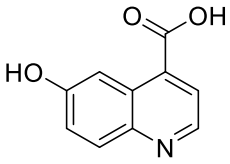

Compound (**2**) (0.987 g, 4.86 mmol) was measured in a round-bottom flask, before the addition of hydrogen bromide (20 mL, 48 %). The reaction mixture was refluxed for 4 hours at 130ºC before it was allowed to reach room temperature. The solvent was evaporated and dried overnight to obtain compound (**3**) as a green powder (1.421 g, 154.56 %). ^{1}H NMR (400 MHz, DMSO) δ 9.06 (d, *J* = 5.2 Hz, 1H), 8.21 – 8.12 (m, 2H), 8.09 (d, *J* = 2.6 Hz, 1H), 7.64 (dd, *J* = 9.2, 2.5 Hz, 1H). MS (ESI) *m/z* 212.032 $[M+Na]^+$

5.1.7 Procedure for the synthesis of 3-((tert-butoxycarbonyl)amino)propyl 6-(3-((tert-butoxycarbonyl)amino)propoxy)quinoline-4-carboxylate (11)

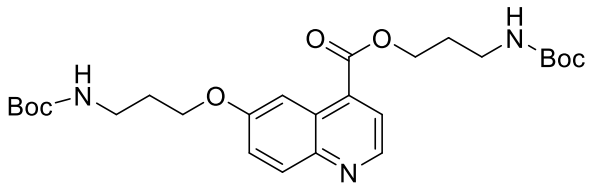

Cesium carbonate (4.760 g, 14.61 mmol) was added to a round-bottom flask containing compound (**3**) (1.421 g, 7.51 mmol) from the previous reaction. DMF (5 mL) was added, and the reaction mixture was stirred in room temperature for 15 minutes. A solution of compound (**12**) (2.260 g, 8.92 mmol) in DMF (5 mL) was then added dropwise to the round-bottom flask. The reaction mixture was refluxed at 60 ºC overnight. After reaching room temperature, the solvent was evaporated. MS (ESI) *m/z* 526.252 $[M+Na]^+$

5.1.8 Procedure for the synthesis of 6-(3-((tert-butoxycarbonyl)amino)propoxy) quinoline-4-carboxylic acid (6)

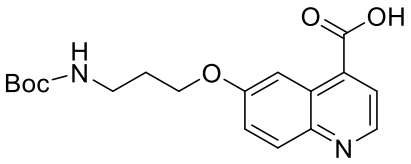

Compound (**11**) was diluted in methanol (20 mL), and NaOH (25 mL, 1.0 M) was added. The reaction mixture was stirred overnight and later neutralized with HCl (12.5 mL, 2.0 M). The mixture was then filtrated before the solvents were evaporated. Purification on prep-HPLC resulted in compound (**6**) as a snow-white powder (0.275 g, 10.57 %). ^{1}H NMR (400 MHz, DMSO) δ 8.85 (d, *J* = 4.4 Hz, 1H), 8.15 (d, *J* = 2.8 Hz, 1H), 8.02 (d, *J* = 9.2 Hz, 1H), 7.92 (d, *J* = 4.4 Hz, 1H), 7.48 (dd, *J* = 9.2, 2.8 Hz, 1H), 6.94 (t, *J* = 5.6 Hz, 1H), 4.11 (t, *J* = 6.2 Hz, 2H), 3.13 (q, *J* = 6.5 Hz, 2H), 1.92 (p, *J* = 6.5 Hz, 2H), 1.36 (s, 9H). MS (ESI) *m/z* 347.10 $[M+H]^+$

5.1.9 Procedure for the synthesis of tert-butyl (S)-(3-((4-((2-(2-cyano-4,4-difluoropyrrolidin-1-yl)-2-oxoethyl)carbamoyl)quinolin-6-yl)oxy)propyl)carbamate (7)

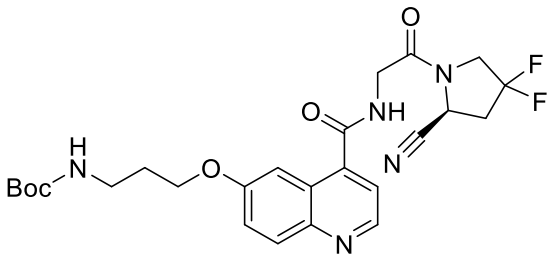

HATU (0.286 g, 0.752 mmol) and compound (**6**) (0.275 g, 0.794 mmol) were measured in a round-bottom flask before the addition of DMF (7 mL) and DIPEA (0.390 mL, 2.239 mmol). The mixture was allowed to stir for 15 minutes before the dropwise addition of compound (**13**) (0.567 g, 2.997 mmol) dissolved in DMF (3 mL) to the round-bottom flask. The reaction mixture was stirred overnight before the solvents were evaporated. Purification on prep-HPLC resulted in compound (**7**) as a white solid (0,154 g, 37.48 %). ^{1}H NMR (400 MHz, $CDCl_3$) δ 8.75 – 8.53 (m, 2H), 7.92 (d, *J* = 9.4 Hz, 1H), 7.79 – 7.59 (m, 2H), 7.35 (dd, *J* = 9.5, 2.6 Hz, 1H), 5.07 (dd, *J* = 8.7, 4.5 Hz, 1H), 4.39 – 3.91 (m, 6H), 3.33 (t, *J* = 6.8 Hz, 2H), 2.82 (dtd, *J* = 18.2, 8.8, 8.1, 4.2 Hz, 2H), 2.03 (p, *J* = 6.6 Hz, 2H), 1.41 (s, 9H). ^{19}F NMR (376 MHz, $CDCl_3$) δ -75.48. MS (ESI) *m/z* 518.15 $[M+H]^+$

5.1.10 Procedure for the synthesis of (S)-6-(3-aminopropoxy)-N-(2-(2-cyano-4,4-difluoropyrrolidin-1-yl)-2-oxoethyl)quinoline-4-carboxamide (8)

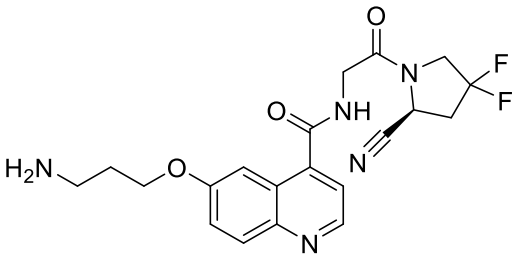

A solution containing TFA (9.5 mL), H_2O (0.25 mL) and TIPS (0.25 mL) was prepared. The solution (5 mL) was added to compound (**7**) and stirred for 30 minutes. The solvent was evaporated, and the remaining contents dried overnight under vacuum. This resulted in compound (**8**) as a brown, viscous solution. MS (ESI) *m/z* 418.1690 $[M+H]^+$

5.1.11 Procedure for the synthesis of (R)-2-((tert-butoxycarbonyl)amino)-3-((3-((4-((2-((S)-2-cyano-4,4-difluoropyrrolidin-1-yl)-2-oxoethyl)carbamoyl)quinolin-6-yl)oxy)propyl)amino)-3-oxopropane-1-sulfonic acid (18)

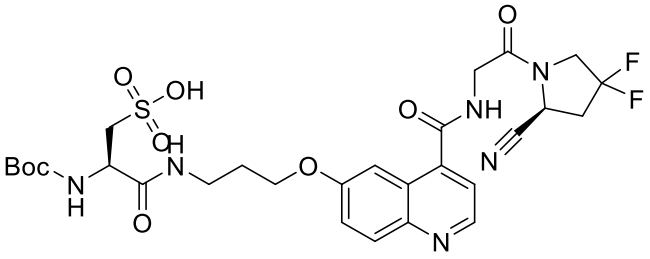

HATU (0.081 g, 0.213 mmol) and compound (**17**) (0.126 g, 0.468 mmol) were weighed in a round-bottom flask and dissolved in DMF (7 mL) before DIPEA (0.110 mL, 0.631 mmol) was added. The solution was stirred for 15 minutes and followed by the dropwise addition of compound (**8**) (0.0871 g, 0.208 mmol) dissolved in DMF (3 mL) to the round-bottom flask. The reaction mixture was stirred overnight, before the solvents were evaporated to afford compound (**18**). ^{1}H NMR (400 MHz, D_2O) δ 9.03 (d, *J* = 5.5 Hz, 1H), 8.24 – 8.19 (m, 1H), 8.11 (d, *J* = 5.6 Hz, 1H), 7.85 (d, *J* = 8.8 Hz, 3H), 5.20 (dd, *J* = 8.7, 4.2 Hz, 1H), 4.52 – 4.09 (m, 11H), 3.61 (dt, *J* = 13.6, 6.7 Hz, 2H), 3.47 – 3.18 (m, 5H), 3.11 – 2.88 (m, 3H), 2.73 (t, *J* = 0.9 Hz, 2H), 2.23 – 2.07 (m, 3H), 1.83 (s, 3H), 1.49 – 1.12 (m, 1H). ^{13}C NMR (101 MHz, D_2O) δ 168.88, 167.70, 167.34, 163.06, 162.70, 159.93, 149.91, 148.07, 141.08, 134.42, 128.91, 127.63, 125.31, 124.97, 122.49, 119.99, 117.76, 117.47, 114.86, 104.41, 66.56, 65.06, 52.02, 51.70, 51.38, 50.34, 50.01, 44.78, 42.21, 38.01, 36.62, 36.55, 36.37, 36.12, 34.48, 28.34, 27.52. MS (ESI) *m/z* 669.14 $[M+H]^+$

5.1.12 Procedure for the synthesis (R)-2-amino-3-((3-((4-((2-((S)-2-cyano-4,4-difluoropyrrolidin-1-yl)-2-oxoethyl)carbamoyl)quinolin-6-yl)oxy)propyl)amino)-3-oxopropane-1-sulfonic acid (1)

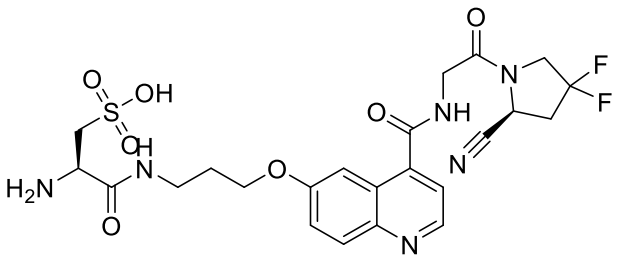

A solution containing TFA (9.5 mL), H_2O (0.25 mL) and TIPS (0.25 mL) was prepared. The solution (5 mL) was added to compound (**18**) and stirred for 30 minutes. The solvents were then

evaporated, and the remaining contents were purified on prep-HPLC to afford compound (**1**) as a yellow solid (0.067 g, 56.65 %). HRMS *m/z* 591.1444 $[M+Na]^+$ (calculated for $C_{23}H_{26}F_2N_6NaO_7S$: 591.1444).

5.1.13 Procedure for the synthesis (R)-3-((3-((4-((2-((S)-2-cyano-4,4-difluoropyrrolidin-1-yl)-2-oxoethyl)carbamoyl)quinolin-6-yl)oxy)propyl)amino)-2-(6-fluoronicotinamido)-3-oxopropane-1-sulfonic acid (19)

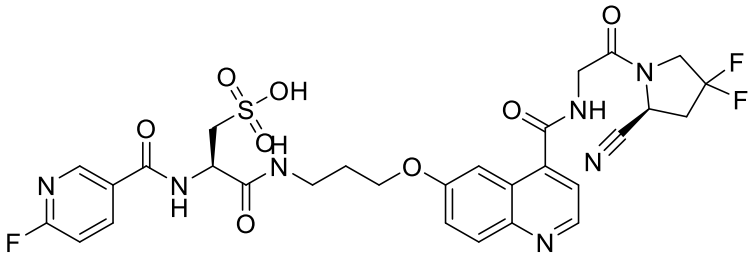

HATU (0.013 g, 0.0341 mmol) and 6-fluoropyrridine-3-carboxylic acid (0.006 g, 0.0425 mmol) were measured in a round-bottom flask and dissolved in DMF (1.0 mL). DIPEA (0.0185 mL, 0.106 mmol) was added, and the mixture was stirred for 15 minutes before the dropwise addition of compound (**1**) (0.019 g, 0.0334 mmol) dissolved in DMF (2.0 mL). The reaction mixture was stirred overnight. The solvent was evaporated, and the residue dried under vacuum for 30 minutes. Purification on prep-HPLC resulted in compound (**19**) as a light yellow and green solid (0.017 g, 73.59 %). ^{1}H NMR (400 MHz, DMSO) δ 9.25 (q, *J* = 7.5, 6.0 Hz, 1H), 9.04 (d, *J* = 4.9 Hz, 1H), 8.86 (d, *J* = 5.9 Hz, 1H), 8.65 (d, *J* = 2.4 Hz, 1H), 8.32 (td, *J* = 8.2, 2.5 Hz, 1H), 8.15 – 7.97 (m, 3H), 7.82 (d, *J* = 4.9 Hz, 1H), 7.68 (dd, *J* = 9.3, 2.7 Hz, 1H), 7.30 (dd, *J* = 8.6, 2.6 Hz, 1H), 5.21 (dd, *J* = 9.4, 2.6 Hz, 1H), 4.50 (q, *J* = 6.3 Hz, 2H), 4.43 – 4.06 (m, 15H), 3.29 (dq, *J* = 12.6, 6.5 Hz, 2H), 2.98 – 2.76 (m, 4H), 1.96 (p, *J* = 6.4 Hz, 2H). ^{19}F NMR (376 MHz, DMSO) δ -65.53 (dd, *J* = 7.8, 2.6 Hz), -75.09. HRMS *m/z* 736.1385 $[M-H+2Na]^+$ (calculated for $C_{29}H_{27}F_3N_7Na_2O_8S$: 736.1384)

5.2 Methods for radiochemistry

5.2.1 Procedure for the radiosynthesis of 6-[^{18}F]fluoronicotinic acid 2,3,5,6-tetrafluorophenyl ester ([^{18}F]F-Py-TFP) (21)

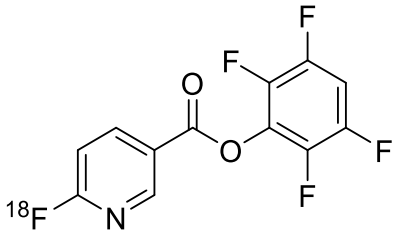

Target water labelled with fluorine-18 was diluted with H_2O (2 mL) and fixated on a Chromabond PS-HCO_3 anion exchange column. The column was washed with anhydrous MeCN (2 mL) and dried for one minute under vacuum. The quaternary ammonium precursor (N,N,N-trimethyl-5-((2,3,5,6-tetrafluorophenoxy)carbonyl)pyridin-2-aminiumtrifluoro methanesulfonate (0.012 g, 0.0364 mmol) was dissolved in MeCN/t-BuOH (0.5 mL) and pushed through the same column in order to produce compound (**21**). The solution was diluted in H_2O (5 mL) and pushed onto a C18 cartridge that was preconditioned. The column containing compound (**21**) was washed with H_2O (5 mL) and thereafter eluted with MeCN (2 mL, 65 %).

5.2.2 Procedure for the radiosynthesis of (R)-3-((3-((4-((2-((S)-2-cyano-4,4-difluoropyrrolidin-1-yl)-2-oxoethyl)carbamoyl)quinolin-6-yl)oxy)propyl)amino)-2-(6-(^{18}F)nicotinamido)-3-oxopropane-1-sulfonic acid (22)

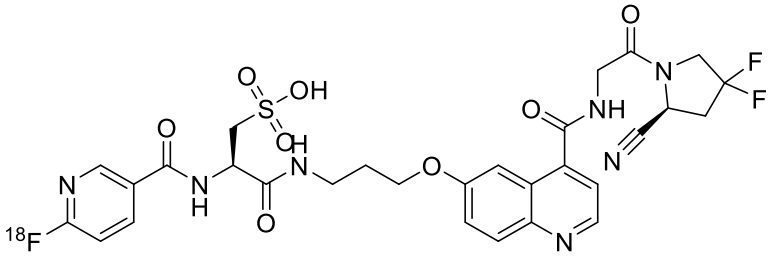

In a vial, the FAPI precursor (**1**) (0.001 g, 0.00176 mmol) was dissolved in DMSO (0.05 mL), before the addition of 2-butanon (0.3 mL) and DIPEA (0.003 mL, 0.0172 mmol). After this, a stock solution containing (**21**) (0.02 mL) was added. The reaction mixture was heated, resulting in compound (**22**).

6 References

1. Pecorino, L. Molecular biology of cancer: Mechanisms, Targets, and Therapeutics, 3rd ed.; Oxford University Press, 2012.

2. Yokota, J. "Tumor progression and metastasis". *Carcinogenesis*., **2000**, *21*(3), 497-503.

3. Clark, W.H. "Tumour progression and the nature of cancer". *Br. J. Cancer*., **1991**, *64*(4), 631-644.

4. Kinzler, K.W.; Vogelstein, B. ''Cancer genes and the pathways they control". *Nat Med*., **2004**, *10*(8), 789-99.

5. Hanahan, D.; Weinberg, R.A. "The hallmarks of cancer". *Cell*., **2000**, *100*(1), 57-70.

6. Hanahan, D.; Weinberg, R.A. "Hallmarks of cancer: the next generation". *Cell*., **2011**, *144*(5), 646-74.

7. All cancers. International Agency for Research on Cancer, 2020. https://gco.iarc.fr/today/data/factsheets/cancers/39-All-cancers-fact-sheet.pdf (accessed 2021-07-22).

8. Cancer in Norway. Cancer Registry of Norway, Institute of Population-based Cancer Research, 2019. https://www.kreftregisteret.no/globalassets/cancer-in-norway/2019/cin_report.pdf (accessed 2021-07-22).

9. Sung, H.; Ferlay, J.; Siegel, R.L.; Laversanne, M.; Soerjomataram, I.; Jemal, Ahmedin.; Bray, F. "Global Cancer Statistics 2020: GLOBOCAN Estimates of Incidence and Mortality Worldwide for 36 Cancers in 185 Countries". *Ca Cancer J Clin*., **2021**, *71*(3), 209-249.

10. Faguet, G.B. "A brief history of cancer: age-old milestones underlying our current knowledge database". *Int J Cancer*., **2015**, *169*(9), 2022-36.

11. Karpozilos, A.; Pavlidis, N. "The treatment of cancer in Greek antiquity". *Eur J cancer*., **2004**, *40*(14), 2033-40.

12. Goodman, L.S.; Wintrobe, M.M, et al. "Nitrogen mustard therapy; use of methyl-bis (beta-chloroethyl) amine hydrochloride and tris (beta-chloroethyl) amine hydrochloride for Hodgkin's disease, lymphosarcoma, leukemia and certain allied and miscellaneous disorders". *J Am Med Assoc.*, **1946**, *132*, 126-32.

13. Chabner, B.A.; Roberts Jr, T.G. "Timeline: Chemotherapy and the war on cancer". *Nat Rev Cancer*., **2005**, *5*(1), 65-72.

14. Kim, K.; Roh, J.K.; Wee, H. Kim, C. Cancer Drug Discovery: Science and History, 1st ed.; Springer, 2016.

15. Altmann, A.; Haberkorn, U.; Siveke, J. “The Latest Developments in Imaging of Fibroblast Activation Protein”. *J Nucl Med*., **2021**, *62*(2), 160-167.

16. Brennen, W.N.; Isaacs, J.T.; Denmeade, S.R.; “Rationale behind targeting fibroblast activation protein-expressing carcinoma-associated fibroblasts as a novel chemotherapeutic strategy”. *Mol Cancer Ther*., **2012**, *11*(2), 257-266.

17. Zi, F.; He, J.; He, D.; Li, Y.; Yang, L.; Cai, Z. “Fibroblast activation protein α in tumor microenvironment: recent progression and implications (review)”. *Mol Med Rep*., **2015**, *11*(5), 3203-3211.

18. Valkenburg, K.C.; De Groot, A.E, Pienta, K.J. “Targeting the tumour stroma to improve cancer therapy”. *Nat Rev Clin Oncol*., **2018**, *15*, 366-381.

19. Wang, M.; Zhao, J.; Zhang, L., et al. “Role of tumor microenvironment in tumorigenesis”. *J Cancer*., **2017**, *8*(5), 761-773.

20. Lindner, T.; Loktev, A.; Giesel, F. et al. “Targeting of activated fibroblasts for imaging and therapy”. *EJNMMI radiopharm*., **2019**, *4*(1).

21. Plava, J.; Cihova, M.; Burikova, M., et al. “Recent advances in understanding tumor stroma-mediated chemoresistance in breast cancer”. *Mol Cancer*., **2019**, *18*(1).

22. Loktev, A.; Lindner, T.; Mier, W., et al. “A Tumor-Imaging Method Targeting Cancer-Associated Fibroblasts”. *J Nucl Med*., **2018**, *59*(9), 1423-1429.

23. Puré, E.; Blomberg, R. “Pro-tumorigenic roles of fibroblast activation protein in cancer: back to the basics”. *Oncogene.*, **2018**, *37*(32), 4343-4357.

24. Liu, R.; Li, H.; Liu, L., et al. “Fibroblast activation protein: A potential therapeutic target in cancer”. *Cancer biol.*, **2012**, *13*(3), 123-129.

25. Aaertgeerts, K.; Levin, I.; Shi, L., et al. “Structural and kinetic analysis of the substrate specificity of human fibroblast activation protein alpha”. *J Biol Chem.*, **2005**, *280*(20), 19441-4.

26. Huang, Y.; Wang, S.; Kelly, T. “Seprase promotes rapid tumor growth and increased microvessel density in a mouse model of human breast cancer”. *Cancer Res*., **2004**, *64*(8), 2712-6.

27. Keane, F.M.; Nadvi, N.A.; Yao, T., et al. “Neuropeptide Y, B-type natriuretic peptide, substance P and peptide YY are novel substrates of fibroblast activation protein-α”. *FEBS J*., **2011**, *278*(8), 1316-32.

28. Giesel, F.L.; Kratochwil, C.; Lindner, T., et al. “68 Ga-FAPI PET/CT: Biodistribution and Preliminary Dosimetry Estimate of 2 DOTA-Containing FAP-Targeting Agents in Patients with Various Cancers”. *J Nucl Med.*, **2019**, *60*(3), 386-392.

29. Liu, F.; Qi, L.; Liu, B., et al. “Fibroblast activation protein overexpression and clinical implications in solid tumors: a meta-analysis”. *PLoS One.,* **2015**, *10*(3).

30. Ramirez-Montagut, T.; Blachere, N.E.; Sviderskaya, E.V., et al. “FAPalpha, a surface peptidase expressed during wound healing, is a tumor suppressor”. *Oncogene*., **2004**, *23*(32), 5435-46.

31. Ariga, N.; Sato, E.; Ohuchi, N., et al. “Stromal expression of fibroblast activation protein/seprase, a cell membrane serine proteinase and gelatinase, is associated with longer survival in patients with invasive ductal carcinoma of breast”. *Int J Cancer.,* **2001**, *95*(1), 67-72.

32. Narra, K.; Mullins, S.R.; Lee, H., et al. “Phase II trial of single agent Val-boroPro (Talabostat) inhibiting Fibroblast Activation Protein in patients with metastatic colorectal cancer”. *Cancer Biol Ther*., **2007**, *6*(11).

33. Scott, A.M.; Wiseman, G.; Welt, S., et al. “A Phase I dose-escalation study of sibrotuzumab in patients with advanced or metastatic fibroblast activation protein-positive cancer”. *Clin Cancer Res*., **2003**, *9*(5), 1639-47.

34. Hofheinz, R-D.; al-Batran, S.E.; Hartmann, F., et al. “Stromal antigen targeting by a humanised monoclonal antibody: an early phase II trial of sibrotuzumab in patients with metastatic colorectal cancer”. *Onkologie.,* **2003**, *26*(1), 44-8.

35. Lindner, T.; Loktev, A.; Altmann., et al. Development of Quinoline-Based Theranostic Ligands for the Targeting of Fibroblast Activation Protein. *J Nucl Med*., **2018**, *59*(9), 1415-1422.

36. Jansen, K.; Heirbaut, L.; Verkerk, R., et al. Extended structure-activity relationship and pharmacokinetic investigation of (4-quinolinoyl)glycyl-2-cyanopyrrolidine inhibitors of fibroblast activation protein (FAP). *J Med Chem*., **2014**, *57*(7), 3053-74.

37. Decker, A.D.; Vliegen, G.; Rompaey, D.V., et al. Novel Small Molecule-Derived, Highly Selective Substrates for Fibroblast Activation Protein (FAP). *ACS Med. Chem. Lett*., **2019**, *10*(8), 1173-1179.

38. Jansen, K.; Heirbaut, L.; Cheng, J.D., et al. Selective Inhibitors of Fibroblast Activation Protein (FAP) with a (4-Quinolinoyl)-glycyl-2-cyanopyrrolidine Scaffold. *ACS Med. Chem. Lett.*, **2013**, *4*(5), 491-496.

39. Lewis, J.S.; Windhorst, A.D.; Zeglis, B. Radiopharmaceutical Chemistry, 1st ed.; Springer, 2019.

40. Treglia, G.; Giovanella, Luca. Evidence-based Positron Emission Tomography, 1st ed.; Springer, 2020.

41. Lu, F-M.; Yuan, Z. PET/SPECT molecular imaging in clinical neuroscience: recent advances in the investigation of CNS diseases. *Quant Imaging Med surg.*, **2015**, *5*(3), 433-447.

42. Sharma, R.; Aboagye, E. Development of radiotracers for oncology – the interface with pharmacology. *Br J Pharmacol.*, **2011**, *163*(8), 1565-1585.

43. Rigo, P.; Paulus, P.; Kaschten, B.J., et al. Oncological applications of positron emission tomography with fluorine-18 fluorodeoxyglucose. *Eur J Nucl Med.*, **1996**, *23*(12), 1641-74.

44. Bailey, D.L.; Townsend, D.W., Maisey, P.E., et al. Positron Emission Tomography: Basic Sciences, 1st ed.; Springer, 2005.

45. Alauddin, M. Positron emission tomography (PET) imaging with (18)F-based radiotracers. *Am J Nucl Med Mol Imaging.*, **2012**, *2*(1), 55-76.

46. Olberg, D.E.; Arukwe, J.M.; Grace, D. One step radiosynthesis of 6-[(^{18})F]fluoronicotinic acid 2,3,5,6-tetrafluorophenyl ester ([(^{18})F]F-Py-TFP): a new prosthetic group for efficient labeling of biomolecules with fluorine-18. *J Med Chem.*, **2010**, *53*(4), 1732-40.

47. Sanches-Crespo, A. Comparison of Gallium-68 and Fluorine-18 imaging characteristics in positron emission tomography. *Appl Radiat Isot.*, **2013**, *76*, 55-62.

48. Khan, M.S.; Kanwal, N.; Rozeen, H. A Systematic Review of Medical Cyclotron, Producing F-18 & FDG Radio Isotopes for Pet Scan Imaging. *Int. J. Eng. Res.*, **2017**, *5*(4), 620-623.

49. Jacobson, O.; Kiesewetter, D.O.; Chen, X. Fluorine-18 radiochemistry, labeling strategies and synthetic routes. *Bioconjug Chem.*, **2015**, *26*(1), 1-18.

50. Nieweg, O.E.; Kim, E.E.; Wong, W.H. Positron emission tomography with fluorine-18-deoxyglucose in the detection and staging of breast cancer. *Cancer.*, **1993**, *71*(12), 3920-5.

51. Glaudemans, A.W.J.M.; de Vries, E.F.J.; Galli, F., et al. The Use of 18F-FDG-PET/CT for Diagnosis and Treatment Monitoring of Inflammatory and Infectious Diseases. *Clin Dev Immunol.*, **2013**, 2013.

52. Pinilla, I.; Rodriguez-Vigil, B.; Gomez-Leon, N. Integrated 18FDG PET/CT: Utility and Applications in Clinical Oncology. *Clin Med Oncol.*, **2008**, *2*, 181-198.

53. Hoh, C.K. Clinical use of FDG PET. *Nucl Med Biol.*, **2007**, *34*(7), 737-42.

54. Carpino, L.A.; Imazumi, H.; El-Faham, A., et al. The Uronium/Guanidinium Peptide Coupling Reagents: Finally the True Uronium Salts. *Angew Chem.*, **2002**, *41*(3), 441-445.

55. Knorr, R.; Trzeciak, A.; Bannwarth, W., et al. New coupling reagents in peptide chemistry. *Tetrahedron Lett.*, **1989**, *30*(15), 1927-1930

56. Vrettos, E.I.; Sayyad, N.; Mavrogiannaki, E.M., et al. Unveiling and tackling guanidinium peptide coupling reagent side reactions towards the development of peptide-drug conjugates. *RSC Adv.*, **2017**, *80*(7), 50519-50526.

57. Valeur, E.; Bradley, M. Amide bond formation: beyond the myth of coupling reagents. *Chem Soc Rev.*, **2009**, *38*(2), 606-631.

58. Hopper, A.V. Recent developments in polymer research, 1st ed.; Nova Science Pub, 2006.

59. Cho, J.M.; Yang, E.H.; Quan, W. Discovery of a novel fibroblast activation protein (FAP) inhibitor, BR103354, with anti-diabetic and anti-steatotic effects. *Sci Rep.*, 2020.

60. Novartis expands targeted radioligand therapy pipeline with in-license for compounds targeting Fibroblast Activation Protein (FAP). Novartis, 2021 https://www.novartis.com/news/media-releases/novartis-expands-targeted-radioligand-therapy-pipeline-license-compounds-targeting-fibroblast-activation-protein-fap (accessed 2021-08-15

61. Haberkorn, U.; Loktev A.; Lindner, T., et al. FAP inhibitor. WO 2019/154886 A1, 15th of August 2019.

62. Feurer, A.; Soeberdt M.; Terinek, M., et al. Substituted benzimidazole derivatives as melanocortin 3 receptor antagonists. EP 2 439 197 A1, 11th of April 2012.

63. Bing, J.; Liu, Z.; Shi, J., et al. Linker effects on biological properties of 111In-labeled DTPA conjugates of a cyclic RGDfK dimer. *Bioconjug Chem.*, **2008**, *19*(1), 201-10.

64. Liu, S. Radiolabeled Cyclic RGD Peptides as Integrin αvβ3-Targeted Radiotracers: Maximizing Binding Affinity via Bivalency. *Bioconjug Chem.*, **2010**, *20*(12), 2199-2213.

65. Olberg, D.E.; Svadberg, A. Automation friendly on-column radiosynthesis of 18F-bifunctional labeling agents from trialkyl pyridin-2-ammonium nicotinic acid precursors.

66. Sureshbabu, V.V.; Naik, S.A.; Nagendra, G. Synthesis of Boc-Amino Tetrazoles Derived from a-Amino Acid. *Synth Commun.,* **2009**, *39*, 395-406.

67. Gawandi, V.; Fitzpatrick, P.F. The synthesis of deuterium-labeled spermine, N1-acetylspermine and N1-acetylspermidine. *J labelled Comp Radiopharm*., **2007**, *50*(7), 666-670.

7 Appendix

A: NMR

Figure A-1: Compound (**2**)

Figure A-2: Compound (**3**)

Figure A-3: Compound (**15**)

Figure A-4: Compound (**16**)

Figure A-5: Compound (**13**)

Figure A-6: Compound (**12**)

Figure A-7: Compound (**17**)

Figure A-8: Compound (**6**)

Figure A-9: Compound (**7**)

Figure A-10: Compound (**7**)

Figure A-11: Compound (**18**)

Figure A-12: Compound (**18**)

Figure A-13: Compound (**19**)

Figure A-14: Compound (**19**)

B: MS

Figure B-1: Compound (**3**)

Figure B-2: Compound (**15**)

Figure B-3: Compound (**16**)

Figure B-4: Compound (**13**)

Figure B-5: Compound (**12**)

Figure B-6: Compound (**11**)

Figure B-7: Compound (**6**)

Figure B-8: Compound (**7**)

Figure B-9: Compound (**8**)

Figure B-10: Compound (**18**)

C: HRMS

Figure C-1: Compound (**1**)

Figure C-2: Compound (**19**)

D: Prep-HPLC

Figure D-1: Compound (**13**)

Figure D-2: Compound (**6**)

Figure D-3: Compound (**7**)

Figure D-4: Compound (**1**)

Figure D-5: Compound (**19**)

E: HPLC/Radio-HPLC

Figure E-1: Compound (**1**)

Figure E-2: Compound (**19**)

Figure E-3: Compound (**21**)

Figure E-4: Compound (**19**) and (**22**)

Figure E-5 – E-12: Compound (**22**)

Appendix A: NMR

Figure A-1. ^{1}H NMR spectrum of 6-methyoxyquinoline-4-carboxylic acid (**2**).

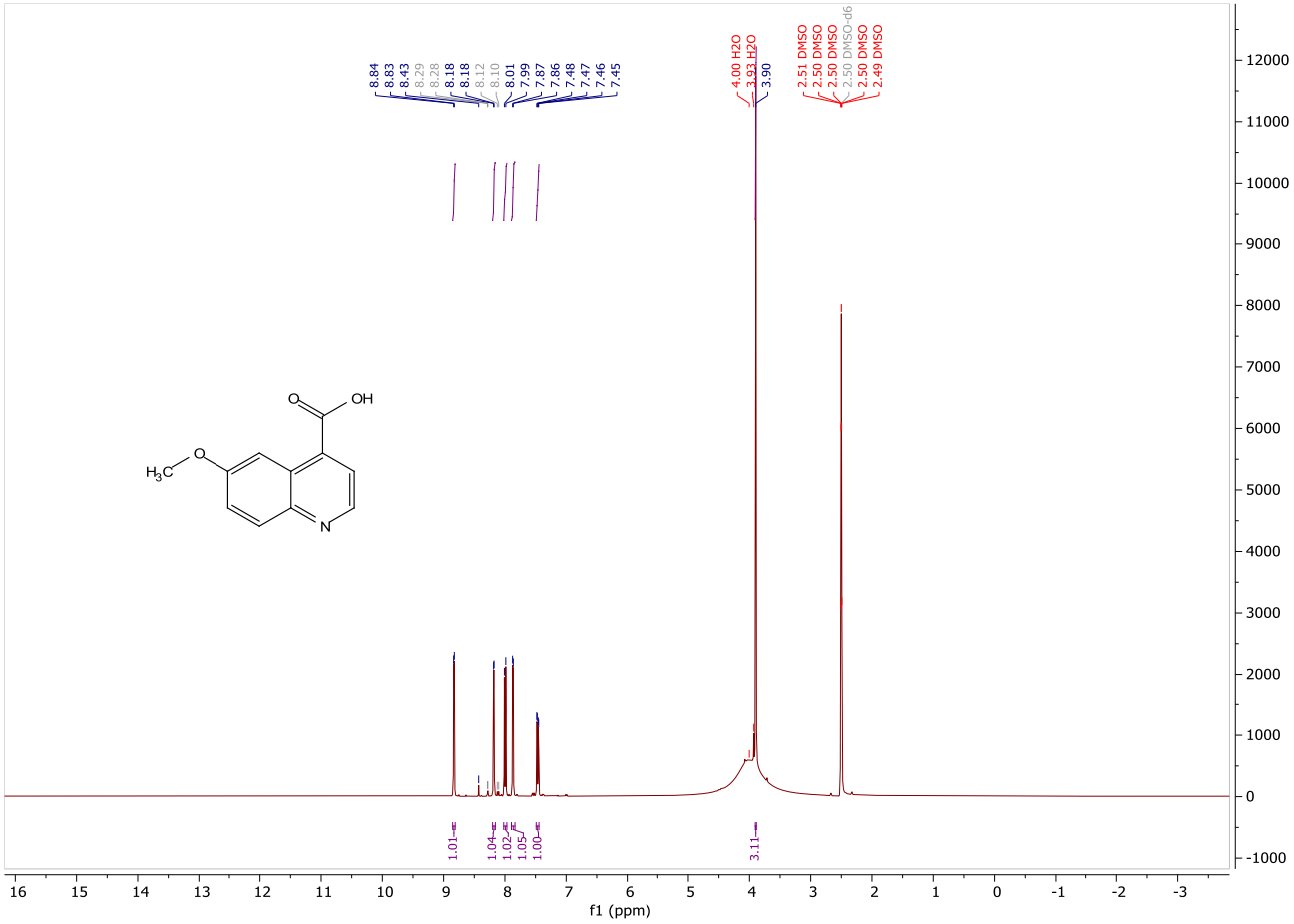

Appendix A: NMR

Figure A-2. ^{1}H NMR spectrum of 6-hydroxyquinoline-4-carboxylic acid (**3**)

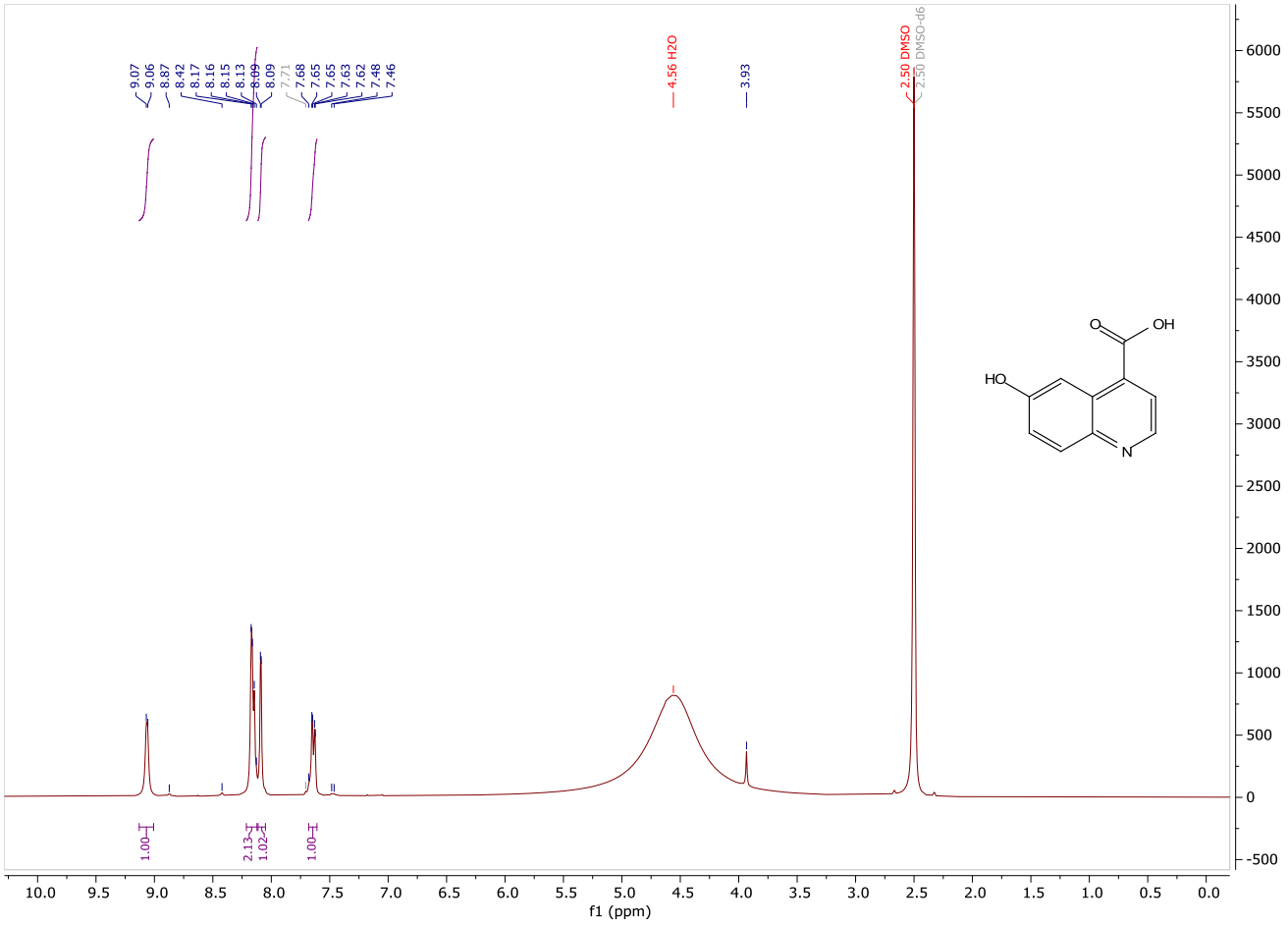

Appendix A: NMR

Figure A-3. ^{1}H NMR spectrum of tert-butyl (S)-(2-(2-carbamoyl-4,4-difluoropyrrolidin-1-yl)-2-oxoethyl)carbamate (**15**)

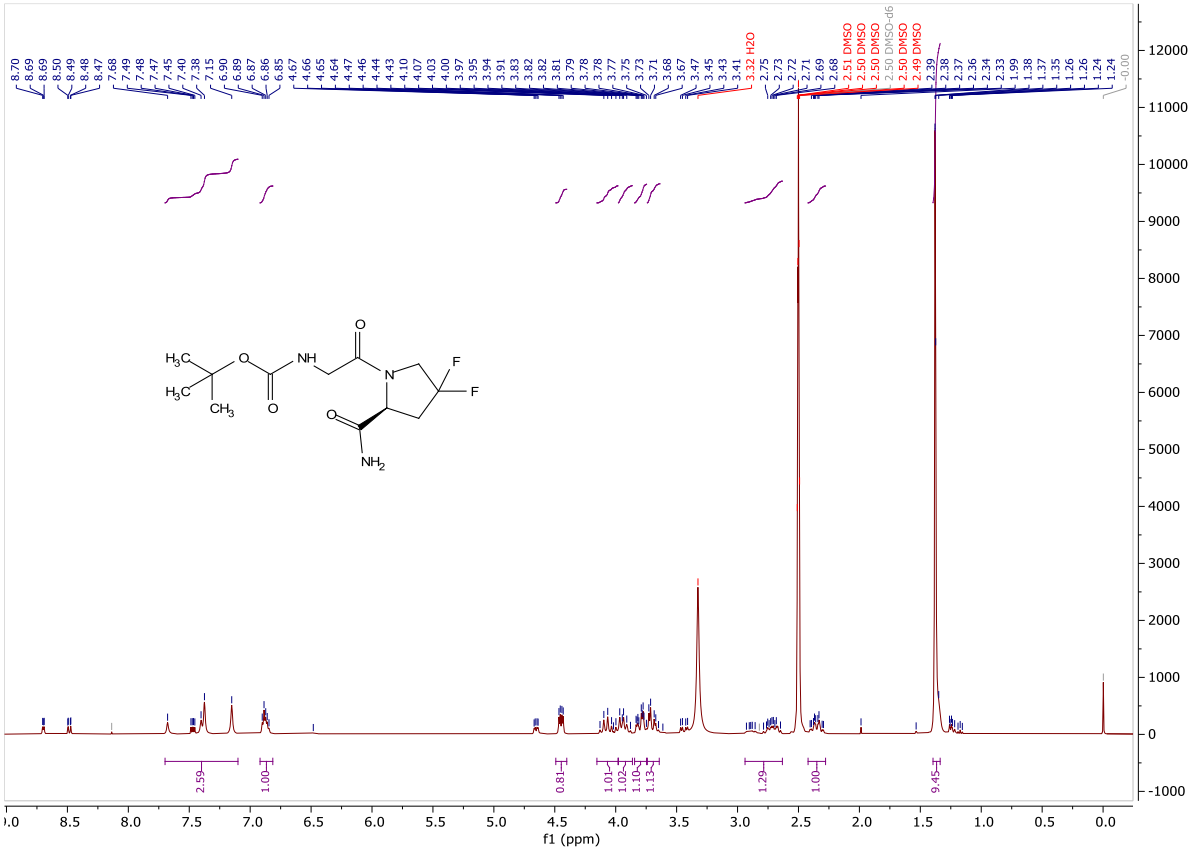

Appendix A: NMR

Figure A-4. ^{1}H NMR spectrum of tert-butyl (S)-(2-2-cyano-4,4-difluoropyrrolidin-1-yl)-2-oxoethyl)carbamate (**16**)

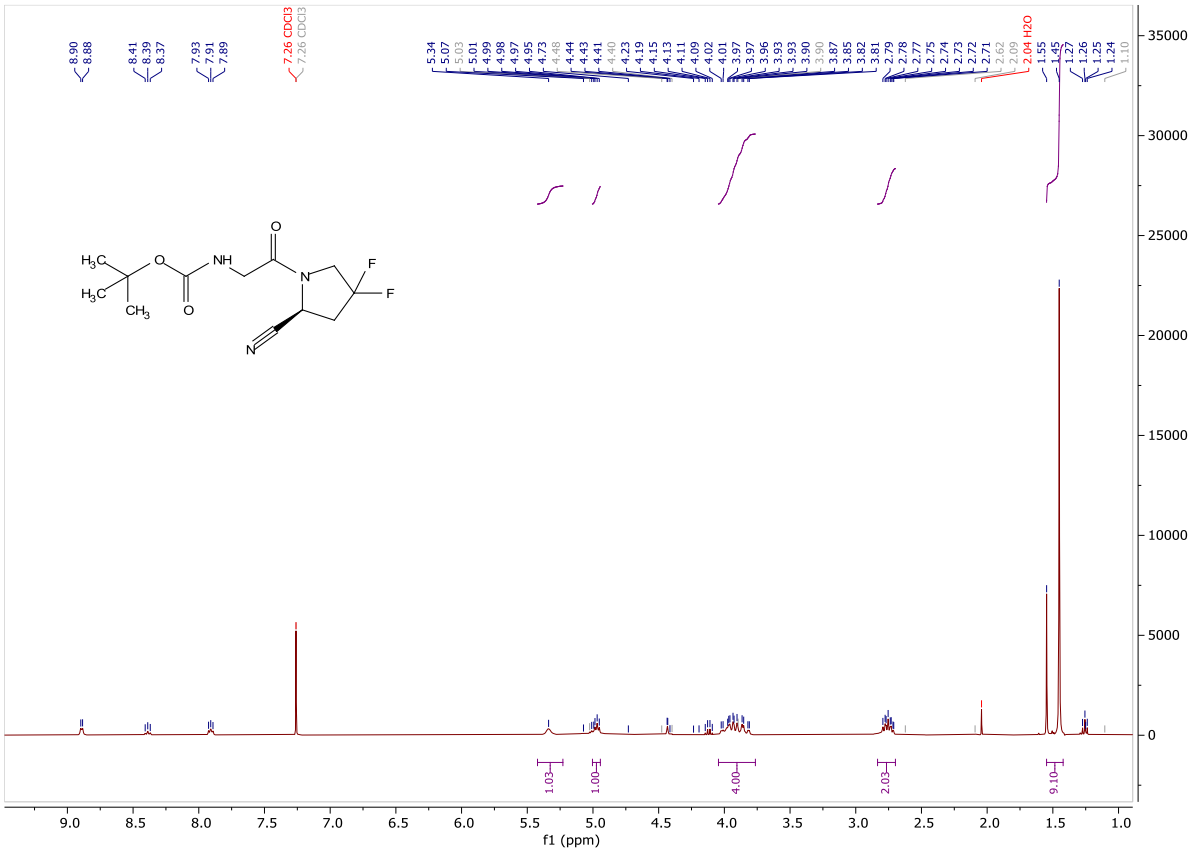

Appendix A: NMR

Figure A-5. ^{1}H NMR spectrum of (S)-4,4-difluoro-1-glycylpyrrolidine-2-carbonitrile (**13**)

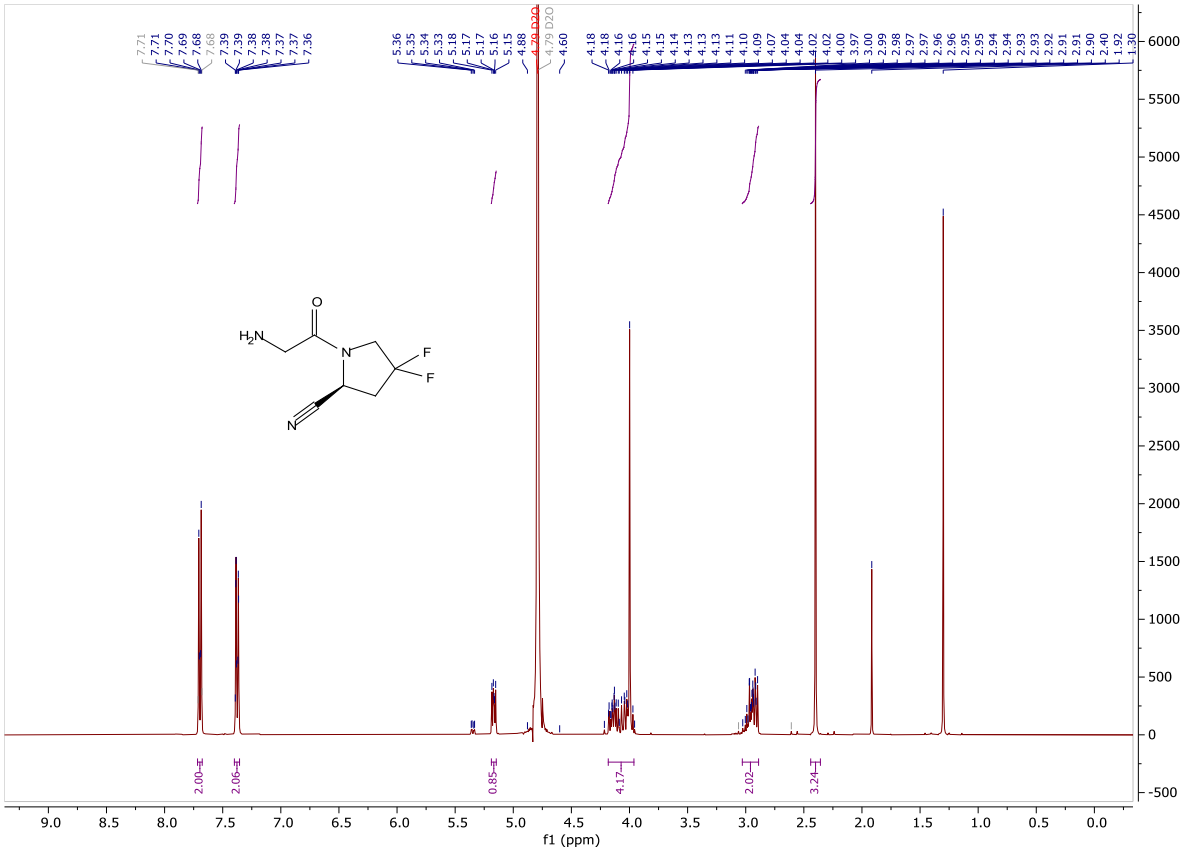

Appendix A: NMR

Figure A-6. ^{1}H NMR spectrum of 3-((tert-butoxycarbonyl)amino)propyl methanesulfonate **(12)**

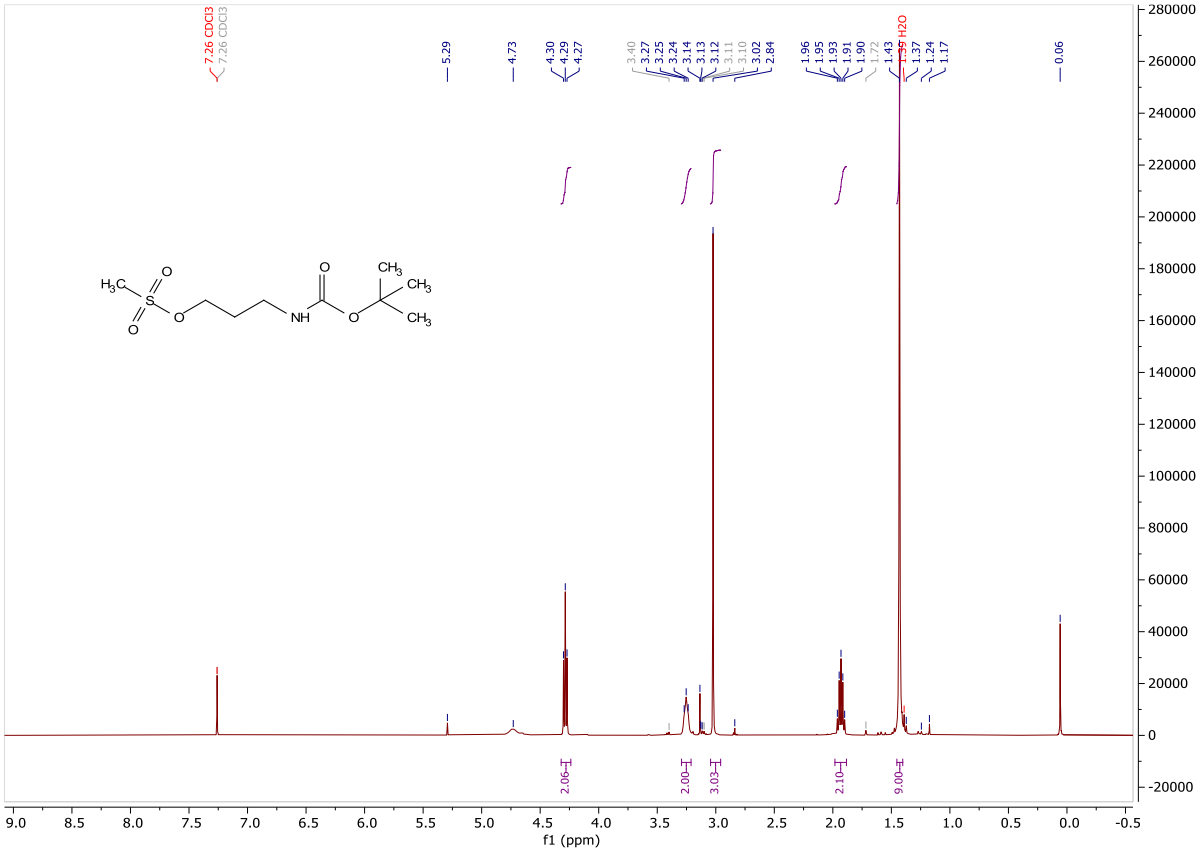

Appendix A: NMR

Figure A-7. ^{1}H NMR spectrum of Boc-L-cysteic acid (**17**)

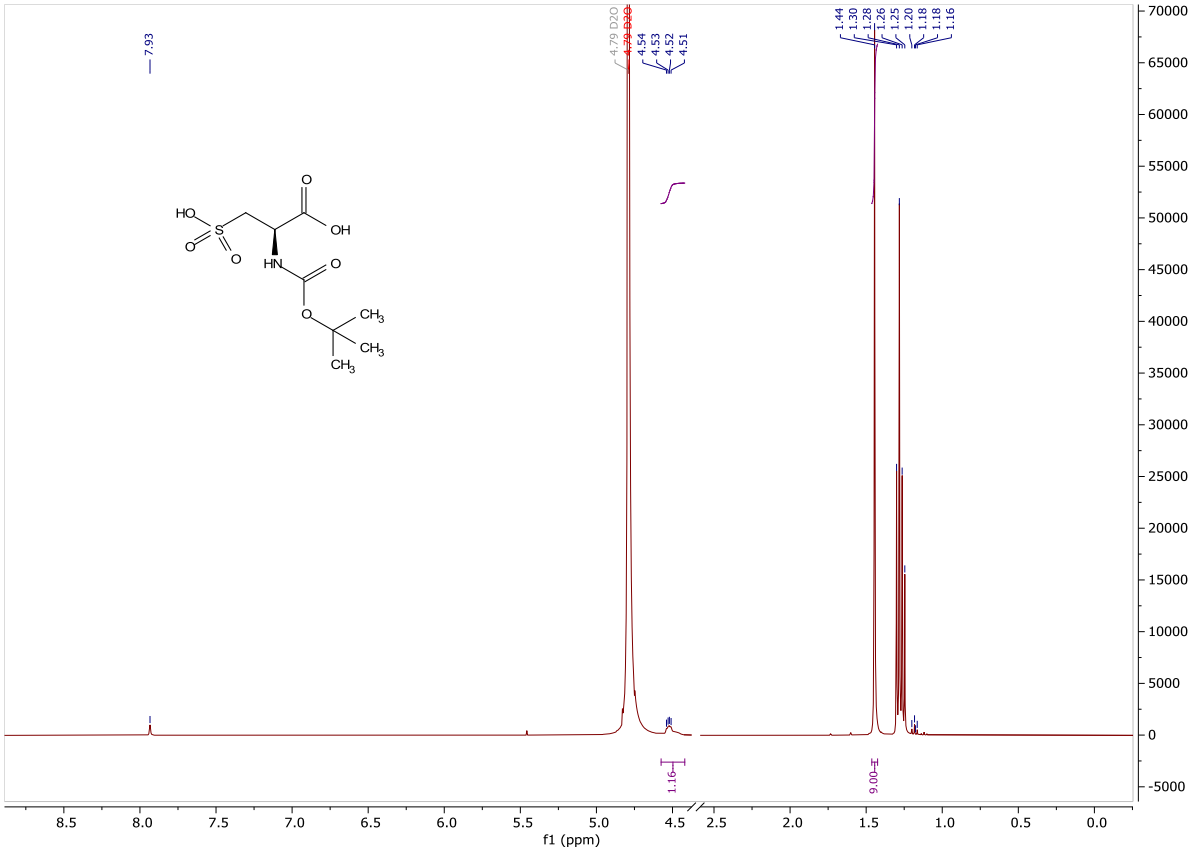

Appendix A: NMR

Figure A-8. ^{1}H NMR spectrum of 6-(3-((tert-butoxycarbonyl)amino)propoxy) quinoline-4-carboxylic acid (**6**)

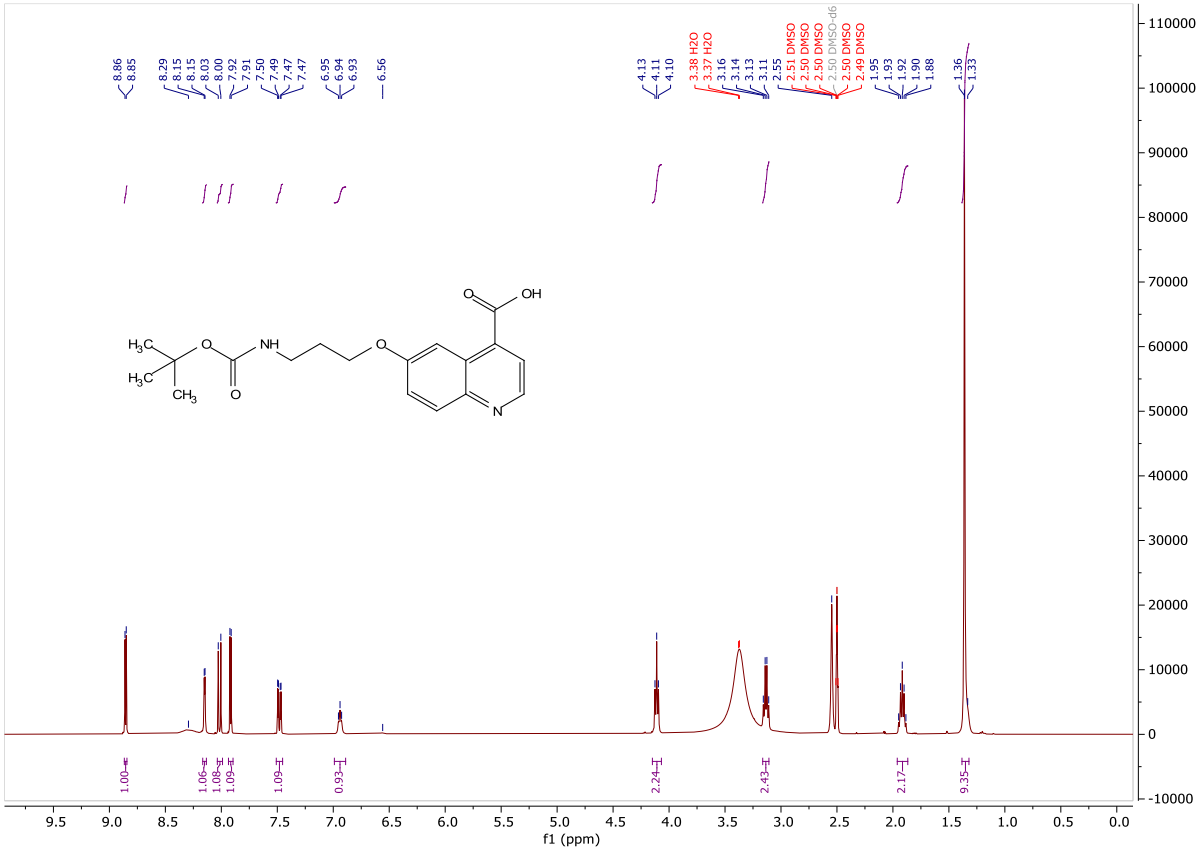

Appendix A: NMR

Figure A-9. ^{1}H NMR spectrum of tert-butyl (S)-(3-((4-((2-(2-cyano-4,4-difluoropyrrolidin-1-yl)-2-oxoethyl)carbamoyl)quinolin-6-yl)oxy)propyl)carbamate (**7**)

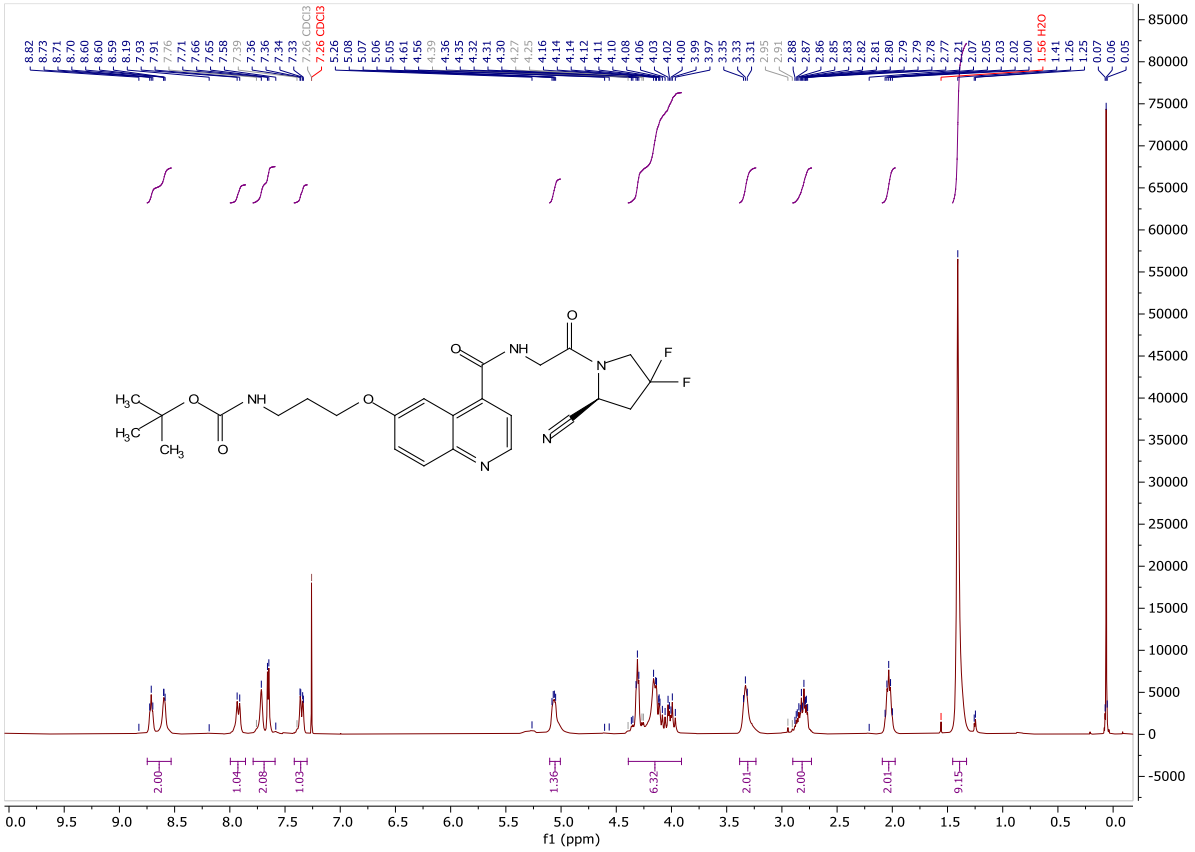

Appendix A: NMR

Figure A-10. ^{19}F NMR spectrum of tert-butyl (S)-(3-((4-((2-(2-cyano-4,4-difluoropyrrolidin-1-yl)-2-oxoethyl)carbamoyl)quinolin-6-yl)oxy)propyl)carbamate (**7**)

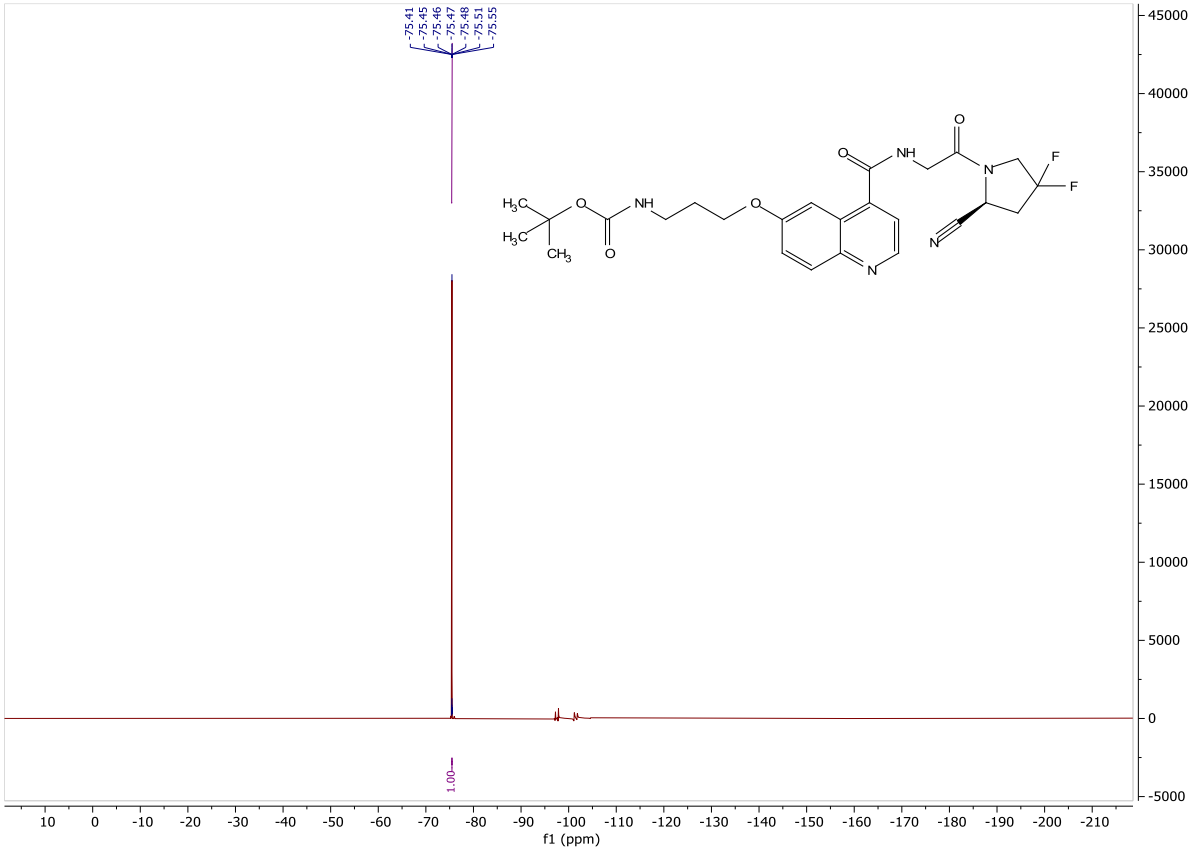

Appendix A: NMR

Figure A-11. ^{1}H NMR spectrum of (R)-2-((tert-butoxycarbonyl)amino)-3-((3-((4-((2-((S)-2-cyano-4,4-difluoropyrrolidin-1-yl)-2-oxoethyl)carbamoyl)quinolin-6-yl)oxy)propyl)amino)-3-oxopropane-1-sulfonic acid (**18**)

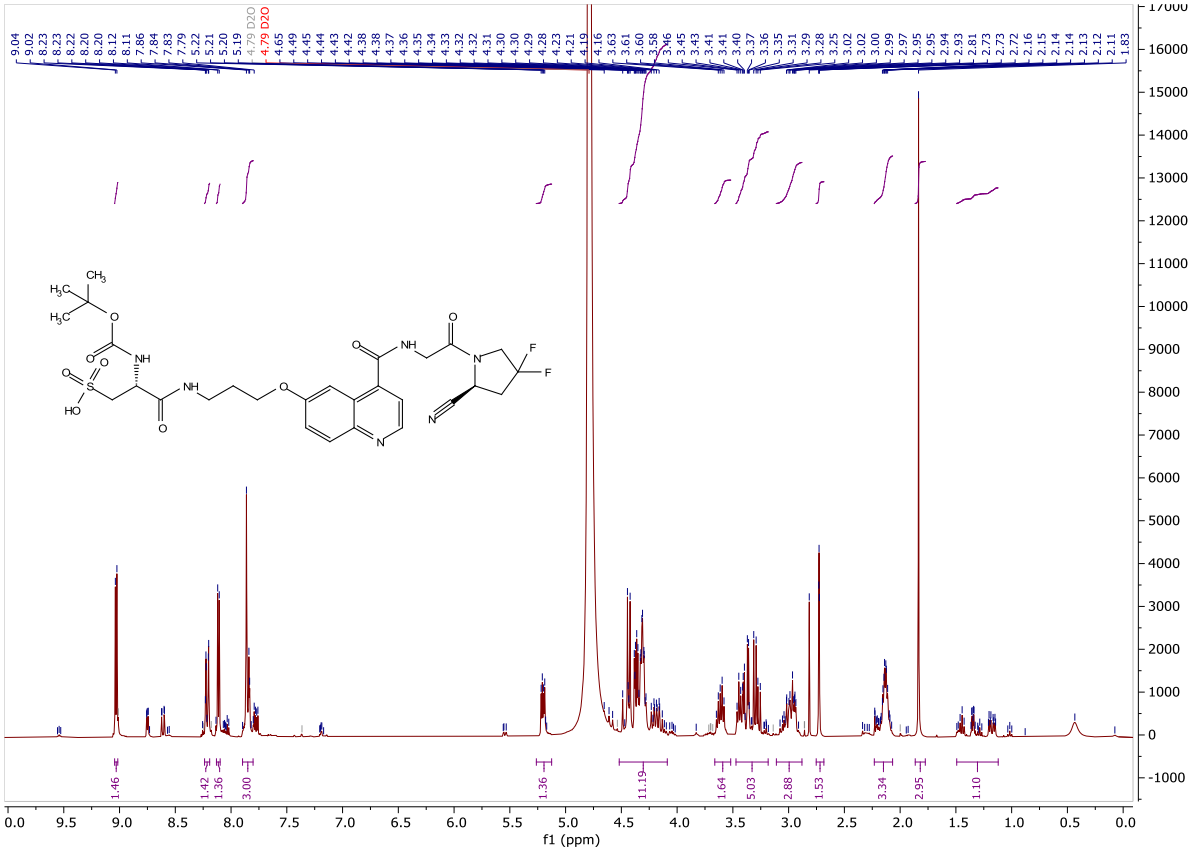

Appendix A: NMR

Figure A-12. ^{13}C NMR spectrum of (R)-2-((tert-butoxycarbonyl)amino)-3-((3-((4-((2-((S)-2-cyano-4,4-difluoropyrrolidin-1-yl)-2-oxoethyl)carbamoyl)quinolin-6-yl)oxy)propyl)amino)-3-oxopropane-1-sulfonic acid (**18**)

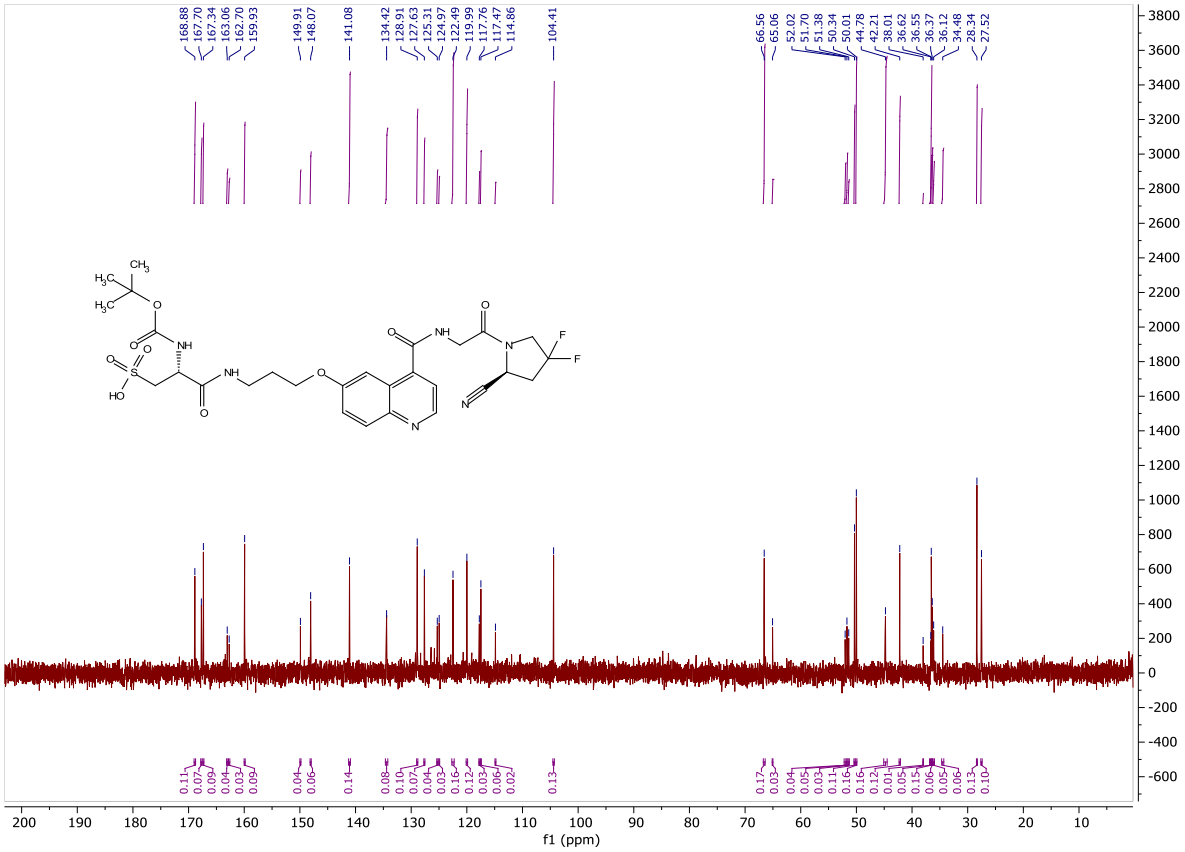

Appendix A: NMR

Figure A-13. ^{1}H NMR spectrum of (R)-3-((3-((4-((2-((S)-2-cyano-4,4-difluoropyrrolidin-1-yl)-2-oxoethyl)carbamoyl)quinolin-6-yl)oxy)propyl)amino)-2-(6-fluoronicotinamido)-3-oxopropane-1-sulfonic acid (**19**)

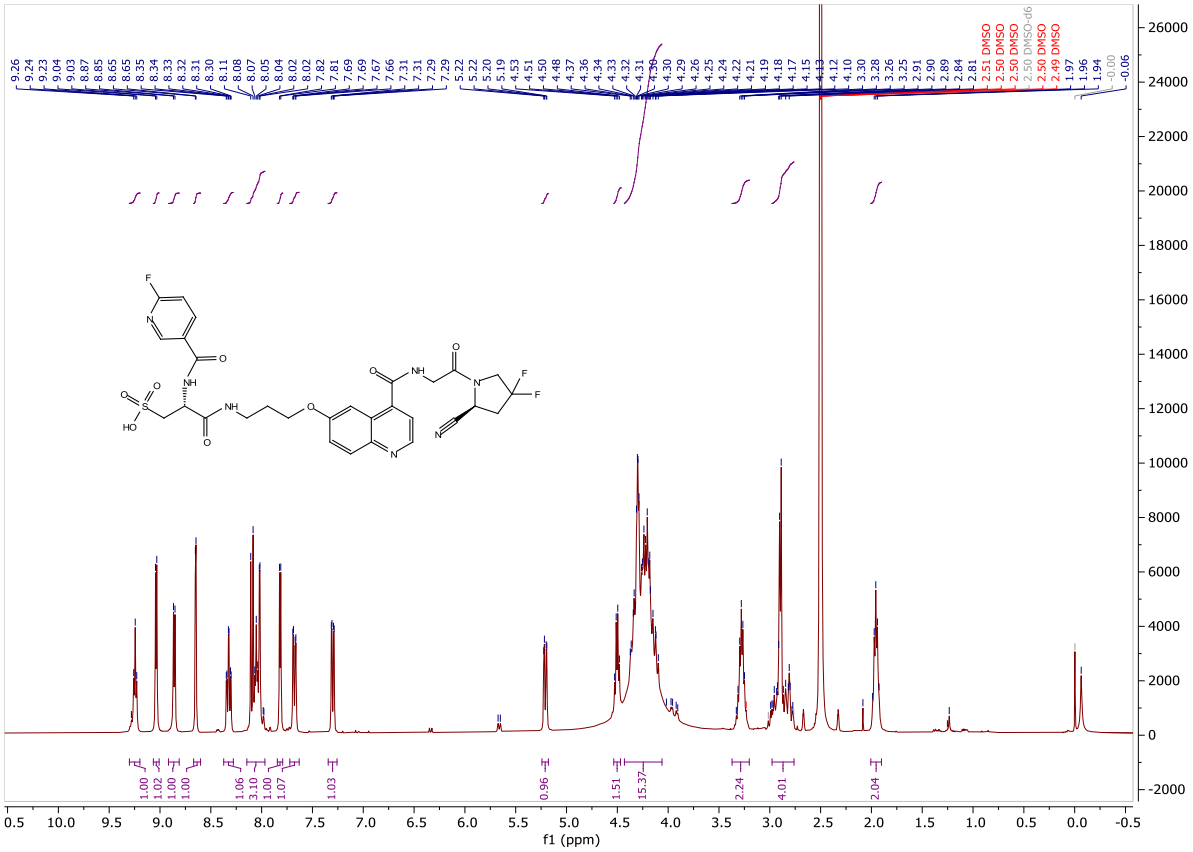

Appendix A: NMR

Figure A-14. ^{19}F NMR spectrum of (R)-3-((3-((4-((2-((S)-2-cyano-4,4-difluoropyrrolidin-1-yl)-2-oxoethyl)carbamoyl)quinolin-6-yl)oxy)propyl)amino)-2-(6-fluoronicotinamido)-3-oxopropane-1-sulfonic acid (**19**)

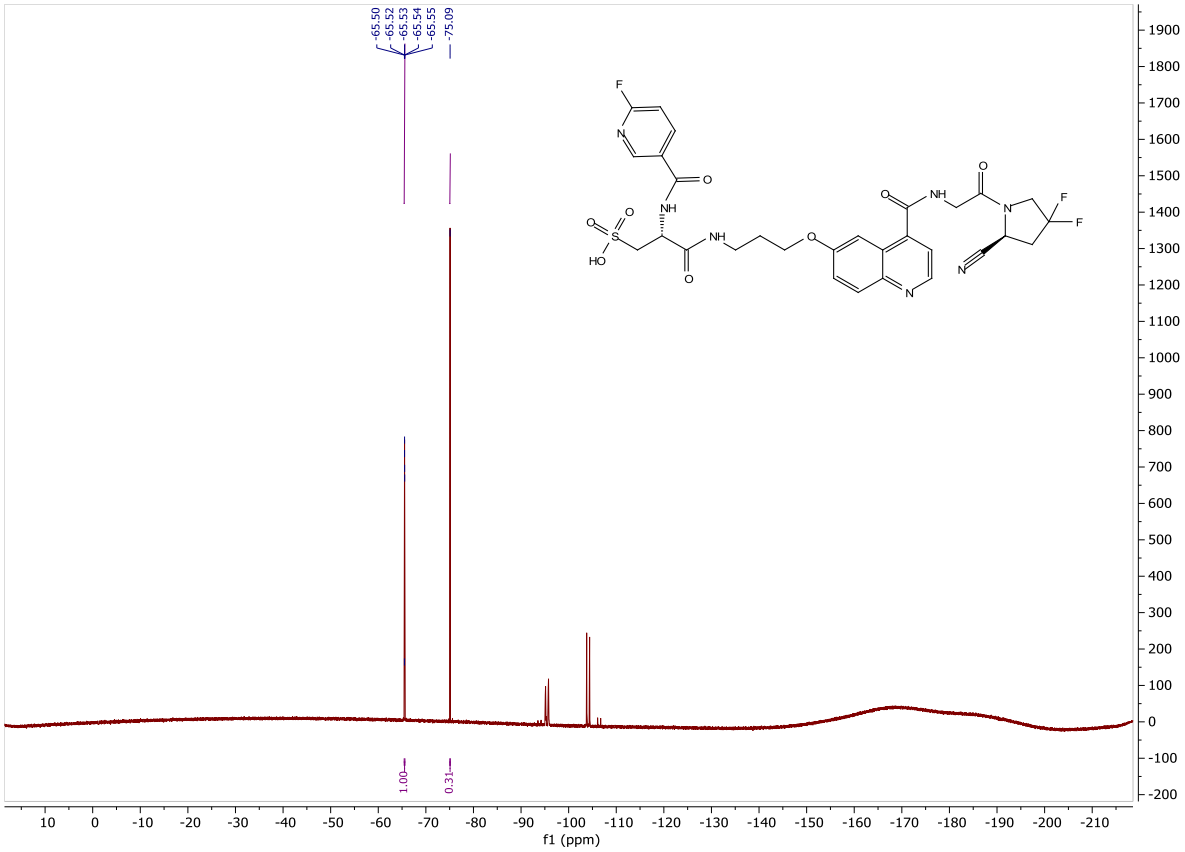

Appendix B: MS

Figure B-1. MS of 6-hydroxyquinoline-4-carboxylic acid (**3**)

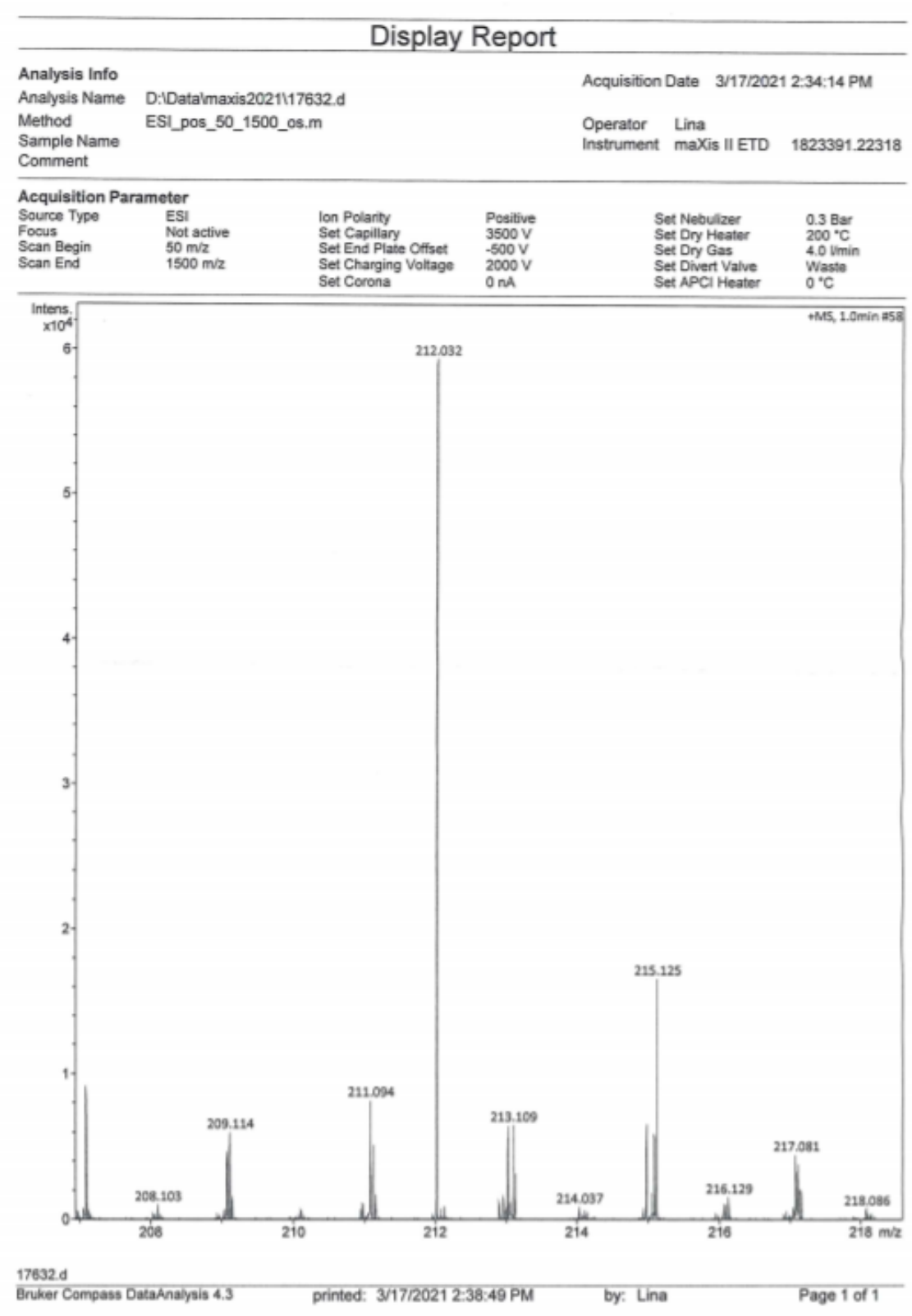

Appendix B: MS

Figure B-2. MS of tert-butyl (S)-(2-(2-carbamoyl-4,4-difluoropyrrolidin-1-yl)-2-oxoethyl)carbamate (**15**)

MS Spectrum Report

Analysis Info

Sample Name
Method ESI_pos_50_1500_os.m

Acquisition Date 4/28/2021 9:39:04 AM
Analysis Name D:\Data\maxis2021\17766.d

Acquisition Parameter

Source Type	ESI	Ion Polarity	Positive	Set Nebulizer	0.3 Bar
Focus	Not active	Set Capillary	3500 V	Set Dry Heater	200 °C
Scan Begin	50 m/z	Set End Plate Offset	-500 V	Set Dry Gas	4.0 l/min
Scan End	1500 m/z	Set Charging Voltage	2000 V	Set Divert Valve	Waste
		Set Corona	0 nA	Set APCI Heater	0 °C

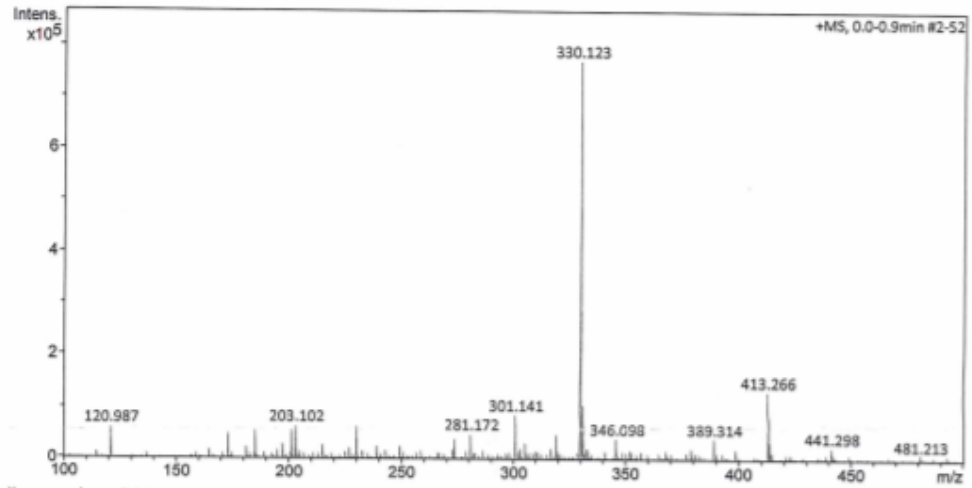

#	m/z	I %
1	120.987	7.9
2	173.078	6.6
3	185.115	7.4
4	197.085	3.8
5	201.110	7.7
6	203.102	8.4
7	215.095	3.5
8	230.071	8.4
9	239.162	3.5
10	274.061	5.0
11	281.172	6.4
12	301.141	11.2
13	305.245	4.0
14	319.261	6.4
15	330.123	100.0
16	331.127	13.8
17	346.098	5.3
18	389.314	5.3
19	413.266	17.2
20	414.270	4.5

17766.d
Bruker Compass DataAnalysis 4.3 printed: 4/28/2021 9:43:29 AM Page 1 of 1

Appendix B: MS

Figure B-3. MS of tert-butyl (S)-(2-2-cyano-4,4-difluoropyrrolidin-1-yl)-2-oxoethyl)carbamate (**16**)

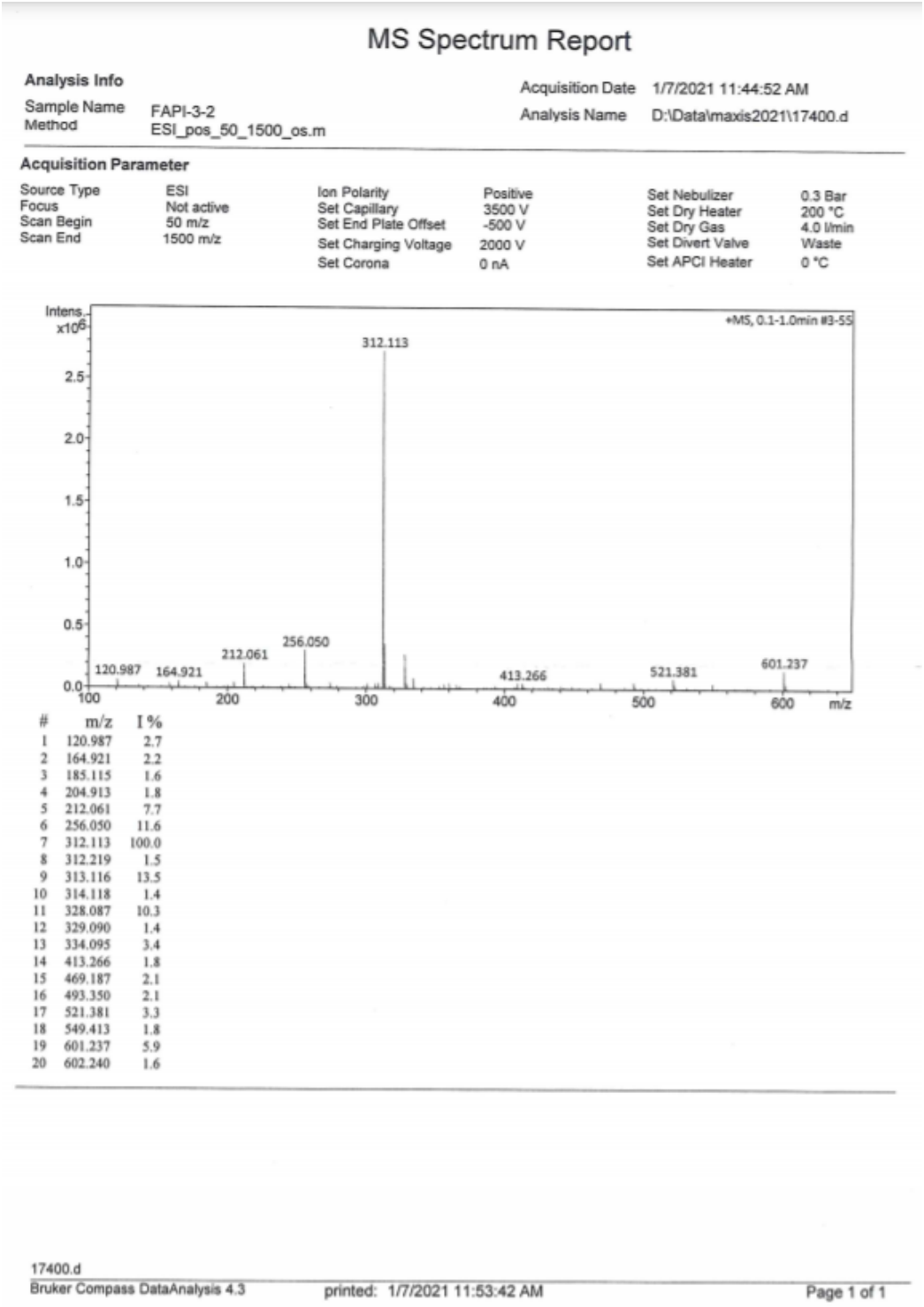

MS Spectrum Report

Analysis Info

Sample Name	FAPI-3-2	Acquisition Date	1/7/2021 11:44:52 AM
Method	ESI_pos_50_1500_os.m	Analysis Name	D:\Data\maxis2021\17400.d

Acquisition Parameter

Source Type	ESI	Ion Polarity	Positive	Set Nebulizer	0.3 Bar
Focus	Not active	Set Capillary	3500 V	Set Dry Heater	200 °C
Scan Begin	50 m/z	Set End Plate Offset	-500 V	Set Dry Gas	4.0 l/min
Scan End	1500 m/z	Set Charging Voltage	2000 V	Set Divert Valve	Waste
		Set Corona	0 nA	Set APCI Heater	0 °C

#	m/z	I %
1	120.987	2.7
2	164.921	2.2
3	185.115	1.6
4	204.913	1.8
5	212.061	7.7
6	256.050	11.6
7	312.113	100.0
8	312.219	1.5
9	313.116	13.5
10	314.118	1.4
11	328.087	10.3
12	329.090	1.4
13	334.095	3.4
14	413.266	1.8
15	469.187	2.1
16	493.350	2.1
17	521.381	3.3
18	549.413	1.8
19	601.237	5.9
20	602.240	1.6

17400.d
Bruker Compass DataAnalysis 4.3 printed: 1/7/2021 11:53:42 AM Page 1 of 1

Appendix B: MS

Figure B-4. MS of (S)-4,4-difluoro-1-glycylpyrrolidine-2-carbonitrile (**13**)

MS Spectrum Report

Analysis Info

Sample Name
Method ESI_pos_50_1500_os.m

Acquisition Date 3/30/2021 9:10:38 AM
Analysis Name D:\Data\maxis2021\17680.d

Acquisition Parameter

Source Type	ESI	Ion Polarity	Positive	Set Nebulizer	0.3 Bar
Focus	Not active	Set Capillary	3500 V	Set Dry Heater	200 °C
Scan Begin	50 m/z	Set End Plate Offset	-500 V	Set Dry Gas	4.0 l/min
Scan End	1500 m/z	Set Charging Voltage	2000 V	Set Divert Valve	Waste
		Set Corona	0 nA	Set APCI Heater	0 °C

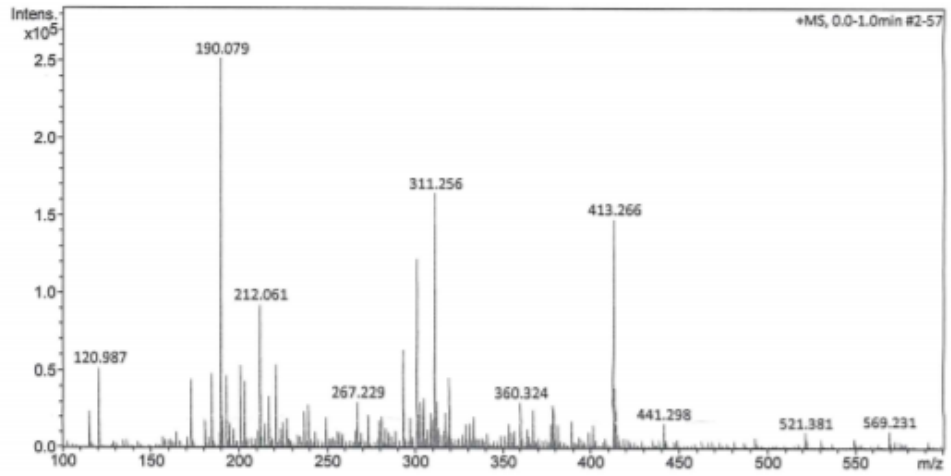

#	m/z	I %
1	120.987	20.6
2	173.078	17.9
3	185.115	19.2
4	190.079	100.0
5	193.070	18.8
6	201.110	21.2
7	203.102	17.3
8	212.061	36.8
9	216.991	13.5
10	221.065	21.6
11	267.229	12.1
12	293.122	25.3
13	301.141	48.7
14	305.245	13.2
15	311.256	65.3
16	312.259	12.3
17	319.261	18.0
18	360.324	12.1
19	413.266	58.7
20	414.270	15.5

17680.d
Bruker Compass DataAnalysis 4.3 printed: 3/30/2021 9:15:12 AM Page 1 of 1

Appendix B: MS

Figure B-5. MS of 3-((tert-butoxycarbonyl)amino)propyl methanesulfonate **(12)**

MS Spectrum Report

Analysis Info

Sample Name	Mesylat-propylkjede (b2)	Acquisition Date	4/8/2021 8:40:10 AM
Method	ESI_pos_50_1500_os.m	Analysis Name	D:\Data\maxis2021\17696.d

Acquisition Parameter

Source Type	ESI	Ion Polarity	Positive	Set Nebulizer	0.3 Bar
Focus	Not active	Set Capillary	3500 V	Set Dry Heater	200 °C
Scan Begin	50 m/z	Set End Plate Offset	-500 V	Set Dry Gas	4.0 l/min
Scan End	1500 m/z	Set Charging Voltage	2000 V	Set Divert Valve	Waste
		Set Corona	0 nA	Set APCI Heater	0 °C

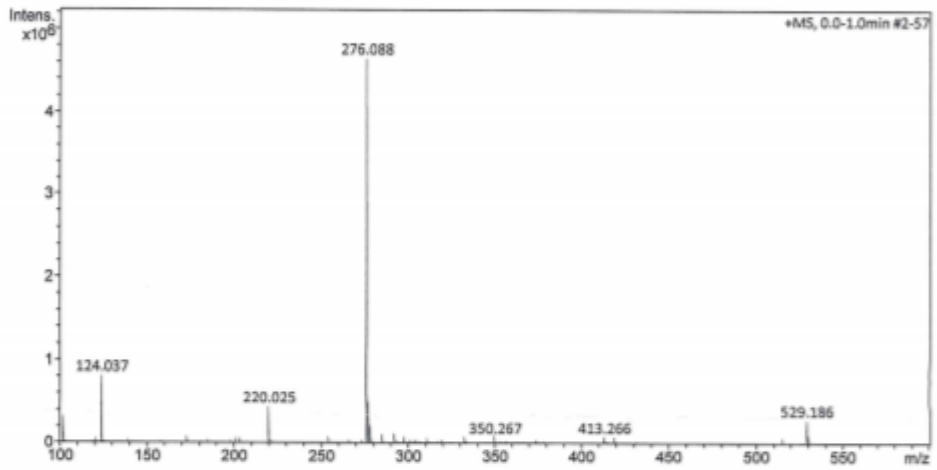

#	m/z	I %
1	102.055	7.1
2	124.037	17.4
3	173.078	1.1
4	220.025	9.5
5	254.173	1.1
6	276.088	100.0
7	276.187	2.0
8	277.091	11.1
9	278.084	4.9
10	285.146	2.4
11	292.062	2.5
12	298.070	1.2
13	311.256	1.0
14	333.146	1.2
15	350.267	1.4
16	413.266	1.6
17	419.182	1.5
18	515.153	0.9
19	529.186	6.2
20	530.189	1.3

17696.d
Bruker Compass DataAnalysis 4.3 printed: 4/8/2021 8:45:32 AM Page 1 of 1

Appendix B: MS

Figure B-6. MS of 3-((tert-butoxycarbonyl)amino)propyl 6-(3-((tert-butoxycarbonyl)amino)propoxy)quinoline-4-carboxylate (**11**)

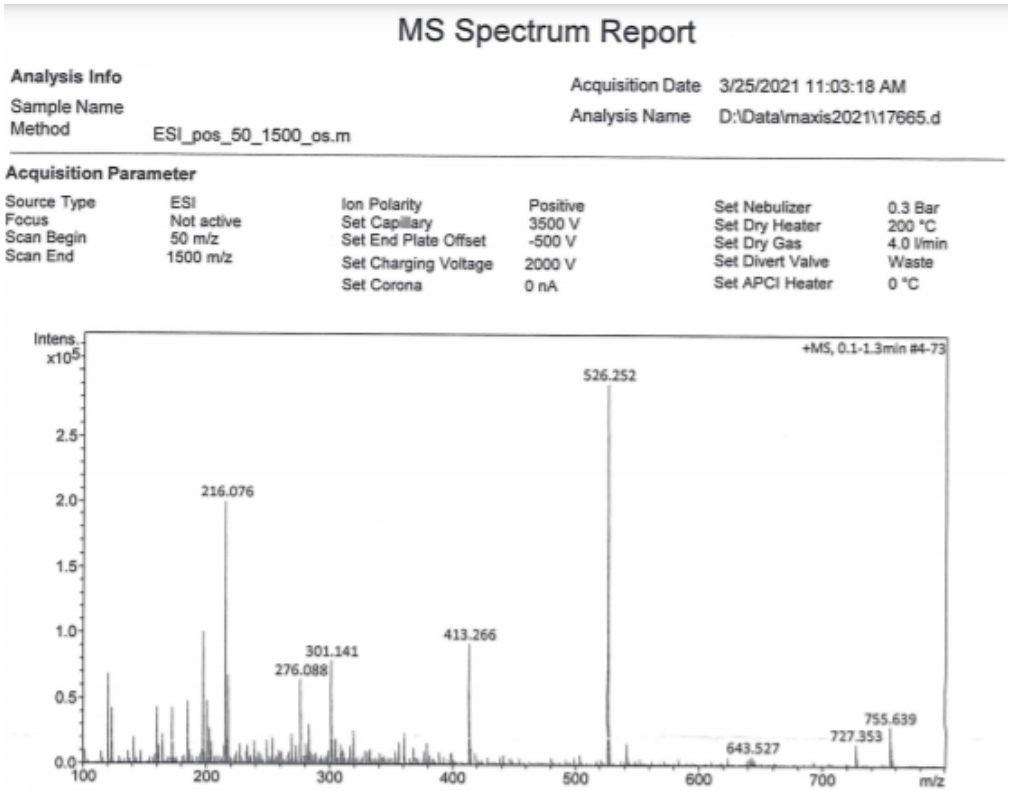

#	m/z	I %
1	120.988	23.6
2	124.037	14.8
3	160.014	15.0
4	173.079	15.2
5	185.115	16.6
6	198.110	34.8
7	201.110	16.7
8	203.102	9.7
9	216.076	68.9
10	218.073	23.4
11	276.088	22.2
12	283.224	10.7
13	301.141	27.2
14	319.261	9.0
15	360.324	8.4
16	413.266	31.8
17	414.270	8.4
18	526.252	100.0
19	527.256	29.5
20	755.639	10.5

17665.d
Bruker Compass DataAnalysis 4.3 printed: 3/25/2021 11:17:23 AM Page 1 of 1

Appendix B: MS

Figure B-7. LC-MS of 6-(3-((tert-butoxycarbonyl)amino)propoxy) quinoline-4-carboxylic acid (**6**)

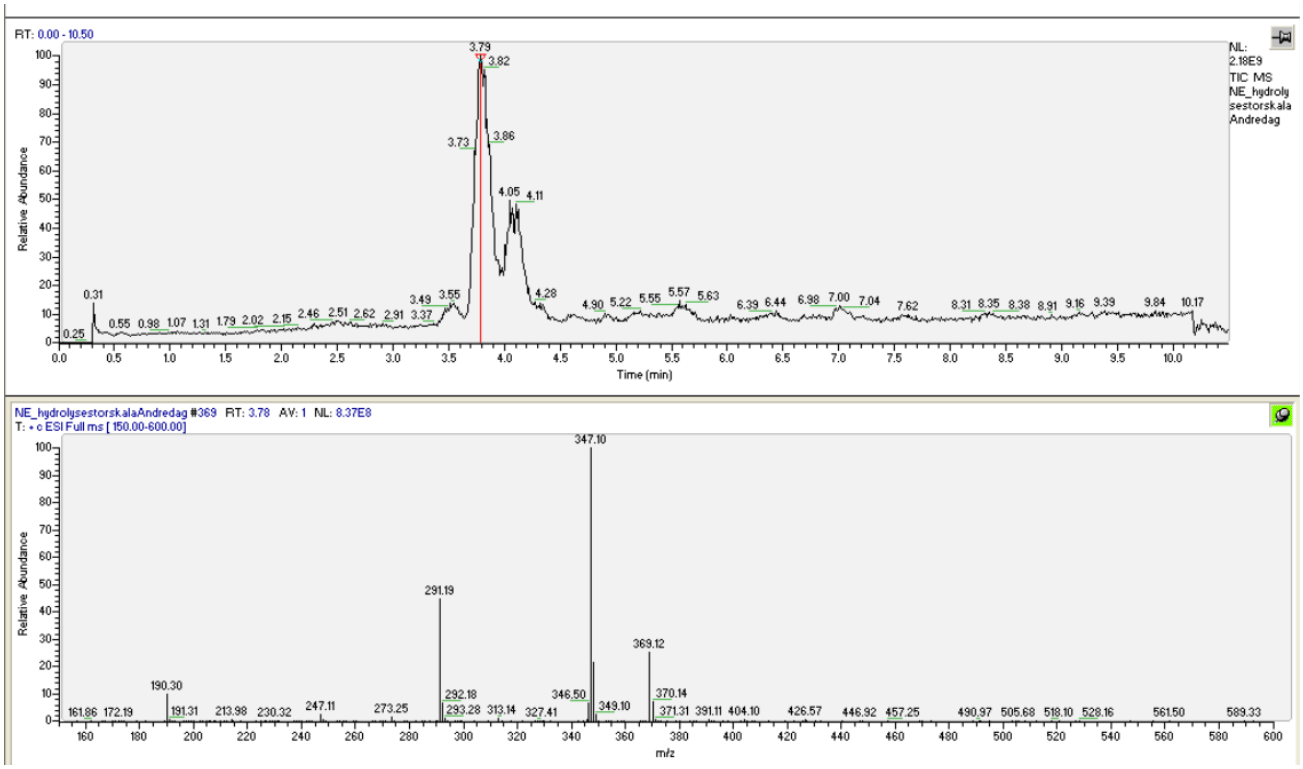

Appendix B: MS

Figure B-8. LC-MS of tert-butyl (S)-(3-((4-((2-(2-cyano-4,4-difluoropyrrolidin-1-yl)-2-oxoethyl)carbamoyl)quinolin-6-yl)oxy)propyl)carbamate (**7**)

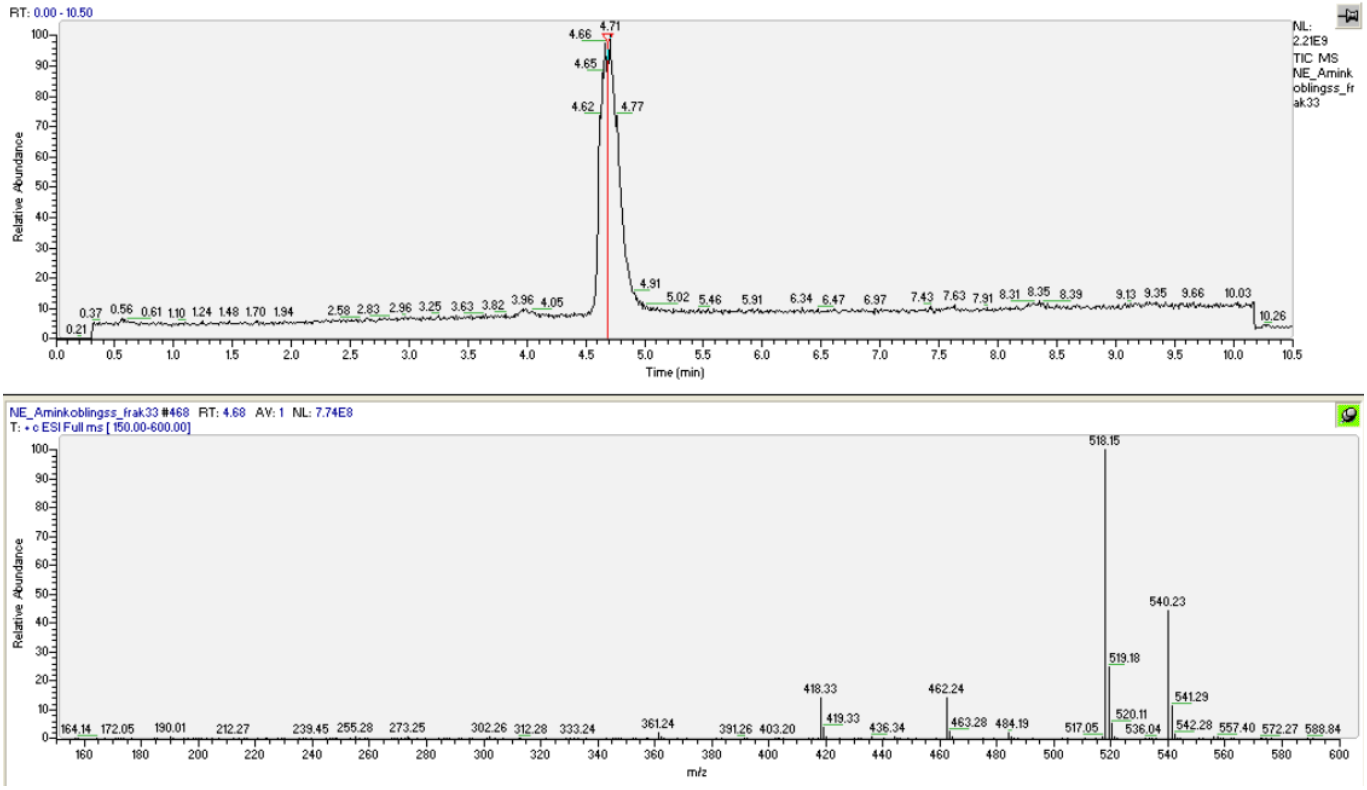

Appendix B: MS

Figure B-9. LC-MS of (S)-6-(3-aminopropoxy)-N-(2-(2-cyano-4,4-difluoropyrrolidin-1-yl)-2-oxoethyl)quinoline-4-carboxamide (**8**)

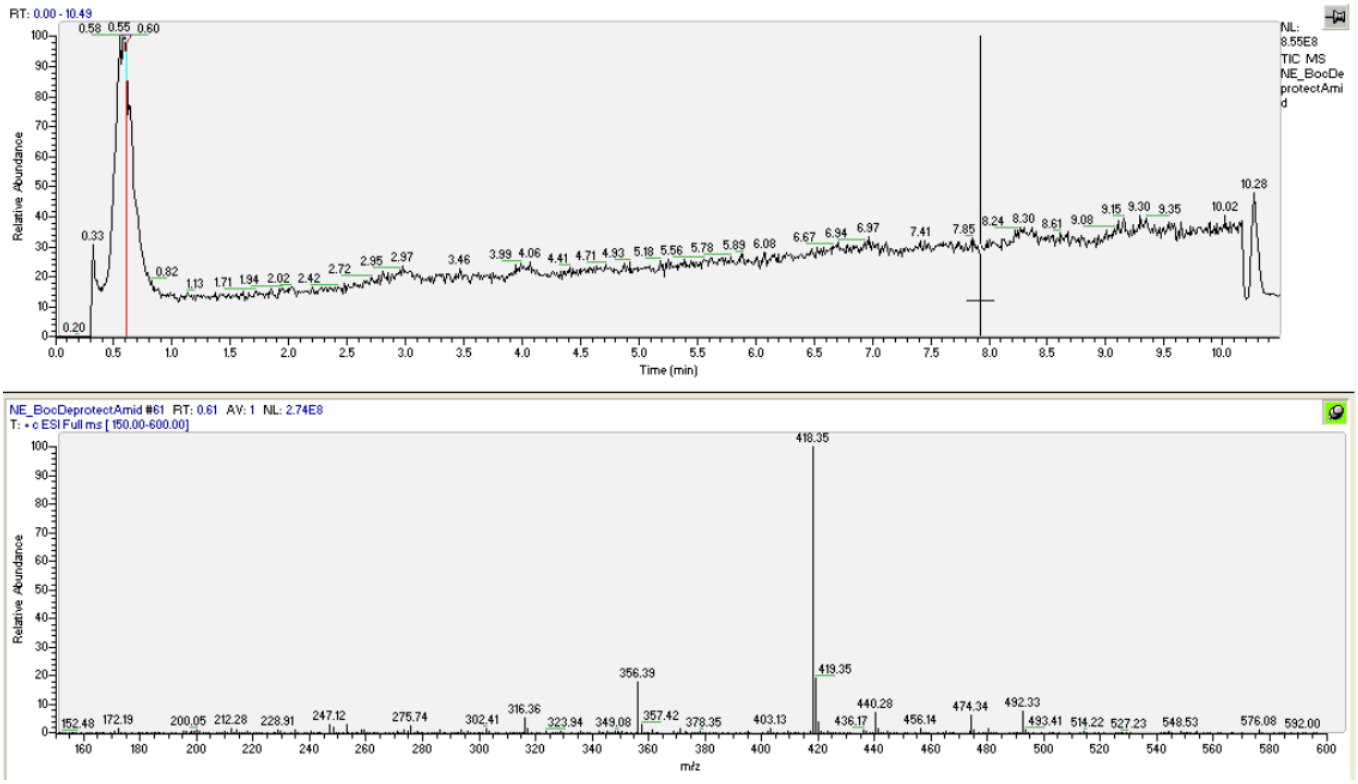

Appendix B: MS

Figure B-10. LC-MS of (R)-2-((tert-butoxycarbonyl)amino)-3-((3-((4-((2-((S)-2-cyano-4,4-difluoropyrrolidin-1-yl)-2-oxoethyl)carbamoyl)quinolin-6-yl)oxy)propyl)amino)-3-oxopropane-1-sulfonic acid (**18**)

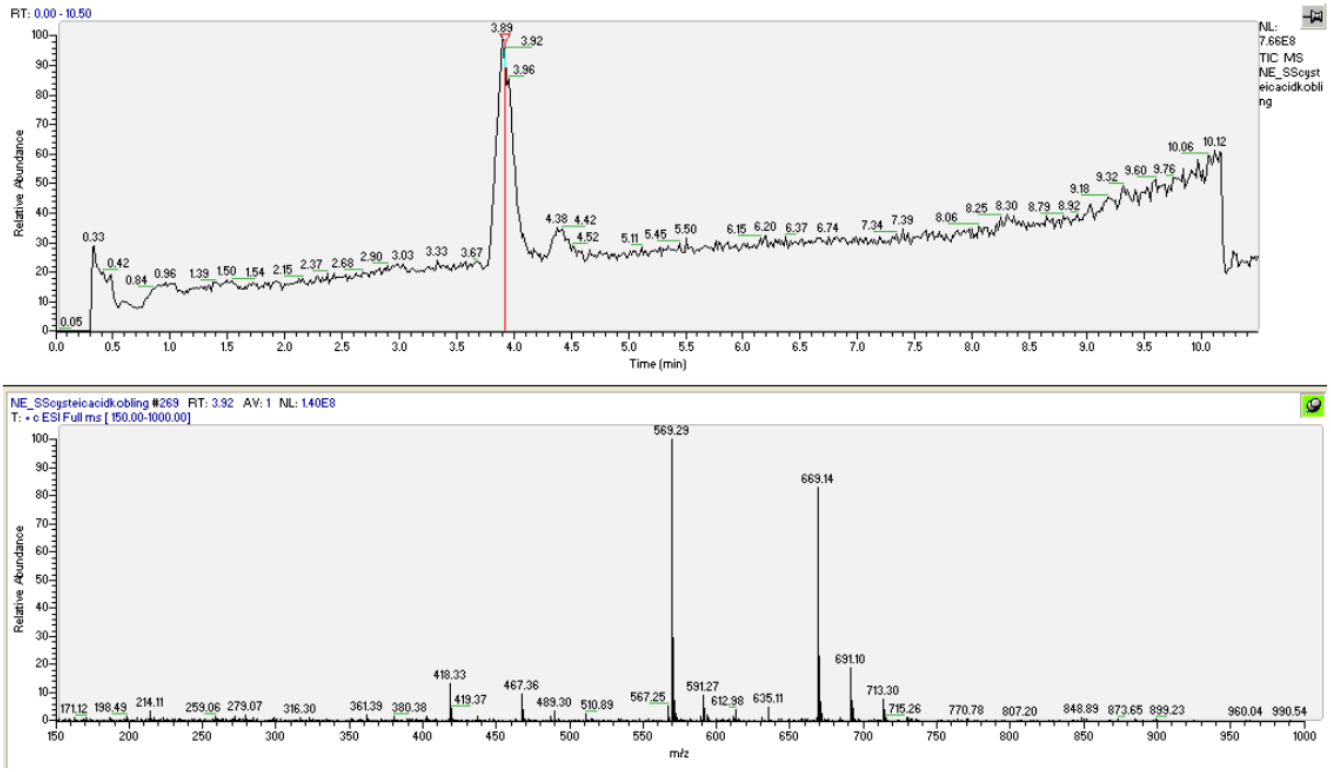

Appendix C: HRMS

Figure C-1. HRMS spectrum of (R)-2-amino-3-((3-((4-((2-((S)-2-cyano-4,4-difluoropyrrolidin-1-yl)-2-oxoethyl)carbamoyl)quinolin-6-yl)oxy)propyl)amino)-3-oxopropane-1-sulfonic acid (**1**)

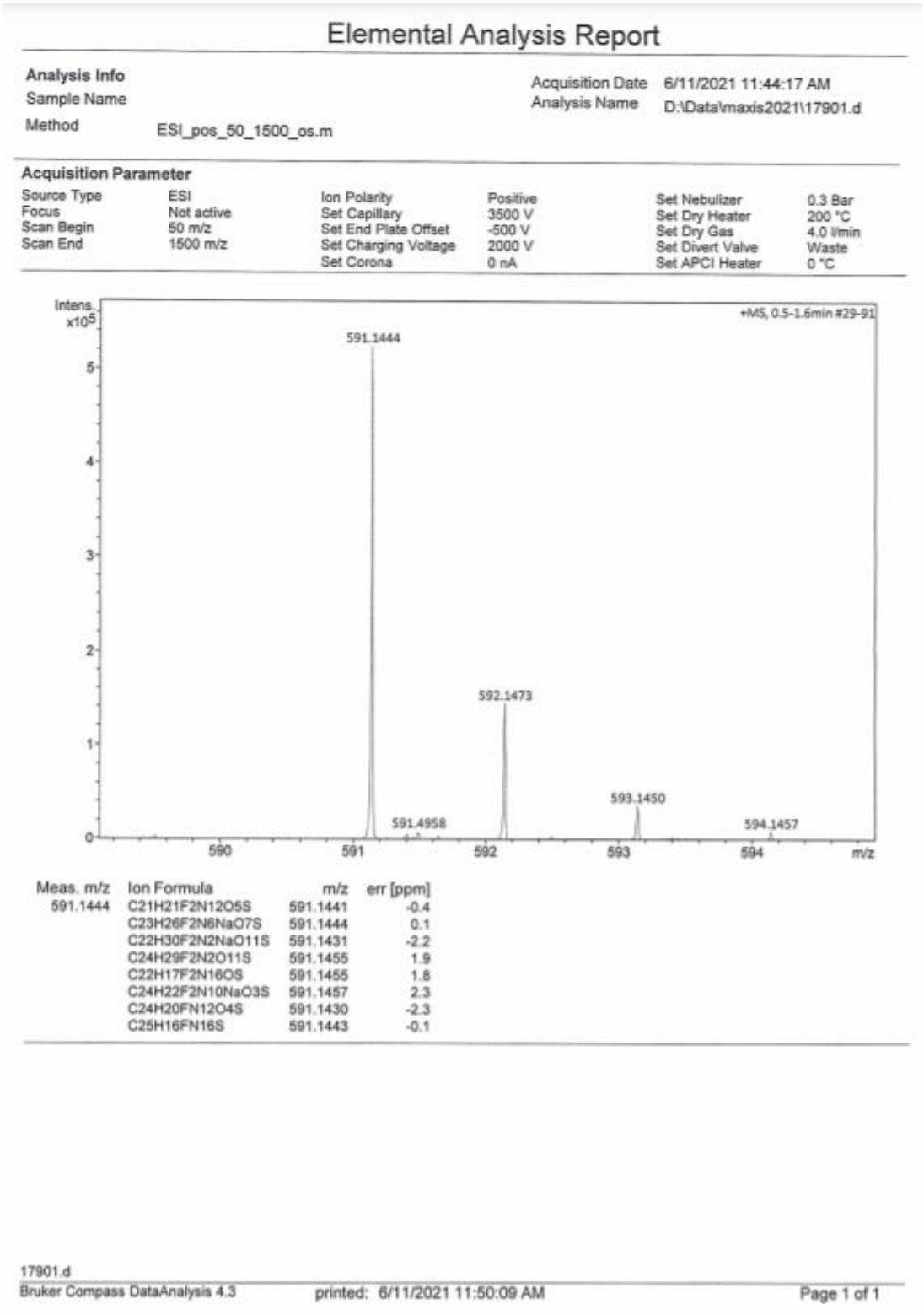

Appendix C: HRMS

Figure C-2. HRMS spectrum of (R)-3-((3-((4-((2-((S)-2-cyano-4,4-difluoropyrrolidin-1-yl)-2-oxoethyl)carbamoyl)quinolin-6-yl)oxy)propyl)amino)-2-(6-fluoronicotinamido)-3-oxopropane-1-sulfonic acid (**19**)

Elemental Analysis Report

Analysis Info

Sample Name	Referansestandard(ny)	Acquisition Date	6/14/2021 9:13:17 AM
Method	ESI_pos_50_1500_os.m	Analysis Name	D:\Data\maxis2021\17905.d

Acquisition Parameter

Source Type	ESI	Ion Polarity	Positive	Set Nebulizer	0.3 Bar
Focus	Not active	Set Capillary	3500 V	Set Dry Heater	200 °C
Scan Begin	50 m/z	Set End Plate Offset	-500 V	Set Dry Gas	4.0 l/min
Scan End	1500 m/z	Set Charging Voltage	2000 V	Set Divert Valve	Waste
		Set Corona	0 nA	Set APCI Heater	0 °C

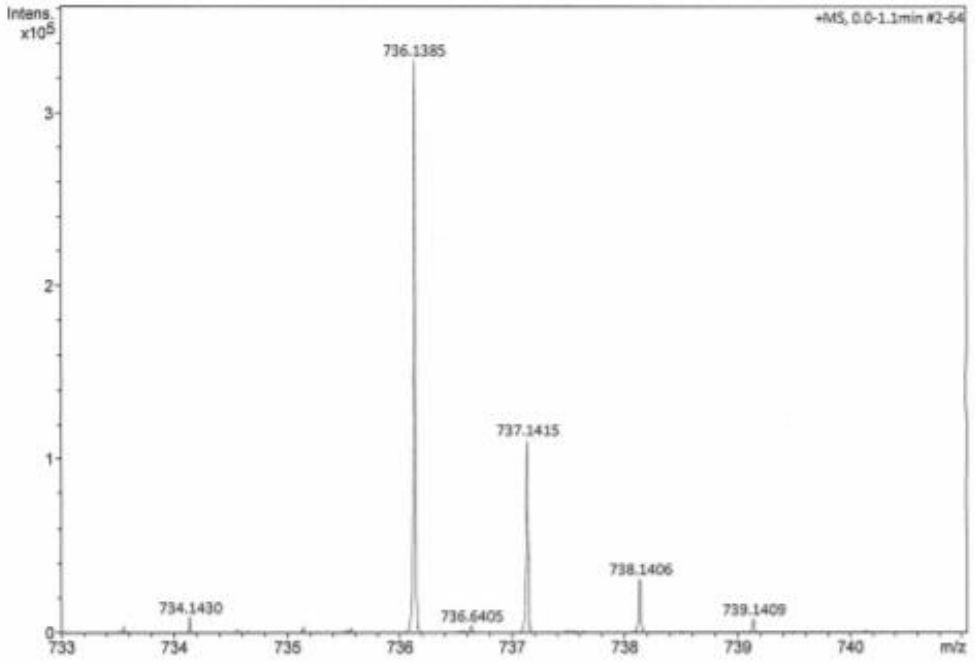

Meas. m/z	Ion Formula	m/z	err [ppm]
736.1385	C24H14F3N23NaS	736.1368	-2.4
	C24H21F3N15O8S	736.1365	-2.8
	C26H19F3N17Na2O2S	736.1370	-2.0
	C25H17F3N19O4S	736.1378	-1.0
	C26H26F3N9NaO10S	736.1368	-2.4
	C27H22F3N13NaO6S	736.1381	-0.6
	C28H31F3N3Na2O12S	736.1370	-2.0
	C29H27F3N7Na2O8S	736.1384	-0.2
	C27H29F3N5O14S	736.1378	-0.9
	C28H25F3N9O10S	736.1392	0.9
	C30H30F3N3NaO12S	736.1394	1.2
	C26H13F3N23S	736.1392	0.9
	C28H18F3N17NaO2S	736.1394	1.2
	C26H33F3NO18S	736.1365	-2.8
	C29H21F3N13O6S	736.1405	2.7
	C30H23F3N11Na2O4S	736.1397	1.6
	C40H21F3N7O3S	736.1373	-1.6
	C42H26F3NNaO5S	736.1376	-1.3
	C41H23F3N5Na2OS	736.1365	-2.7

17905.d
Bruker Compass DataAnalysis 4.3 printed: 6/14/2021 9:20:14 AM Page 1 of 2

Appendix D: Prep-HPLC

Figure D-1. Prep-HPLC of (S)-4,4-difluoro-1-glycylpyrrolidine-2-carbonitrile (**13**)

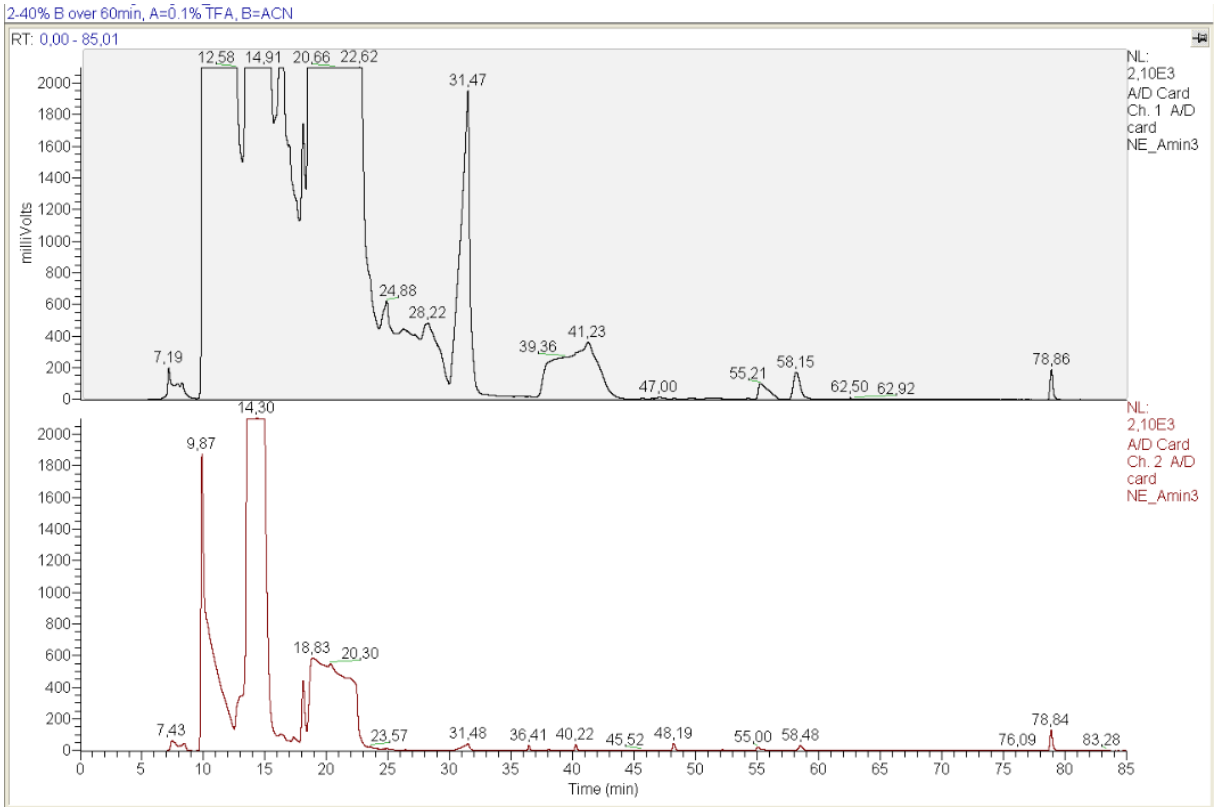

Appendix D: Prep-HPLC

Figure D-2. Prep-HPLC of 6-(3-((tert-butoxycarbonyl)amino)propoxy) quinoline-4-carboxylic acid (**6**)

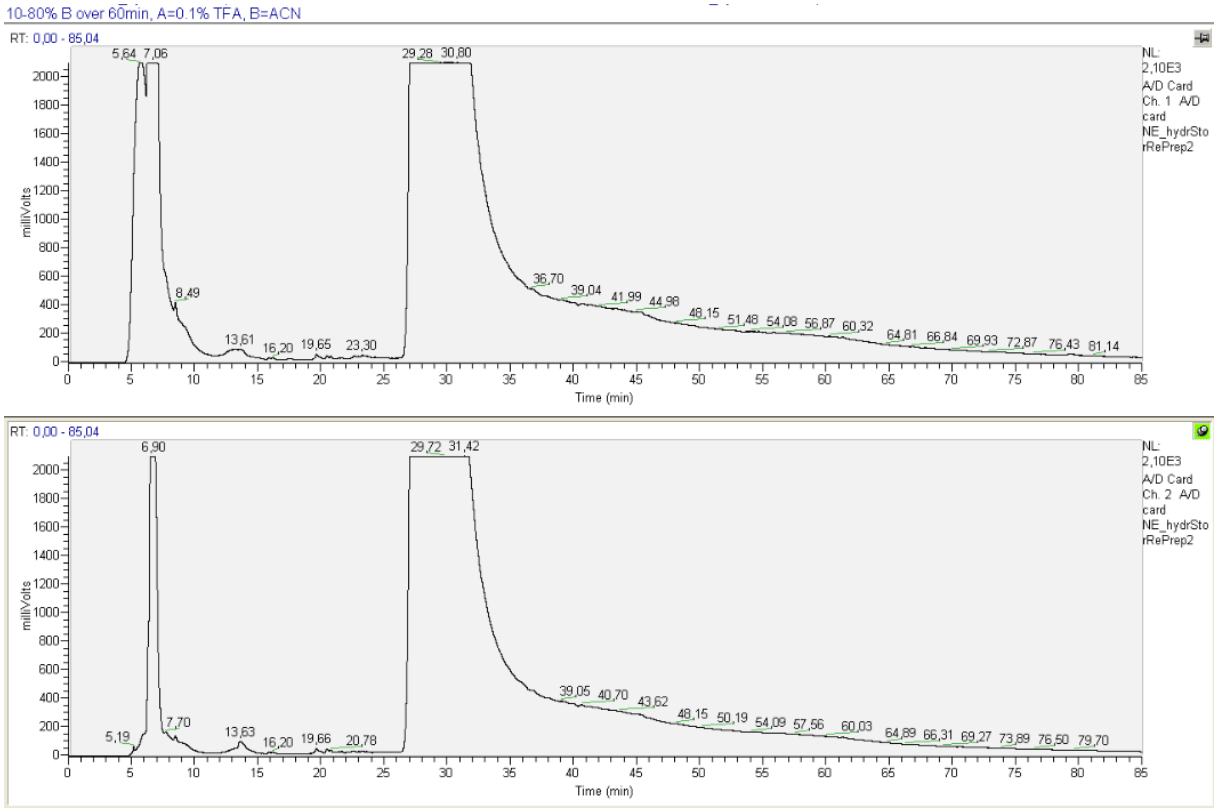

Appendix D: Prep-HPLC

Figure D-3. Prep-HPLC of tert-butyl (S)-(3-((4-((2-(2-cyano-4,4-difluoropyrrolidin-1-yl)-2-oxoethyl)carbamoyl)quinolin-6-yl)oxy)propyl)carbamate (**7**)

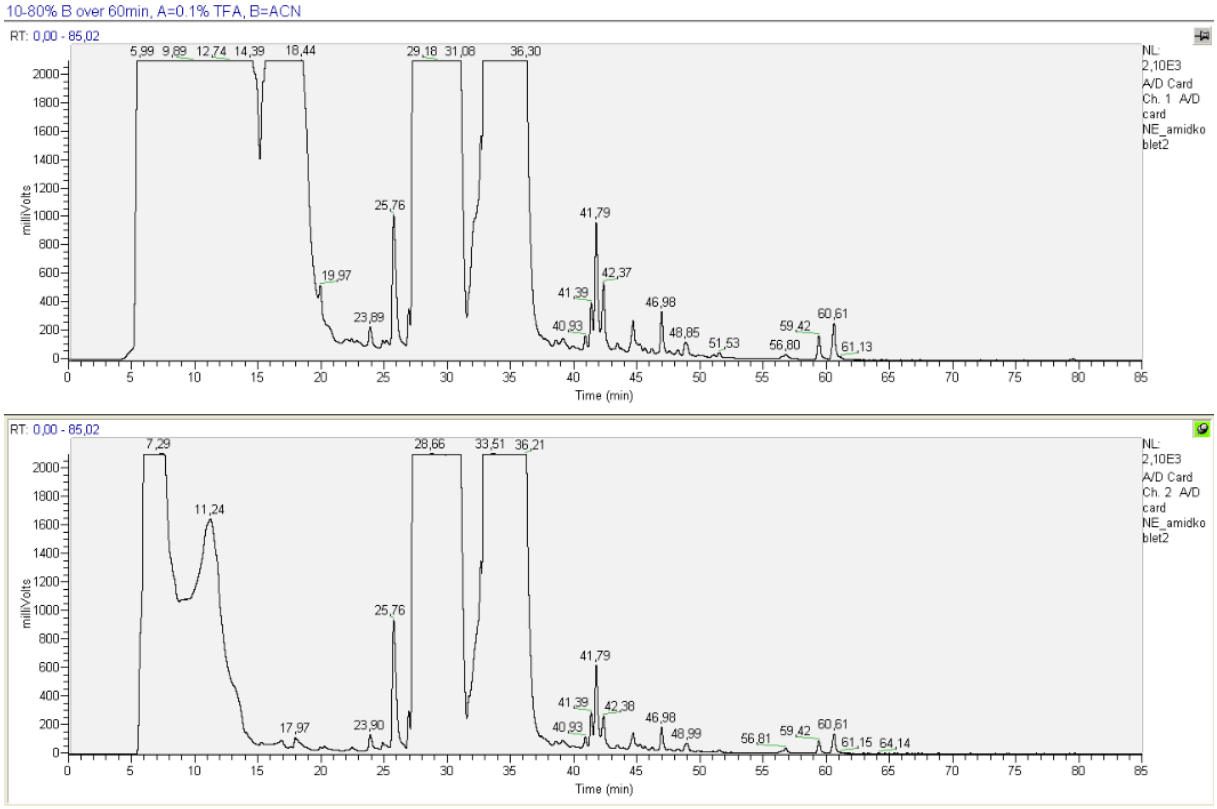

Appendix D: Prep-HPLC

Figure D-4. Prep-HPLC of (R)-2-amino-3-((3-((4-((2-((S)-2-cyano-4,4-difluoropyrrolidin-1-yl)-2-oxoethyl)carbamoyl)quinolin-6-yl)oxy)propyl)amino)-3-oxopropane-1-sulfonic acid (**1**)

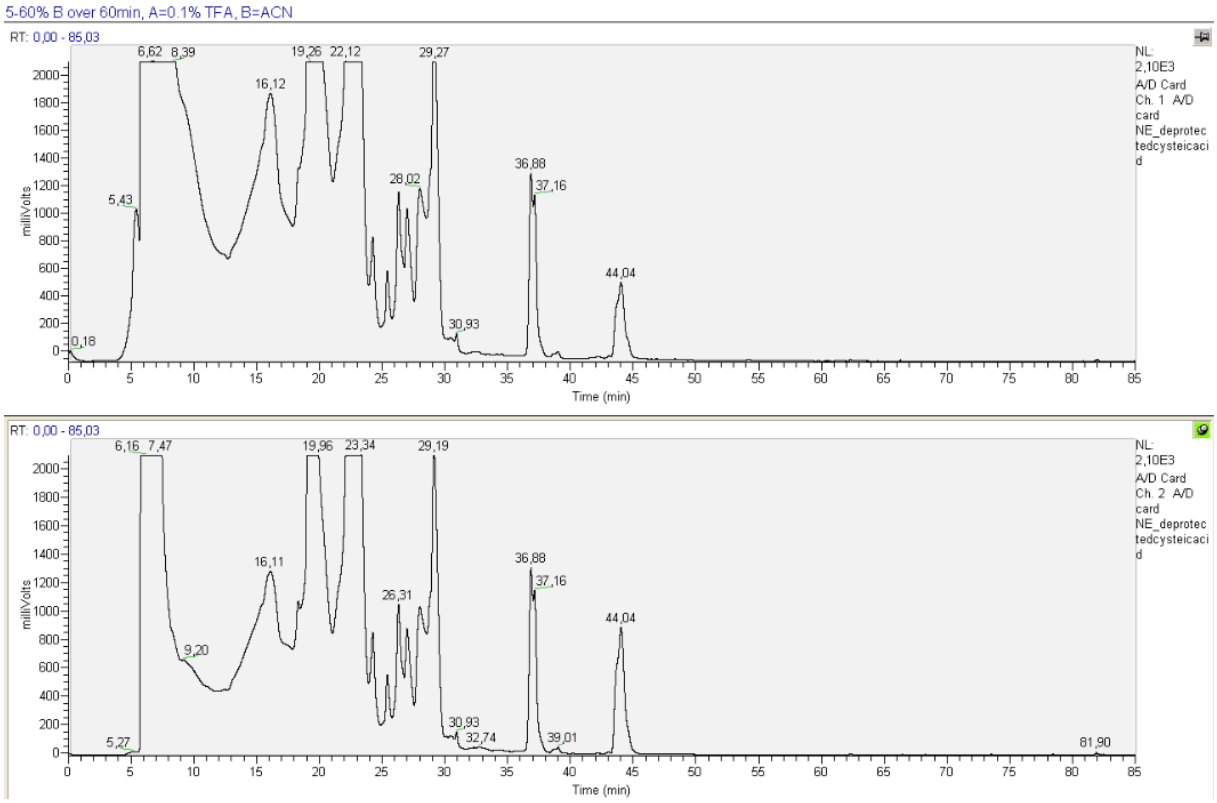

Appendix D: Prep-HPLC

Figure D-5. Prep-HPLC of (R)-3-((3-((4-((2-((S)-2-cyano-4,4-difluoropyrrolidin-1-yl)-2-oxoethyl)carbamoyl)quinolin-6-yl)oxy)propyl)amino)-2-(6-fluoronicotinamido)-3-oxopropane-1-sulfonic acid (**19**)

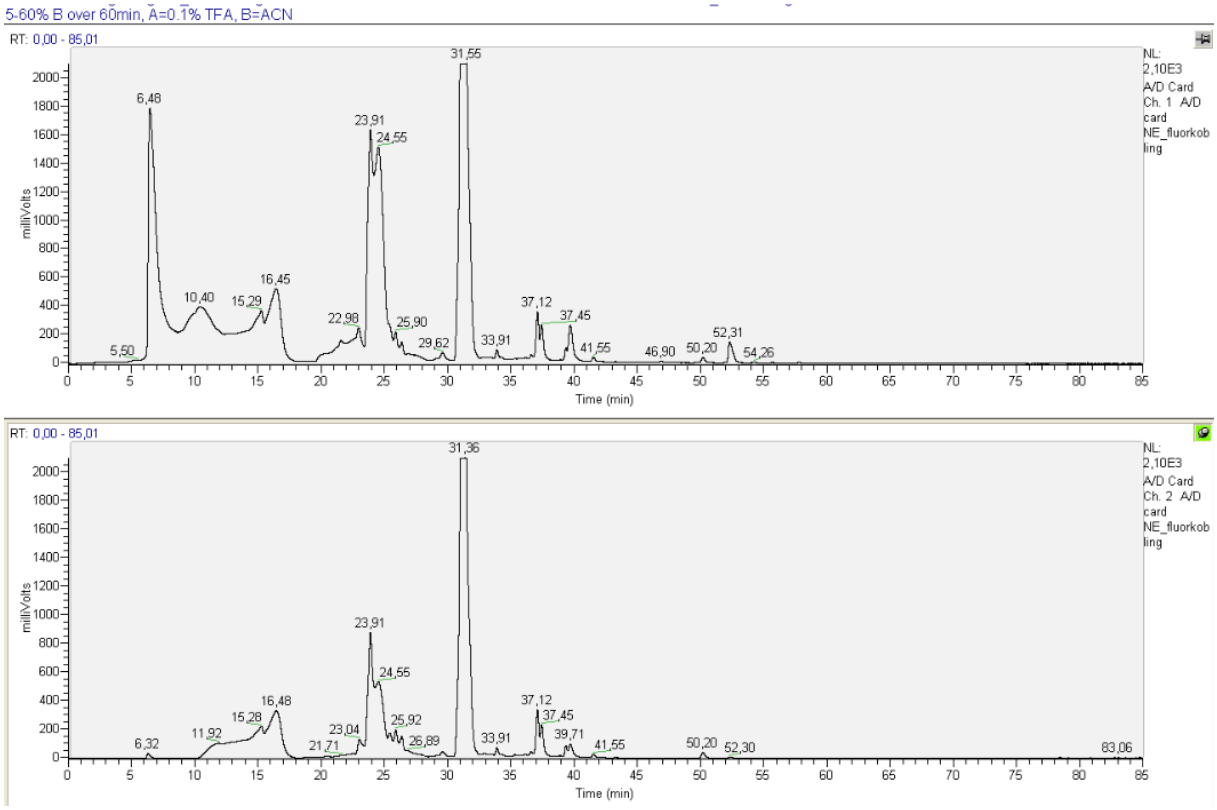

Appendix E: HPLC/Radio-HPLC

Figure E-1. HPLC of (R)-2-amino-3-((3-((4-((2-((S)-2-cyano-4,4-difluoropyrrolidin-1-yl)-2-oxoethyl)carbamoyl)quinolin-6-yl)oxy)propyl)amino)-3-oxopropane-1-sulfonic acid (**1**)

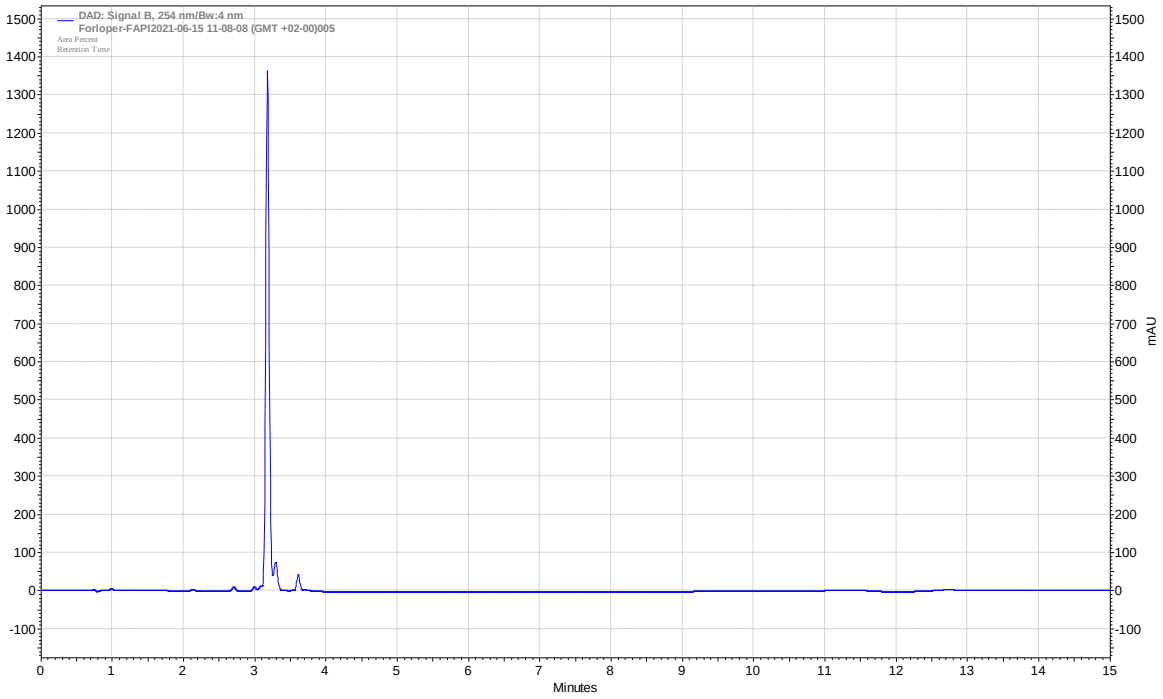

Appendix E: HPLC/Radio-HPLC

Figure E-2. HPLC of (R)-3-((3-((4-((2-((S)-2-cyano-4,4-difluoropyrrolidin-1-yl)-2-oxoethyl)carbamoyl)quinolin-6-yl)oxy)propyl)amino)-2-(6-fluoronicotinamido)-3-oxopropane-1-sulfonic acid (**19**)

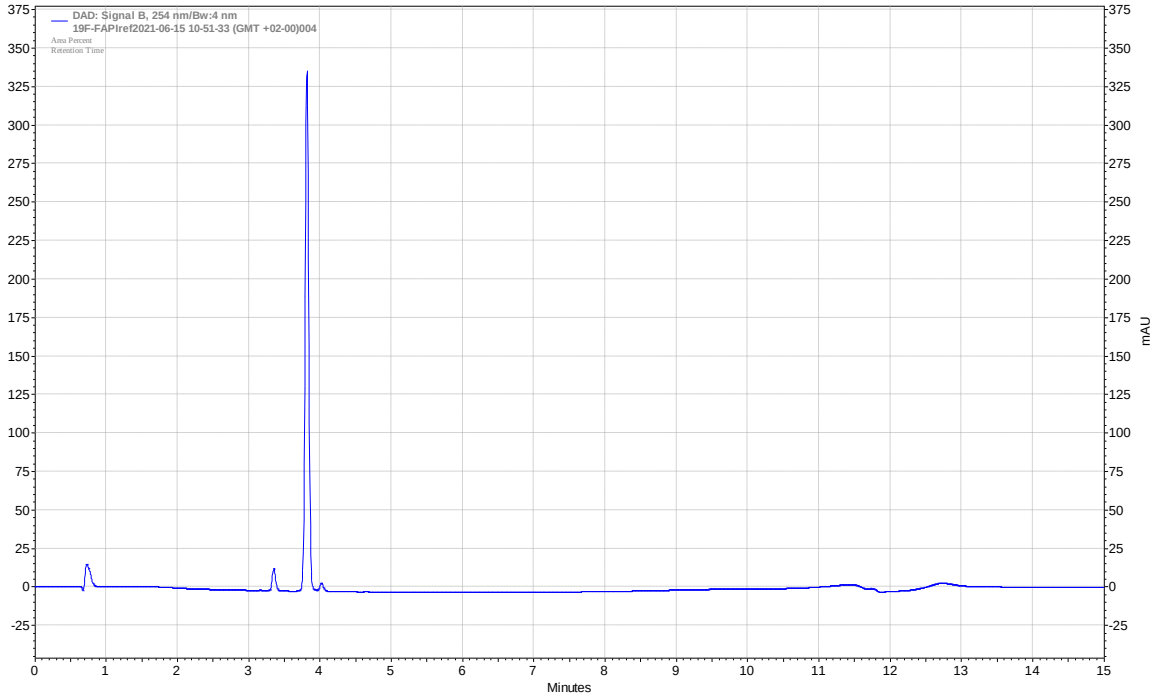

Appendix E: HPLC/Radio-HPLC

Figure E-3. Radio-HPLC of 6-[^{18}F]fluoronicotinic acid 2,3,5,6-tetrafluorophenyl ester ([18F]F-Py-TFP) **(21)**

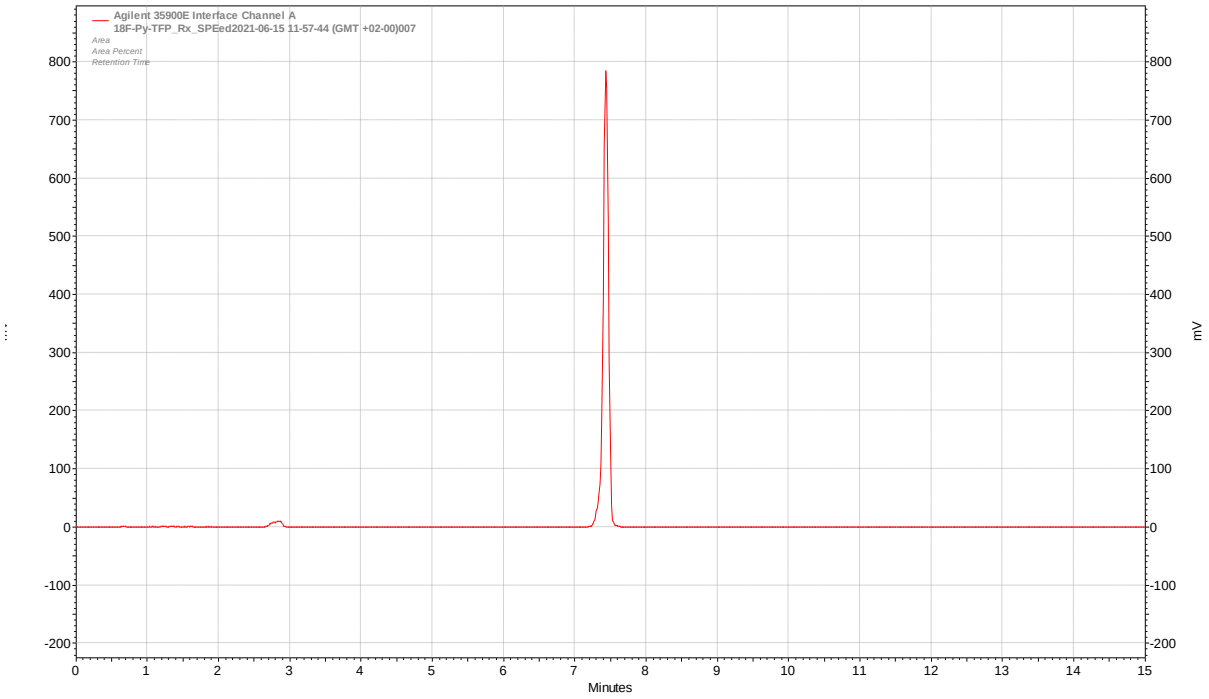

Appendix E: HPLC/Radio-HPLC

Figure E-4. Co-elution of (R)-3-((3-((4-((2-((S)-2-cyano-4,4-difluoropyrrolidin-1-yl)-2-oxoethyl)carbamoyl)quinolin-6-yl)oxy)propyl)amino)-2-(6-fluoronicotinamido)-3-oxopropane-1-sulfonic acid (**19**) in blue and (R)-3-((3-((4-((2-((S)-2-cyano-4,4-difluoropyrrolidin-1-yl)-2-oxoethyl)carbamoyl)quinolin-6-yl)oxy)propyl)amino)-2-(6-(^{18}F)nicotinamido)-3-oxopropane-1-sulfonic acid (**22**) in red on radio-HPLC.

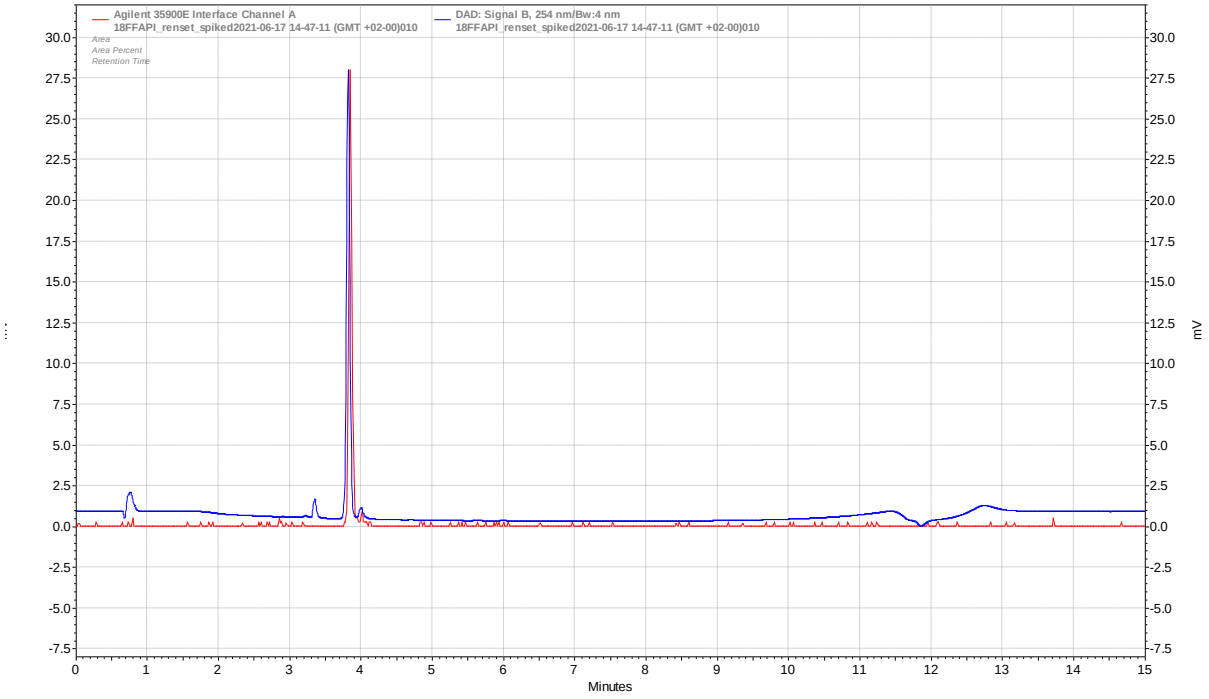

Appendix E: HPLC/Radio-HPLC

Figure E-5. Radio HPLC of (R)-3-((3-(((4-((2-((S)-2-cyano-4,4-difluoropyrrolidin-1-yl)-2-oxoethyl)carbamoyl)quinolin-6-yl)oxy)propyl)amino)-2-(6-(^{18}F)nicotinamido)-3-oxopropane-1-sulfonic acid (**22**). The conditions include DMSO, 2-butanone, DIPEA and heat.

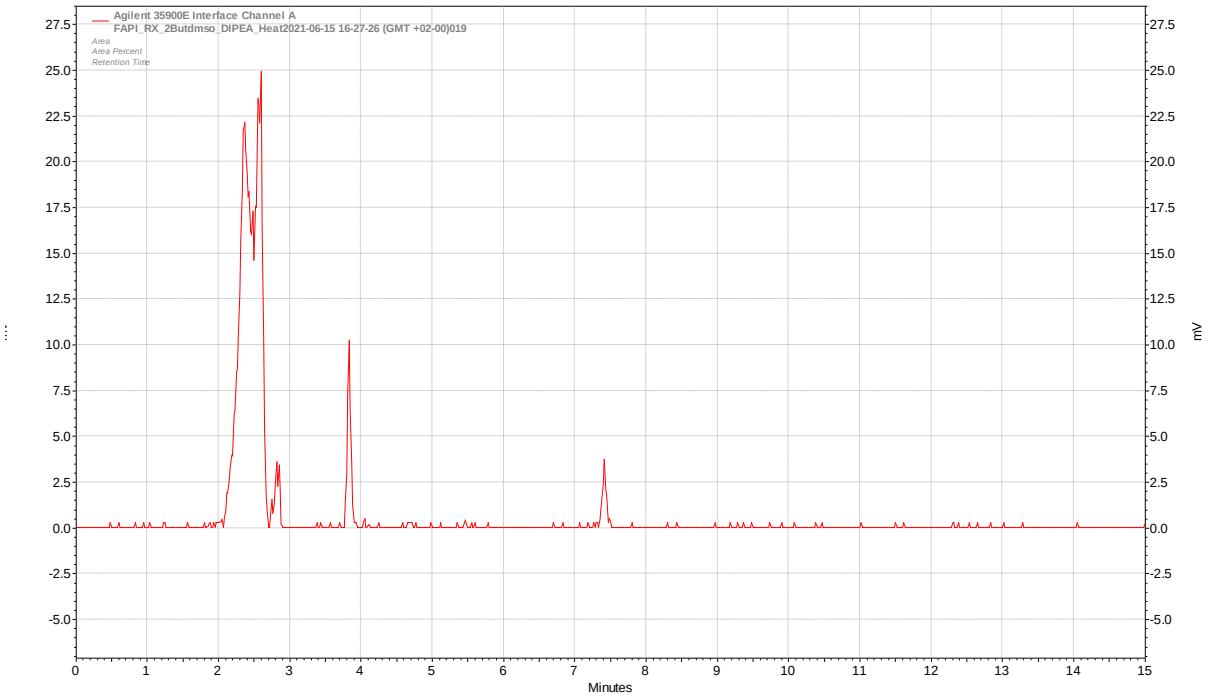

Appendix E: HPLC/Radio-HPLC

Figure E-6. Radio HPLC of (R)-3-((3-(((4-((2-((S)-2-cyano-4,4-difluoropyrrolidin-1-yl)-2-oxoethyl)carbamoyl)quinolin-6-yl)oxy)propyl)amino)-2-(6-(^{18}F)nicotinamido)-3-oxopropane-1-sulfonic acid (**22**). The conditions include DMSO and DIPEA.

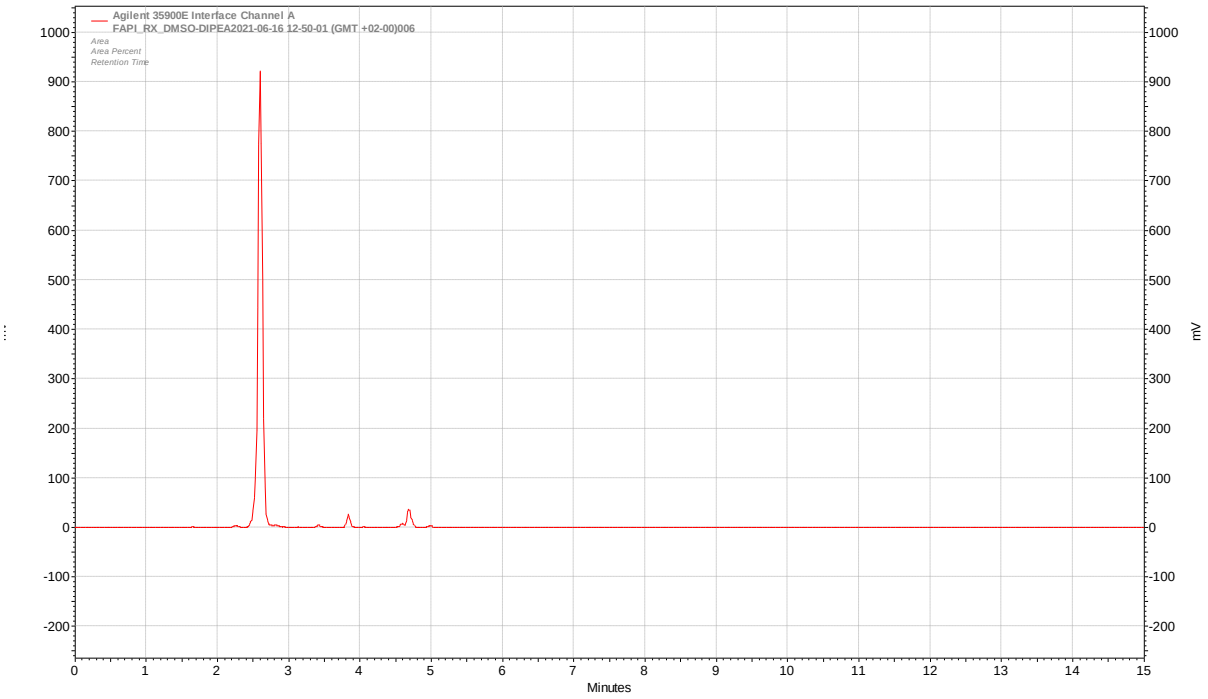

Appendix E: HPLC/Radio-HPLC

Figure E-7. Radio HPLC of (R)-3-((3-((4-((2-((S)-2-cyano-4,4-difluoropyrrolidin-1-yl)-2-oxoethyl)carbamoyl)quinolin-6-yl)oxy)propyl)amino)-2-(6-(^{18}F)nicotinamido)-3-oxopropane-1-sulfonic acid (**22**). The conditions include ethanol absolute, triethylamine, hydrogen carbonate and heat.

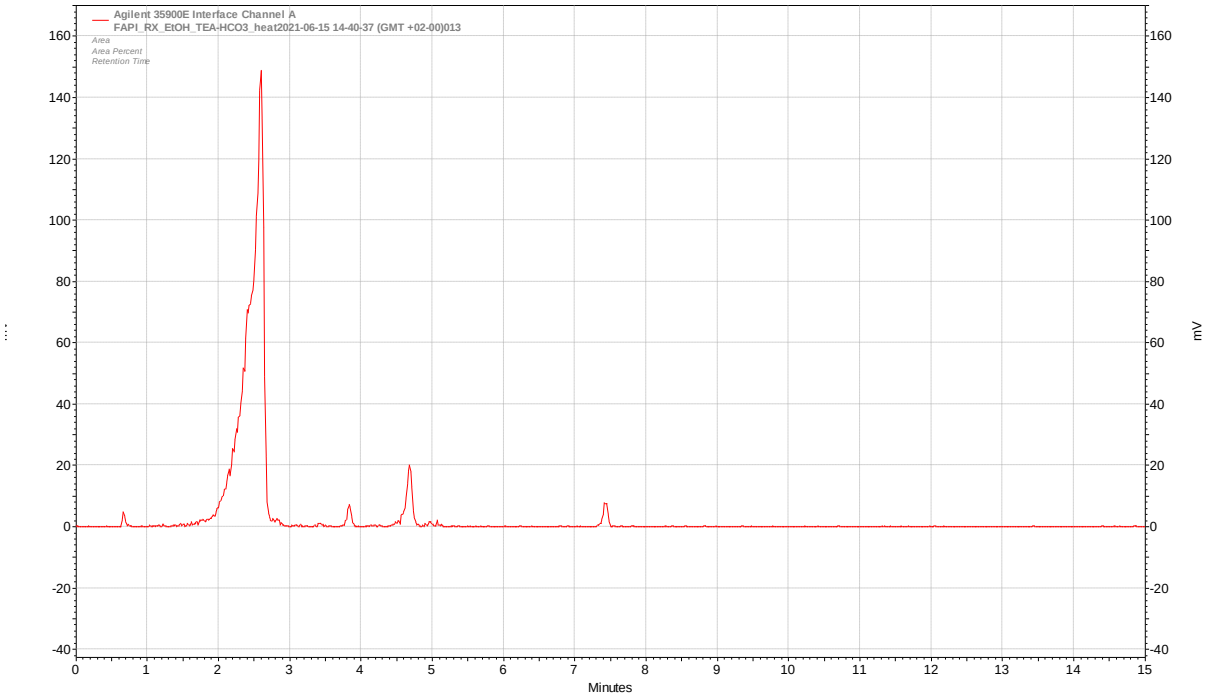

Appendix E: HPLC/Radio-HPLC

Figure E-8. Radio HPLC of (R)-3-((3-((4-((2-((S)-2-cyano-4,4-difluoropyrrolidin-1-yl)-2-oxoethyl)carbamoyl)quinolin-6-yl)oxy)propyl)amino)-2-(6-(^{18}F)nicotinamido)-3-oxopropane-1-sulfonic acid (**22**). The conditions include ethanol absolute, 2,6-lutidine and DIPEA.

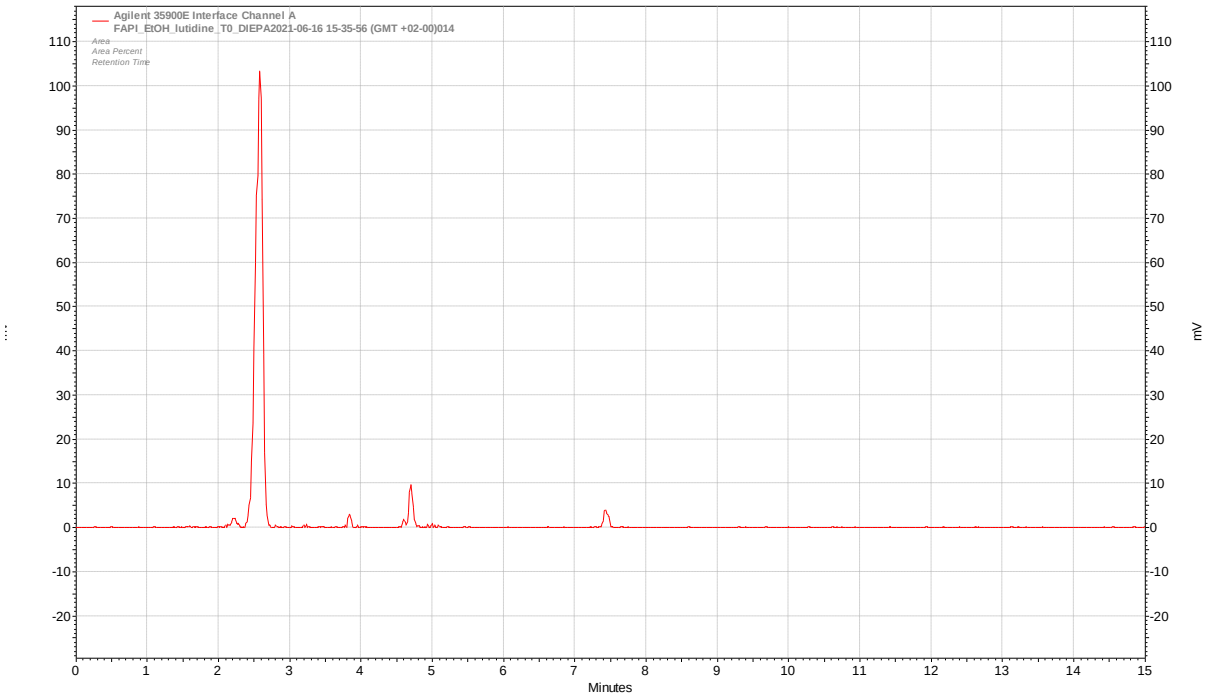

Appendix E: HPLC/Radio-HPLC

Figure E-9. Radio HPLC of (R)-3-((3-((4-((2-((S)-2-cyano-4,4-difluoropyrrolidin-1-yl)-2-oxoethyl)carbamoyl)quinolin-6-yl)oxy)propyl)amino)-2-(6-(^{18}F)nicotinamido)-3-oxopropane-1-sulfonic acid (**22**). The conditions include a phosphate buffer (pH 7.75).

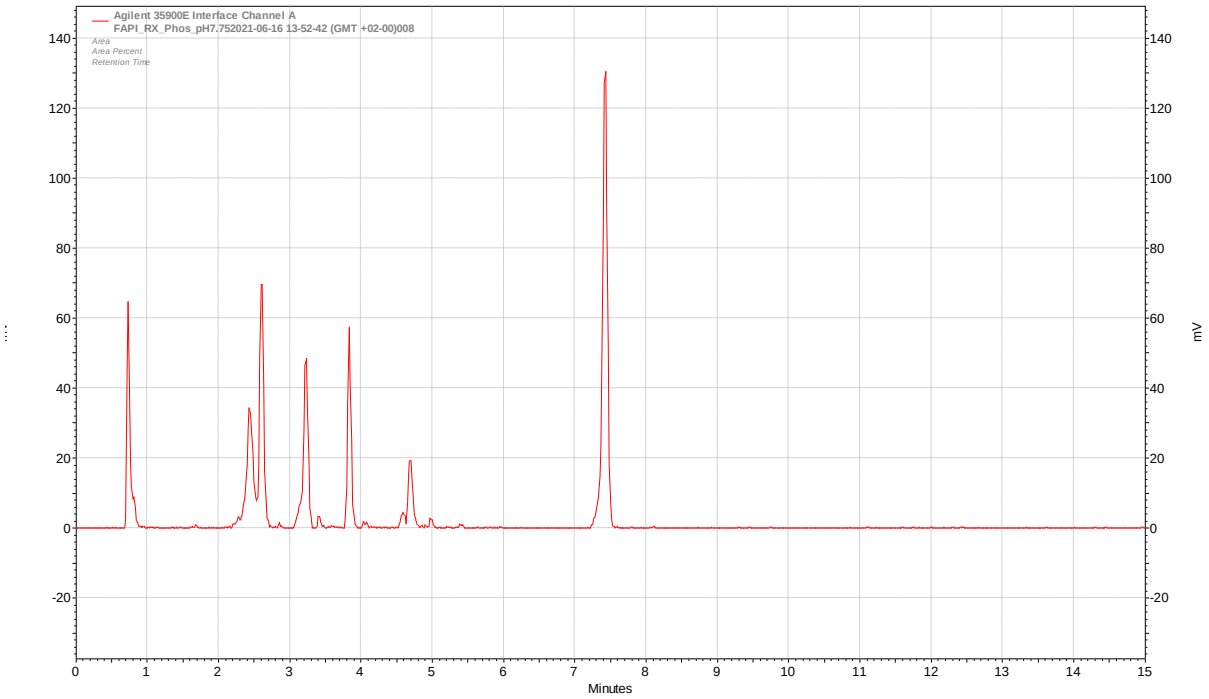

Appendix E: HPLC/Radio-HPLC

Figure E-10. Radio HPLC of (R)-3-((3-((4-((2-((S)-2-cyano-4,4-difluoropyrrolidin-1-yl)-2-oxoethyl)carbamoyl)quinolin-6-yl)oxy)propyl)amino)-2-(6-(^{18}F)nicotinamido)-3-oxopropane-1-sulfonic acid (**22**). The conditions include a phosphate buffer (pH 7.75) and heat.

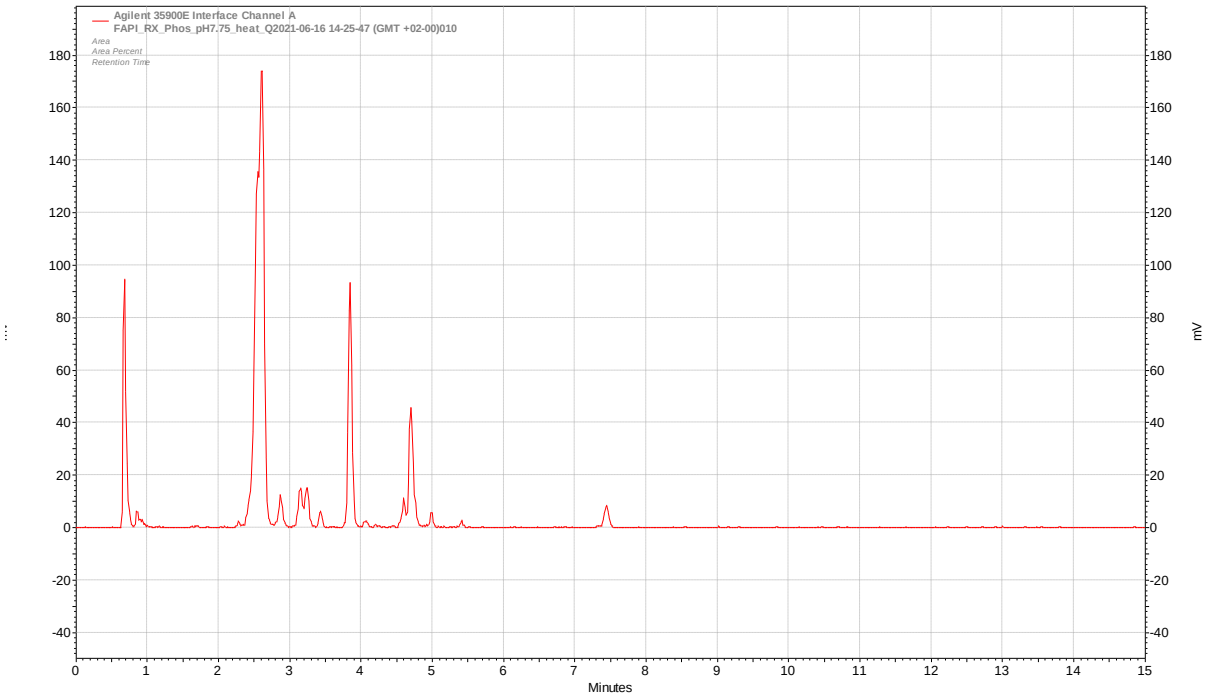

Appendix E: HPLC/Radio-HPLC

Figure E-11. Radio HPLC of (R)-3-((3-((4-((2-((S)-2-cyano-4,4-difluoropyrrolidin-1-yl)-2-oxoethyl)carbamoyl)quinolin-6-yl)oxy)propyl)amino)-2-(6-(^{18}F)nicotinamido)-3-oxopropane-1-sulfonic acid (**22**). The conditions include a phosphate buffer (pH 8.6).

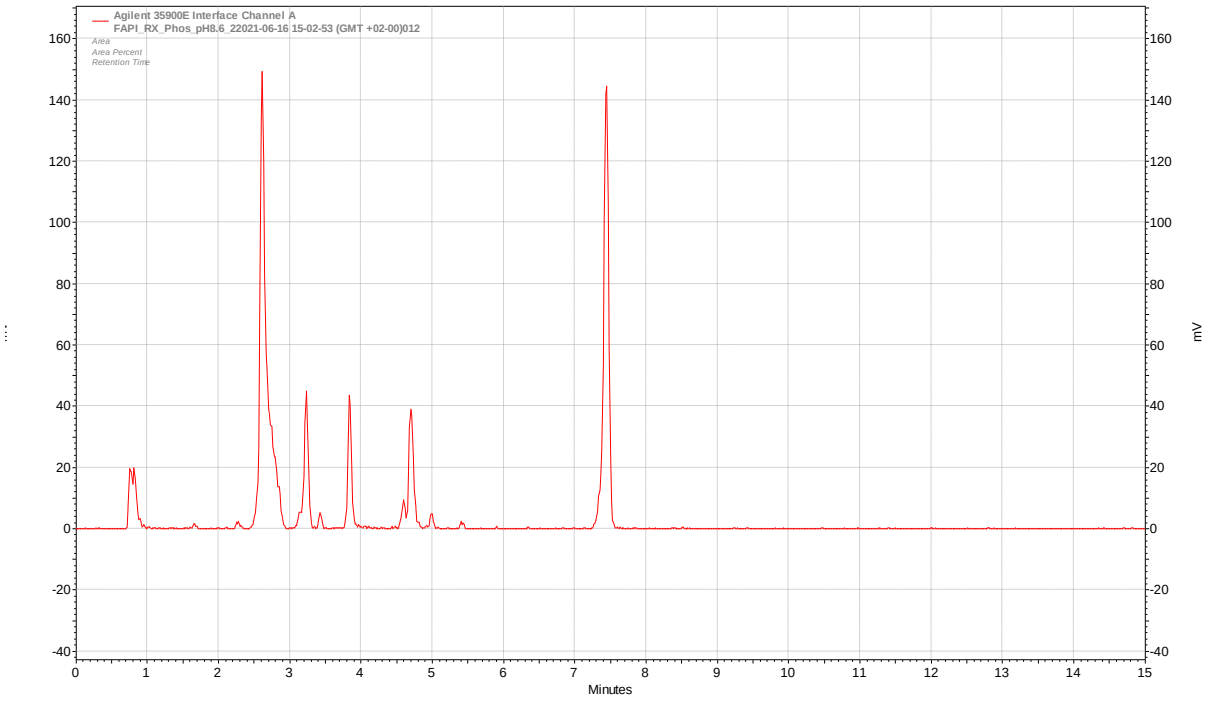

Appendix E: HPLC/Radio-HPLC

Figure E-12. Radio HPLC of (R)-3-((3-((4-((2-((S)-2-cyano-4,4-difluoropyrrolidin-1-yl)-2-oxoethyl)carbamoyl)quinolin-6-yl)oxy)propyl)amino)-2-(6-(^{18}F)nicotinamido)-3-oxopropane-1-sulfonic acid (**22**). The conditions include THF, DIPEA and heat.